Seismicity at Newdigate, Surrey, during 2018-2019: A candidate mechanism indicating causation by nearby oil production

Rob Westaway[1]

[1]University of Glasgow

November 21, 2022

Abstract

During 2018-2019, oil was intermittently produced from the Late Jurassic Upper Portland Sandstone in the Weald Basin, southeast England, via the Horse Hill-1 and Brockham-X2Y wells. Concurrently, a sequence of earthquakes of magnitude ?3.25 occurred near Newdigate, ˜4 km and ˜8 km from these wells. The pattern, with earthquakes concentrated during production from this reservoir, suggests a cause-and-effect connection. It is proposed that this seismicity occurred on a patch of fault transecting permeable Dinantian limestone, beneath the Jurassic succession of the Weald Basin, hydraulically connected to the Portland reservoir via this permeable fault and the permeable calcite 'beef' fabric within the Portland sandstone; oil production depressurizes this reservoir and draws groundwater from the limestone, compacting it and 'unclamping' the fault, reaching the Coulomb failure criterion and causing seismicity. In principle this model is testable, but required data, notably the history of pressure variations in the wells, are not currently in the public domain. The recognition that this instance of seismicity is arguably caused by human activity may well help inform understanding of anthropogenic seismicity in other settings. The initial response, including claims that any connection between this seismicity and oil production was implausible, before any geomechanical analysis was done, was inappropriate.

Seismicity at Newdigate, Surrey, during 2018-2019:
A candidate mechanism indicating causation by nearby oil production

Rob Westaway,
James Watt School of Engineering, University of Glasgow, Glasgow G12 8QQ, UK
robert.westaway@gla.ac.uk

Abstract
During 2018-2019, oil was intermittently produced from the Late Jurassic Upper Portland Sandstone in the Weald Basin, southeast England, via the Horse Hill-1 and Brockham-X2Y wells. Concurrently, a sequence of earthquakes of magnitude ≤3.25 occurred near Newdigate, ~4 km and ~8 km from these wells. The pattern, with earthquakes concentrated during production from this reservoir, suggests a cause-and-effect connection. It is proposed that this seismicity occurred on a patch of fault transecting permeable Dinantian limestone, beneath the Jurassic succession of the Weald Basin, hydraulically connected to the Portland reservoir via this permeable fault and the permeable calcite 'beef' fabric within the Portland sandstone; oil production depressurizes this reservoir and draws groundwater from the limestone, compacting it and 'unclamping' the fault, reaching the Coulomb failure criterion and causing seismicity. In principle this model is testable, but required data, notably the history of pressure variations in the wells, are not currently in the public domain. The recognition that this instance of seismicity is arguably caused by human activity may well help inform understanding of anthropogenic seismicity in other settings. The initial response, including claims that any connection between this seismicity and oil production was implausible, before any geomechanical analysis was done, was inappropriate.

Key words:
Anthropogenic seismicity, geomechanics, calcite 'beef', Weald Basin, Jurassic, Surrey

Introduction
A 'swarm' of earthquakes with magnitudes up to ~3, starting on 1 April 2018, has affected the Newdigate area of Surrey, in the Weald Basin of southeast England (Figures 1, 2, 3). As is detailed in the online supplement, a potential connection with local oilfield activities, in the nearby Brockham-X2Y (BRX2Y) and Horse Hill-1 (HH1) wells, was immediately suspected, but dismissed by petroleum developers (e.g., BBC, 2018; Hayhurst, 2018). Concerns about the possibility that activities in these oilfields were indeed causing these earthquakes were raised through correspondence in The Times newspaper in August 2018 (Gilfillan et al., 2018). A workshop, convened by the Oil & Gas Authority (OGA), followed on 3 October 2018, the OGA being a UK government body with responsibilities that include the licensing of exploration and development of onshore oil and gas resources in England, including managing the risk of seismicity from such operations. A summary of the proceedings of this workshop was reported (OGA, 2018), including the statement that 'the workshop participants concluded that, based on the evidence presented, there was no causal link between the seismic events and oil and gas activity although one participant was less certain and felt that this could only be concluded on "the balance of probabilities" and would have liked to see more detailed data on recent oil and gas surface and subsurface activity' (OGA, 2018, p.1). It has subsequently been argued that there is indeed no such cause and effect connection (Baptie et al., 2019; Hicks et al., 2019); developers have repeatedly issued strong public statements to this effect (e.g., BBC, 2018; Horse Hill Developments Ltd., 2018a; UKOG, 2019a). However, a major issue, not noted in any of the above-mentioned works, is the clear temporal pattern of earthquake occurrence (Fig. 4), with earthquakes strongly concentrated at times when oil is being produced from the Portland reservoir via the HH1 and/or BRX2Y wells. Production will reduce the fluid pressure in the petroleum reservoir being pumped. Fluid pressure changes within faults are well known as a cause of anthropogenic seismicity (e.g., Davies et al., 2013; Hitzman et al., 2013); however, rather than a decrease, the causative change

is usually an increase in fluid pressure as, for example, for the Preese Hall earthquake sequence in 2011, caused by injection of water under pressure during 'fracking' for shale gas (e.g., Westaway, 2017).

Figure 1 here: Map based on Hicks et al. (2019)
Figure 2 here: Cross section based on Hicks et al. (2019)
Figure 3 here: UKOGL seismic profile excerpt.
Figure 4 here: Timelines

Given the geology of the Weald Basin, a conceptual model can be envisaged whereby pressure reduction the Portland reservoir might bring nearby faults to the Coulomb condition for slip, as illustrated in Fig. 5. Nonetheless, testing this model is difficult, for several reasons. The map and cross-section reported by Hicks et al. (2019) provide the most detailed documentation of the Newdigate seismicity that is available, and thus serve as a basis for further discussion. However, a first reason why model testing is difficult is that use of these outputs is problematic because of mistakes in their preparation; before they can be used their geolocation has to be improved (this task occupies much of the present online supplement). A second reason is uncertainty in the hydraulic properties of elements of the proposed model; this includes the distribution of the permeable fabric known as 'calcite "beef"' within clay-dominated lithologies that are otherwise impermeable. Each of these aspects will be investigated in this study. A third reason why testing the proposed model is difficult is that key operational data, such as pressure variations in oil wells and logs of wellsite activities that might affect reservoir conditions, have been found to be unavailable. Indeed, preparation of this manuscript was delayed pending an attempt to obtain such data from the OGA under UK law using a Freedom of Information (FOI) request. However, this request was unsuccessful on the basis that the OGA did not hold such data, notwithstanding the extent of public interest in this topic and the statutory duties of the OGA. In the absence of pressure data, testing the proposed model will be limited to investigating the magnitudes of pressure perturbations that can be anticipated in the model fault and the time delays for their propagation between the oil reservoirs and this fault.

Figure 5 here: Cartoon illustrating conceptual model

Geological structure and stratigraphy

The study area is in southeast England, near the boundary between the counties of Surrey and West Sussex, ~40 km WSW of central London, on the northern flank of the Weald Basin (Figs 1, 6). The outcrop geology and shallow subsurface structure of this area are documented by Dines and Edmunds (1933) and Gallois and Worssam (1993); Trueman et al. (2003), DECC (2013), and others have discussed the history of petroleum exploration. Many authors have discussed the origin and structure of the Weald Basin, or Weald sub-basin of the wider Wessex Basin (e.g., Stoneley, 1982; Chadwick et al., 1983; Chadwick, 1986; Karner et al., 1987; Lake and Karner, 1987; Butler and Pullan, 1990; Hawkes et al., 1998; Andrews, 2014; Wigley, 2015; Pullan and Butler, 2018). As these and many other works demonstrate, this basin has developed near the northern margin of the Variscan orogenic belt, Variscan reverse faults having been reactivated as normal faults during the Mesozoic. Chadwick (1986) resolved two phases of Mesozoic extension in the Weald Basin, during the Early Jurassic (Hettangian to Toarcian; extension factor, β, 1.12) and Late Jurassic and earliest Cretaceous (late Oxfordian to Valangian; β=1.10). The succession of Jurassic and Cretaceous sedimentary formations that accompanied and followed this extension is documented in many works and summarised in the British Geological Survey (BGS) stratigraphic lexicon (https://www.bgs.ac.uk/lexicon/). This basin experienced Cenozoic inversion, during which some of the Mesozoic normal faults were reactivated as reverse faults (e.g., Lake and Karner, 1987). As a result of this history, some faults have normal offsets within the syn-rift succession but show reverse slip in younger sediments, as illustrated in Fig. 2. Table 1 summarises the local stratigraphy, based on the record from the HH1 well.

Figure 6 here: Fault map from Butler and Pullan (1990)
Table 1 here: Horse Hill 1 record

The oil reservoir now recognized at Horse Hill is in the Upper Portland Sandstone, with a permeability of up to ~20 mD, sealed above by the overlying impermeable Purbeck Anhydrite (e.g., Xodus, 2018; Table 1). The base of the reservoir has been inferred as in the range 580-602 m TVDSS (Xodus, 2018), thus roughly at the mid-point of the Upper Portland Sandstone. The modelled extent of this reservoir is illustrated in detail in Fig. 6.6 of Xodus (2018). At its most conservative extent, it extends for ~2 km SSE of the HH1 wellhead, ending at a contact with a fault, downthrown to the SSE by up to ~60 m, which appears to act as a seal. To the WSW the reservoir only extends for ~600 m before it is cut out by the gentle WSW dip of the base Purbeck Anhydrite. Under these conservative assumptions the reservoir has overall dimensions of ~4 km east-west by ~3 km north-south. With a base at 602 m TVDSS, this reservoir would have the same faulted contact to the SSE, but would extend for ~2.5 km SW of the wellhead, its overall dimensions being ~6 km east-west by ~4 km north-south (Xodus, 2018). The dimensions of this reservoir are not shown in Fig. 1 as its large size would clutter other detail. This reservoir, hydraulically connected to the HH1 well, is much larger than the hydraulic 'radius of influence' depicted by Hicks et al. (2019) in Fig. 1.

The base of the Jurassic sequence lies at ~2100-2200 m depth in the study area (e.g., Butler and Pullan, 1990; Pullan and Butler, 2018; Fig. 6). This sequence is locally underlain by thin Triassic deposits overlying pre-Variscan (Palaeozoic) 'basement' at depths of >~2200 m (Busby and Smith, 2001). The uppermost 'basement' in much of this area is known from borehole records to be Dinantian (Early Carboniferous) limestone (Busby and Smith, 2001; Pullan and Butler, 2018). Thus, the HH1 well log (Table 1) indicates that the Jurassic Lias Group is underlain by ~60 m of latest Triassic Penarth Group ('Rhaetic') rocks, then ~50 m of the Triassic Mercia Mudstone, then ~10 m of dolomitic conglomerate of uncertain age, then ~70 m of Dinantian limestone, above a mudstone-dominated Upper Devonian succession. Busby and Smith (2001) estimated using gravity modelling that these Devonian rocks are typically ~1-2 km thick, their base at a typical depth of ~3.5-4 km, being underlain in the central Weald Basin by many kilometres of Lower Palaeozoic metamorphic basement. Around the northern margin of the basin and the southern margin of the adjoining London Platform the Dinantian limestone and underlying Devonian rocks are well imaged seismically at <1 s two way time (TWT), indicating depth <~1500 m (e.g., Andrews, 2014). Both these subdivisions are locally several hundred metres thick, the limestone being relatively unreflective and the Devonian succession highly reflective. Moving southward, as the overlying Mesozoic succession thickens, the Dinantian limestone gradually becomes thinner and its boundaries become more difficult to interpret seismically (e.g., Andrews, 2014). Busby and Smith (2001) noted reports of this limestone in many boreholes beneath the Weald Basin; in their view it persists southward beneath most of the basin, almost to the English Channel coastline.

More recently, Pullan and Butler (2018) have presented a new map (their Fig. 21) showing the pre-Variscan subcrop beneath much of the Weald Basin (including most of the area of Fig. 1, except its NE corner) as Devonian, the Dinantian limestone being inferred to be absent. As interpreted by these workers, this limestone dies out ~2.5 km SW of the HH1 well, indicating that it is absent in the vicinity of the Newdigate fault and the associated seismicity. However, seismic lines in this area (e.g., that in Fig. 2) do not clearly resolve whether this limestone is present or not; as Pullan and Butler (2018) showed, there is no well control for ~20 km distance SW of the HH1 well, so no direct evidence either way. Pullan and Butler (2018) noted dipmeter evidence that in the HH1 well this limestone dips northward at ~20-30°; their inference that it dies out not far away seems based on structural projection given its thickness (Table 1) and assuming continued northward dip. However, it is clear from other seismic sections (e.g., Andrews, 2014) that in other parts of the basin the Dinantian limestone is folded. At this stage it is unclear whether this lithology is present across the study area or

not. The proposed conceptual model (Fig. 5) requires a highly permeable lithology, such as this, beneath the Mesozoic sediment in this area.

The two key issues already noted will now be addressed. The distribution and properties of calcite 'beef' will first be discussed. Second, the geolocation of features, mislocated by Hicks et al. (2019), will be considered.

Calcite 'beef' and its significance
Calcite 'beef', first reported by Webster (1826), consists of bedding-parallel veins of diagenetic calcite (e.g., Cobbold and Rodrigues, 2007; Zanella et al., 2015). Buckland and De la Beche (1835) adopted this nomenclature for veins of fibrous calcite within claystone beds in what is now known as the Purbeck Group in Dorset, the term 'beef' having originally been used by quarry workers on account of similarity to the fibrous structure of meat. This fabric (illustrated by many authors, including Tarney and Schreiber, 1977, Cobbold et al., 2013, and Meng et al., 2017) is now recognized in mudstone formations worldwide (e.g., Cobbold et al., 2013). Following the above-mentioned early reporting its mode of origin was widely debated; the view has become accepted relatively recently that 'beef' develops by natural hydraulic fracturing associated with overpressure during hydrocarbon maturation and migration (e.g., Parnell et al., 2000; Lash and Engelder, 2005; Cobbold and Rodrigues, 2007; Cobbold et al., 2013; Al Duhailan et al., 2015; Zanella et al., 2015; Zhang et al., 2015; cf. Maher et al., 2017; Meng et al., 2017). This fabric is indeed sometimes designated as 'hydrocarbon-expulsion fractures' (e.g., Al Duhailan and Sonnenberg, 2014). The conditions for calcite 'beef' development include palaeo-temperature in the range 70-120 °C (Cobbold et al., 2013). In the central Weald Basin, palaeo-temperatures as high as this are expected throughout the Jurassic succession, given the estimated ≥~2 km of burial during the Cretaceous sedimentation, before the Cenozoic erosion (e.g., Andrews, 2014).

In southern England, calcite 'beef' is best known in the Early Jurassic Shales-With-Beef Member (https://www.bgs.ac.uk/lexicon/lexicon.cfm?pub=SHWB) of the Charmouth Mudstone Formation, part of the Lias Group, which crops out around Lyme Regis in Dorset (e.g., Lang, 1914; Lang et al., 1923; Hesselbo and Jenkyns, 1995; Meng et al., 2017). Calcite 'beef' is also well known in the Late Jurassic of the Weald Basin from both outcrop and borehole sections (e.g., Howett, 1964). In the Howett (1964) stratigraphy, this fabric occurs within the 'Shales with Beef and Clay-ironstone' unit, which occurs at the top of the Middle Purbeck succession and is typically ~20 m thick. This fabric (reported as 'calcite veining') is also known from older Late Jurassic deposits, for example in core recovered between 701 and 710 m depth (below ground level 80.3 m O.D.) in the Collendean Farm borehole (drilled in 1964; BGS ID TQ24SW1; at TQ 2480 4429) near the Horse Hill site (Fig. 1).

In the Collendean Farm borehole log, 'beef' was interpreted as occurring in glauconitic sandstone forming the lower part of the Portland Group. However, Gallois and Worssam (1993) placed this stratigraphic level in what they regarded as the sandy upper part of the underlying Kimmeridge Clay Formation. Nonetheless, in recent petroleum exploration reports (e.g., Xodus, 2018), as in the summary in Table 1, this glauconitic sandstone with calcite 'beef' is reinstated within the Lower Portland Sandstone. Its inclusion within the Portland Group explains why this group is portrayed as much thicker in the recent petroleum-oriented literature (e.g., ~130 m thick in Table 1) than by Gallois and Worssam (1993), who gave its thickness as only 54 m at Collendean Farm. As these latter authors noted, the Portland Group in the Weald Basin is not well correlated with the 'type' Portlandian of the Portland area of Dorset, which is in the Portland – South Wight Basin, not the Weald Basin (e.g., Hawkes et al., 1998). The 'type' Portlandian includes the Portland Limestone (now known as the Portland Stone Formation), an important building stone; the sediments of this age being not sandstone-dominated as in the Weald Basin.

The significance of all the above for the present study is as follows. It has previously been noted that the combination of processes responsible for 'beef' formation will create permeability anisotropy, permeability being far greater parallel to the fabric and bedding than in the perpendicular direction (e.g., Lash and Engelder, 2005; Bisdom et al, 2016). Various workers have estimated the permeability of such bedding-parallel fractures, the highest estimate identified during the present work, ~900 mD ($\sim 9 \times 10^{-13}$ m^2), being by Carey et al. (2015) for the Ordovician Utica Shale of eastern North America. This is many orders-of-magnitude higher than the expected nanodarcy permeability of shale perpendicular to bedding, and is quite a high value for rocks in general.

Other workers (e.g., Wang, 2016; Maher et al., 2017; Meng et al., 2018) have investigated the aperture, or width, of bedding-parallel fractures (typically filled with 'beef') in shale. In a study spanning several shale provinces, Wang (2016) found fractures with width varying between 15 μm and 87 mm. Many of the wider ones could be seen to form as a result of multiple increments to opening, each adding a few tens of microns of width, prior to cementation due to growth of calcite. Permeability and fracture aperture can be interrelated by comparing the Darcy equation for laminar fluid flow, $Q = (k \ A \ / \ \eta) \ dP/dx$, and the Poiseulle equation for laminar flow between parallel boundaries, $Q = (D \ W^2 \ / \ (12 \ \eta)) \ dP/dx$, which is a solution to the more general Navier-Stokes equation for fluid flow (e.g., Zimmerman and Bodvarsson, 1996). Here Q is the volume flow rate, η the viscosity of the fluid, dP/dx the pressure gradient in the direction of flow, k the permeability of the medium, A the cross-sectional area of the flow, and W and D the width of the channel and its length in the direction perpendicular to the flow. Combining these two formulae, equating A to D×W, gives $k \equiv W^2/12$. This formula gives the permeability equivalent to W=15 μm as ~20 D ($\sim 2 \times 10^{-11}$ m^2). Overall, it is inferred that the ~900 mD value, from Carey et al. (2015), rounded to ~1 D ($\sim 10^{-12}$ m^2), might be applicable to 'beef' in the present study area. As will become clear below, the present analysis also requires knowledge of the specific storage S_S of calcite 'beef', although no published estimate for this parameter is known to the present author. Other fractured rocks have S_S ~10^{-6} m^{-1} or thereabouts (e.g., Younger, 1993; Jones et al., 2000; Blake et al., 2010); pending any direct determination, this value will be adopted here.

Geolocation
The study area has been illustrated using the map (Fig. 1), and seismic cross-section (Fig. 2) from Hicks et al. (2019). However, the original versions of both these figures have required significant amendment regarding accuracy issues. This map was originally geolocated using geographical co-ordinates; to make it easier to use British National Grid (BNG) co-ordinates have been added. This map also shows seismic lines and faults. The source of information for positions of seismic lines, including line TWLD-90-15 that is illustrated in Figs 2 and 3, was not reported by Hicks et al. (2019); it is evident that they are from the UK Onshore Geophysical Library (OGL; https://ukogl.org.uk/) location map, which is itself indexed to the BNG, so this information must have been first transformed to geographical co-ordinates by Hicks et al. (2019). Hicks et al. (2019) also explained that (rather than using the existing literature, including geological maps and structural analyses by BGS and petroleum developers, as might be expected) they located faults in the study area through their own interpretation of 2-D seismic reflection profiles. Furthermore, the velocity model used by Hicks et al. (2019) for earthquake location (Table 2) is significantly slower than the set of interval velocities from the HH1 well (Table 1), causing their hypocentres to be mislocated at depths that are too shallow.

Table 2 here: Hicks et al. (2019) velocity model

The seismic section in Fig. 2 clearly has higher resolution than older ones, including those which informed earlier fault maps such as that by Butler and Pullan (1990) (Fig. 6). Some of the faults depicted in Fig. 2 are, thus, recognized for the first time. However, additional faults are also evident in the uninterpreted version, provided by Hicks et al. (2019) as their supplementary Figure S13, which

lacks the overwhelming interpretation applied to Fig. 2, and in the raw seismic section provided by UKOGL (Fig. 3). Of particular significance, it is suggested, is the nature of the Newdigate Fault which, in the lower part of the Jurassic sediment and upper part of the underlying Palaeozoic basement, consists of multiple fault strands distributed across a zone with width, in the north-south direction, approaching ~2 km. Careful inspection of supplementary Figure S13 of Hicks et al. (2019) and Fig. 3 indicates broken and offset seismic reflectors which delineate these subsidiary strands of the Newdigate fault zone, some evidently near the limit of seismic resolution (cf. Bond et al., 2007), which merge upwards by ~0.5 s two way time (TWT).

Depth conversion of the seismic section in Fig. 2 and location of the earthquakes, both using the same velocity model derived from the set of interval velocities (Table 1), would adjust the earthquake hypocentres downward relative to the detail in the seismic section by an estimated ~400 m (see online supplement). The key consequence of this adjustment is to move the earthquake population from within the Jurassic sedimentary section to within the Palaeozoic 'basement'. These earthquakes presumably occurred on one of the steeply north-dipping subsidiary strands of the Newdigate fault zone, given the steeply north-dipping nodal planes, identified as the fault planes, of the focal mechanisms (Fig. 1 and Table 3), rather than on the main Newdigate Fault that dips south.

The mislocation of faults in Fig. 1 is discussed in detail in the online supplement. Its most significant aspect concerns the depiction of faulting south of the Brockham oil reservoir. Figure 1 shows two faults, the Brockham Fault and Holmwood Fault, separating this reservoir from the block farther south, which leads south to the Newdigate fault zone. Hicks et al. (2019) thus proposed that the faulting in this vicinity will act as a 'baffle' to fluid flow or pressure changes, arising in the Brockham reservoir, reaching the seismogenic zone. However, when the more accurate depiction of the faulting from the petroleum industry (e.g., Xodus, 2018), is adopted, only the Brockham Fault offsets the Portland Sandstone between the Brockham oil reservoir and the seismogenic zone. Furthermore, given the seismic velocity listed in Table 1, the ~40 ms TWT offset on the Brockham Fault in this vicinity indicates a throw of ~50 m, rather less than the thickness of the Portland Group in this area (cf. Table 1). Thus, although the seal at the southern margin of the Brockham oil reservoir is provided by the downthrow against it of the impermeable Purbeck Anhydrite, the same downthrow means that at depths of a few tens of metres greater the Lower Portland Sandstone in the footwall is juxtaposed against the Upper Portland Sandstone in the hanging-wall. Since both subdivisions of the Portland Group are highly permeable, the Brockham Fault in this vicinity is unlikely to act as a 'baffle' to fluid flow or pressure changes. Amendment of the structure in this area means that reconsideration of the role of pressure changes in well BRX2Y as a causal factor for the Newdigate seismicity is warranted.

Seismicity and its correlation with well activities

As already noted, multiple publications have already documented the 2018-2019 Newdigate 'earthquake swarm', notably those by Baptie and Luckett (2018), Verdon et al. (2019), and Hicks et al. (2019). Baptie and Luckett (2018) presented a preliminary analysis of 14 earthquakes that occurred between 1 April and 18 August 2018. Their results are significant primarily because they informed the OGA workshop. The more extensive analysis by Hicks et al. (2019) will now be appraised. These latter authors determined hypocentres and other source parameters for 168 earthquakes between 1 April 2018 and 28 June 2019, some with local magnitude $M_L < -1$, their location patterns and timeline being depicted in Figs 1, 2 and 4 and summarized in Table 3. The first nine earthquakes up to 10 July 2018 (including one of the largest, with M_L 3.02, on 5 July) were located before any local seismograph stations were operational, using only data from permanent regional stations. Hicks et al. (2019) explained that due to the limited available data these events were located by assigning each a fixed focal depth. The resulting reported depths vary between 2.33 and 3.08 km (see Table S2 of Hicks et al., 2019), it being unclear on what basis different depths were assumed for different events. The next sixteen events, until 11 July, were located conventionally but including data from local stations. For

the rest of the events, both 'double difference' relocations (after Waldhauser and Ellsworth, 2000) and conventional locations were determined, using the velocity structure in Table 2. Table 4 lists earthquakes in this area that post-date the Hicks et al. (2019) study.

Table 3 here: Summary of Newdigate seismicity
Table 4 here: Most recent Newdigate earthquakes

Focal mechanisms were determined by Hicks et al. (2019) for six events, including the largest, of M_L 3.18 and moment magnitude M_W 3.25, on 27 February 2019, as illustrated in Fig. 1 and listed in Table 3. All six events have a nodal plane striking roughly east-west and dipping steeply north. As already noted, this plane is inferred to be the fault plane, indicating predominant right-lateral slip. Available data regarding the state of stress in the Weald Basin are extremely limited; Kingdon et al. (2016) and Fellgett et al. (2017) provided syntheses of in situ stress data across much of Britain. However, these authors wrote little about the Weald Basin, Fellgett et al. (2017) noting that many hydrocarbon wells in this area have yielded stress data but these data had not yet been placed in the public domain. The stress dataset available for the Weald Basin thus remains that presented by Evans and Brereton (1990). As is detailed in the online supplement, this limited dataset indicates a NW-SE maximum principal stress and a NE-SW minimum principal stress. The Newdigate earthquake focal mechanisms (Fig. 1) are consistent with this stress field orientation, given the standard requirement for the maximum principal stress to lie within dilatational quadrants (McKenzie, 1969).

Temporal clustering
As detailed by Hicks et al. (2019), the Newdigate seismicity between April 2018 and June 2019 involved four 'clusters' of activity (Fig. 4). The first began at 11:10 on 1 April (M_L 2.66), followed by two events later on the same day, another on 9 April, and a final event on 28 April. The smallest of these events (on 9 April) had M_L 1.28. No local seismograph stations were then in operation; Hicks et al. (2019) estimated that the completeness threshold for earthquake detection was circa M_L 2, so many smaller events were undoubtedly missed.

The second 'cluster' (Fig. 4) began at 12:28 on 28 June (M_L 2.52), and included four other events above M_L 2.0 (on 29 June and 5 July, and two on 18 July) including the second largest event overall (M_L 3.02), at 10:53 on 5 July. The installation of local seismograph stations in mid June and early July lowered the completeness threshold for earthquake detection to below M_L 0 (Hicks et al., 2019), resulting in many small events being thereafter detected and enabling use of the relative location procedure that was adopted. After these initial relatively large events this 'cluster' of earthquakes began to tail off, in terms of both magnitude and frequency of occurrence. The last event with M_L>0 occurred at 03:21 on 18 August (M_L 0.30), with infrequent smaller events persisting into early 2019.

The third 'cluster' (Fig. 4) began on 14 February 2019 with a relatively large event at 07:43 (M_L 2.47), followed by two other events of M_L≥ ~2, at 17:03 on 19 February (M_L 1.98) and at 03:42 on 27 February (M_L 3.18), this being the largest event of the overall sequence. After these initial relatively large events this 'cluster' of earthquakes also tailed off, although two events with M_L>0 occurred during April 2019 (on 11 and 22 April; M_L 0.73 and 0.56).

The fourth 'cluster' (Fig. 4) began with a relatively large event (M_L 2.35) at 00:19 on 4 May 2019. As for the preceding 'clusters', this seismicity thereafter began to tail off, although events with M_L ~0 persisted until the end of June 2019. Locations by BGS confirm the tailing-off trend through July and August 2019 (Table 4), with a M_L 1.1 event on 2 September, three smaller events later that month, one during October, and none more before the end of 2019 (Table 3).

Overall, this pattern of seismicity, consisting of event 'clusters', each involving activity tailing off after a peak, with the largest event increasing during successive 'clusters', bears a striking resemblance to other earthquake swarms that are inferred to be caused by fluid pressure changes in a fault (e.g., Hainzl, 2004). However, the Newdigate earthquake population is insufficient to permit statistical testing of the patterns expected for this mechanism.

Correlation of seismicity with well activities
As detailed in the online supplement, during prolonged production from Brockham well BRX2Y prior to 2016, the reservoir pressure had decreased from ~900 to ~500 psi. Angus Energy (2018a) reported that at the end of production in 2016 the reservoir pressure was ~490 psi or ~3.4 MPa. At its depth of ~622 m the expected hydrostatic pressure would be ~6.1 MPa; the reservoir was evidently under-pressured. It is to be expected that flow of groundwater towards this reservoir, during 2016-2018, would re-pressurize this reservoir. Figure 4(c) indicates how the four 'clusters' of earthquakes discussed above correlate with activities affecting the Portland reservoir in the HH1 or BRX2Y wells. Production from well BRX2Y resumed in late March 2018: from Hicks et al. (2016) ~4.0 m^3 (~25 barrels) of oil were produced on 23 March followed by ~1.1, ~0.9 and ~1.0 m^3 (~7, ~6 and ~6 barrels) on 25-27 June. Reservoir pressure during this and subsequent production has not been reported, but from standard theory (e.g., Dake, 1998; Guo et al., 2008) one expects it to have decreased. This start of production occurred nine days before the first Newdigate earthquake on 1 April 2018. Furthermore, as is detailed in Fig. 4 and in the online supplement, other brief 'pulses' of production occurred from well BRX2Y in June, respectively 20, 19, 16 and 6 days before the start of the second 'cluster' of seismicity on 27 June.

Although the activities that were planned in the HH1 well in 2018 have been disclosed (Horse Hill Developments Ltd., 2018b), most of the actual activities that took place, and any associated variations in pressure within the well, have not been, other than in the very general terms reported by Hicks et al. (2019). An attempt is made in the online supplement to piece together the sequence of events, based on fragments of information available. It is thus evident that before 4 July 2018, the Portland reservoir was reported as isolated from the surface by a removable bridge plug in this well. Claims have been made that the reservoir might have been influenced before this date by surface activities at the site and by activities in the shallow part of the well (Hayhurst, 2018); if so, this would imply that the bridge plug had failed. With the exception indicated below, no pressure data from well HH1 have been made public; as already noted, an attempt to obtain such data from the OGA as a FOI request has been unsuccessful. As detailed in the online supplement, during the flow testing of the Portland reservoir in well HH1 in July-August 2018, the developer reported production rates of 140-160 bopd, with stable bottom hole pressures ~1.4 MPa below the initial reservoir pressure of ~6.3 MPa, and that bottom hole pressures recovered rapidly during periods of shut-in, indicating good connectivity within this reservoir.

It is evident from Fig. 4 that production ceased from well BRX2Y in October 2018; production at HH1 switched from the Portland reservoir to the Kimmeridgian reservoirs around the same time. Around this time, seismicity at Newdigate tailed off significantly.

The seismicity then re-intensified as the third 'cluster', recognized by Hicks et al. (2019), starting on 14 February 2019, which followed the resumption on 11 February 2019 of production from well HH1, now at rates of up to 220 bopd, from the Portland reservoir. As is detailed in the online supplement, production from this reservoir continued until late June 2019, after which it switched back to the Kimmeridgian reservoir, then during December 2019 to the newly-completed horizontal lateral, off well Horse Hill-2 (designated HH2Z), in the Portland reservoir. Seismicity at Newdigate remained significant during this phase of production from the Portland reservoir at HH1. However, production was not continuous; Hicks et al. (2019) reported shutdowns during 9-12 April and 4-10 May, the latter

corresponding to the start of the fourth 'cluster' of seismicity as recognized by these authors. Seismicity subsequently tailed off following the end of production at HH1 from the Portland reservoir in late June 2019 and the switch to production from the Kimmeridgian reservoir in early July (Fig. 4 and Table 4). Furthermore, seismicity did not resume during the initial flow testing of well HH2Z in December 2019, even though the production rates from the Portland reservoir well were much greater, up to 1087 bpd of fluid production, than they had been from well HH1 (see the online supplement).

Overall, the correlation between phases of production from the Portland reservoir, from well HH1 or well BRX2Y or both, and 'clusters' of earthquakes has been compelling (Fig. 4). Hicks et al. (2019) did not recognize this pattern, apparently because their account did not differentiate between the Portland and Kimmeridgian reservoirs as sources of production from well HH1, as is now done (based on details in the online supplement). Moreover, there are clear patterns of cause and effect for the first and third 'clusters' of seismicity: the first began 9 days after the resumption of production from well BRX2Y in March 2018; the third began 3 days after the resumption of production from well HH1 in February 2019. Nonetheless, there are no clear patterns for the other two 'clusters' of seismicity, nor any seismicity associated with the flow testing of well HH2Z during December 2019.

Conceptual geomechanical model

The conceptual geomechanical model already summarized (Fig. 5), which can account for seismicity beneath Newdigate, caused by pressure decreases in the Portland reservoir resulting from production (or other activities) from the HH1 or BRX2Y wells, will now be described in detail. The basis of this model (Fig. 5) is as follows. The Upper Portland Sandstone reservoir adjoining these wells is assumed to make a subhorizontal hydraulic connection with the seismogenic fault strand within the Newdigate fault zone via a permeable fabric formed in calcite 'beef' in the stratigraphically adjacent Lower Portland Sandstone. The seismogenic fault is assumed highly permeable and to provide a downward hydraulic connection to the rocks beneath the Jurassic succession. These rocks are assumed to include the dolomitic conglomerate and Dinantian limestone, as in the HH1 well (Table 1), which are themselves permeable. It is further assumed that the Newdigate seismicity has occurred at locations where these permeable lithologies are in contact across this fault. Pressure reduction in the Portland reservoir will thus reduce the fluid pressure in this fault, which will cause flow from within the adjoining permeable lithologies into the fault. The associated reduction in fluid volume within these lithologies will cause them to compact. This will result in surfaces in these lithologies that were previously in contact across this fault to separate slightly, reducing the normal stress across the fault. This will 'unclamp' the fault (as in Fig. 5(b)), moving it closer to the Coulomb failure condition. The fault is itself assumed to be 'critically stressed', already near this failure condition, potentially enabling relatively small change in the state of stress to cause coseismic slip (cf. Townend and Zoback, 2000; Zoback and Zoback, 2007).

Regarding the assumptions thus made, the presence of calcite 'beef' within the Portland Group sediments and its permeability have already been discussed. The permeability of faults is a major issue in Earth science (e.g., Caine et al., 1996; Evans et al., 1997; Lunn et al., 2008; Bense et al., 2013; Haines et al., 2016). There is no information regarding the permeability of any strand of the Newdigate fault zone; however, the view that faults are generally permeable, especially when critically stressed (e.g., Barton et al., 1995) is widely accepted, as is the precautionary principle that faults are assumed permeable, in the absence of contrary evidence, when assessing the possibility of subsurface fluid migration (e.g., Westwood et al., 2017; Wilson et al., 2018). Nonetheless, counterexamples exist, such as faults made impermeable by cemented fault gouge (e.g., Agosta et al., 2007). The question of the continuity of the Dinantian limestone from the HH1 area to the vicinity of the seismogenic strand of the Newdigate fault zone has already been discussed. The uncertainty regarding the state of stress in the Weald Basin is considered in the online supplement. As will become clear below, if the differential

stress here is anything like as high as it is the Preese Hall area (after Westaway, 2017), then any fault with the orientation of that which slipped will be very close to the Coulomb failure condition.

To facilitate first-order calculations regarding the feasibility of this model, the model fault is made vertical and the permeable seismogenic layer is assumed to have thickness H, hydraulic diffusivity D, hydraulic conductivity K, permeability k, and porosity ϕ. Depressurization within the Portland reservoir adjoining one or other of the nearby wells is assumed to result in a constant reduction in groundwater pressure ΔP_O at each point on the fault within the permeable seismogenic layer. As a result, the drawdown δP in groundwater pressure within this permeable layer, at a horizontal position x from the model fault at time t after the start of the imposed pressure drawdown, is given by

$$\delta P \quad = \quad \Delta P_O \, \mathrm{erfc} \, (x / (2 \, \sqrt{(D \, t)})) \tag{1}$$

(e.g., Costain, 2017), where erfc() denotes the complementary Gaussian error function. For z>0, the function erfc(z) decreases as z increases, reaching ~0.0047 when z=2. As Detournay and Cheng (1993) noted, this condition can be taken as indicating an effective outer limit to significant pressure perturbations, at distance x_M from the model fault. It thus follows that

$$x_M \quad = \quad 4 \, \sqrt{(D \, t)} \, . \tag{2}$$

As time progresses, an ever-widening volume of rock, perpendicular to the model fault, will thus become depressurized, water previously stored within this volume being released into the fault.

Carbonate rocks such as these are likely to be complex, being fractured, so water storage within them will be in part by opening of fractures and in part by opening of pore space. The bulk hydraulic properties already defined, D, K, k and ϕ, characterise the rock volume without consideration of such detail. However, as is well known (e.g., Newson, 1973), Dinantian limestone typically has low matrix porosity, often ~1%, its ability to store and transmit groundwater being largely via fractures. The storage capacity of an aquifer can be quantified as its specific storage, S_S, defined as the volume of water released from a unit volume of the aquifer under a unit decline in hydraulic head. By definition, S_S is related to other hydraulic properties, thus:

$$S_S \quad \equiv \quad K / D \, . \tag{3}$$

K and k are interrelated thus:

$$K \quad \equiv \quad k \, \rho_w \, g / \eta \tag{4}$$

where ρ_w and η are the density and viscosity of water, and g is the acceleration due to gravity. Permeability k is a constant of proportionality in Darcy's equation, which can be written thus

$$v \quad = \quad \frac{k \, \Delta P}{\eta \, L} \, , \tag{5}$$

where v is the average flow velocity and ΔP is the pressure drop for flow over distance L.

Specific storage is also related to elastic moduli thus:

$$S_S \quad = \quad \rho_w \, g / B \tag{6}$$

where B is the effective bulk modulus of the material, defined thus:

B $\quad\equiv\quad$ $1 / ((1 / B_R + \phi / B_W)$, $\hspace{4cm}$ (7)

where B_R and B_W are the bulk moduli of the rock and water (e.g., Jacob, 1940; De Wiest, 1966). Bulk modulus is itself defined as

B $\quad\equiv\quad$ $-V\, \partial P/\partial V$, $\hspace{5cm}$ (8)

V denoting volume.

The poroelastic response of the rocks surrounding the model source of pressure variations in the Portland reservoir, to the imposed pressure variation, can now be investigated. In general, poroelastic responses can be complex (e.g., Detournay and Cheng, 1993). Costain (2017) applied the one-dimensional diffusion equation for the pressure of a fluid of constant density and viscosity through a medium of constant permeability,

$$\frac{\partial P}{\partial t} = D\, \frac{\partial^2 P}{\partial x^2} ,\hspace{4cm} (9)$$

where t is time and x is position. He thus obtained a solution for the one-dimensional propagation (in the x-direction) of a hydraulic pressure pulse of amplitude ΔP_P and duration Δt over distance r through rocks of hydraulic diffusivity D. He showed that at times $\gg \Delta t$ the pressure variation δP is given to a good approximation by

$$\delta P(r,t) = \frac{\Delta P_P\, D\, r\, \Delta t\, \exp(-r^2 /(4\, D\, t))}{2\, \sqrt{\pi}\, (D\, t)^{3/2}} .\hspace{3cm} (10)$$

The maximum pressure perturbation at distance r occurs after a time delay t_D given by

$$t_D = r^2 /(6\, D) .\hspace{4cm} (11)$$

It follows that the maximum pressure perturbation at distance r and time t_D is given by δP_M where

$$\delta P_M(r,t) = \frac{3\, \sqrt{6}\, \Delta P_P\, D\, \Delta t\, \exp(-3 / 2)}{\sqrt{\pi}\, r^2} .\hspace{3cm} (12)$$

The alternative empirical analysis by Hettema et al. (2002), based on 'rules of thumb' rather than derivation from first principles, predicts a value for t_D that differs only by a numerical factor but does not predict pressure perturbations.

Parameter values adopted for Dinantian limestone include B_R=50 GPa and ϕ=0.04, along with Young's modulus E_R=75 GPa and Poisson's ratio ν_R=0.25, from Bell (1981), with standard values of B_W=2.2 GPa, ρ_W=1000 kg m^{-3}, and g=9.81 m s^{-2}. With this set of values, B is ~27 GPa and S_S is ~3.6×10^{-7} m^{-1}. Bell (1981) noted a range of values of K for laboratory samples of Dinantian limestone, ranging from 0.07×10^{-9} m s^{-1} to 0.3×10^{-9} m s^{-1}. Lewis et al. (2006) reported much higher values ranging from ~10^{-6} m s^{-1} to ~10^{-2} m s^{-1} in karstified regions. Using the latter set of values, equation (3) gives values for D ranging upward from ~3 m^2 s^{-1}. For comparison, Shepley (2007) determined an upper bound to D for Dinantian limestone in the Peak District of central England by modelling the hydrology of Meerbrook Sough, a disused mine drainage adit that drains a ~40 km^2 area. His analysis reported an upper bound of 50,000 m^2 day^{-1} or ~0.6 m^2 s^{-1}. However, this analysis did not reproduce the observed magnitude of seasonal fluctuations in flow in parts of this subsurface catchment, favouring a higher value of D. Overall, it is inferred that that D ~1 m^2 s^{-1} is appropriate for karstified Dinantian limestone. For comparison, Hornbach et al. (2016) deduced that a poroelastic pressure pulse resulting from large-scale injection of waste water propagated for up to ~40 km through the Ellenburger Formation, a karstified limestone of Ordovician age, in ~6 years, resulting in earthquakes in the vicinity of Dallas,

Texas. Using equation (11) gives an upper bound to D for the Ellenburger Formation of ~1.4 m^2 s^{-1}, in reasonable agreement. Zhang et al. (2013) had previously reported a nominal value of 1 m^2 s^{-1} for this karstified Ordovician limestone.

Figure 7 here: Graphs of pressure variations

Figure 7(a) illustrates the pressure variations predicted over time, alongside the model seismogenic fault, assuming D=1 m^2 s^{-1}, with ΔP_0=-10 kPa. It indicates that any pressure reduction in this fault will cause significant pressure reductions on short timescales in the surrounding rocks, out to distances of many hundreds of metres.

Notwithstanding the complexity of poroelastic responses in general (e.g., Detournay and Cheng, 1993), the ultimate response following equilibration of pressure between pores and other spaces inside a rock volume is relatively straightforward, and can be expressed as simple proportionality between the change in internal pressure δP and the associated volumetric strain ε,

$$\varepsilon \quad = \quad -\delta P / B \quad , \tag{13}$$

B being, once again, the 'effective' bulk modulus of the rock (cf. equation (7)). A reduction in internal pressure, as anticipated for the seismogenic fault, will lead to compaction. As the outer ends, away from the fault, of the blocks alongside the fault are 'pinned', compaction will cause their inner ends, facing each other across the fault, to separate slightly, by distance Δx, as depicted schematically in Fig. 5(b).

Since volumetric strain is being assumed, the strain in the x-direction, ε_{xx}, will be $\varepsilon/3$. The quantity Δx defined above can thus be estimated as

$$\Delta x \quad = \quad 2 \int_{x=0}^{x\to\infty} \varepsilon_{xx}\, dx\,, \tag{14}$$

the factor of 2 taking into account that the rocks on both sides of the fault will move away from it. Likewise, the volume ΔV of water released as a result of this compaction can be estimated as

$$\Delta V \quad = \quad 2\,H\,L \int_{x=0}^{x\to\infty} \varepsilon_{xx}\, dx\,, \tag{15}$$

where H is the thickness of the Dinantian Limestone and L is the along-strike length of the seismogenic fault.

To evaluate these quantities one needs the integral of erfc(). From Abramowicz and Stegun (1972, p. 299) and Weisstein (2019),

$$E(x) \quad \equiv \quad \int_{z=0}^{z=x} \mathrm{erfc}(z)\, dz \quad = \quad x\,\mathrm{erfc}(x) \quad + \quad \frac{(1 - \exp(-x^2))}{\sqrt{\pi}} \tag{16}$$

so

$$E(\infty) \quad \equiv \quad \int_{z=0}^{z\to\infty} \mathrm{erfc}(z)\, dz \quad = \quad \frac{1}{\sqrt{\pi}} \tag{17}$$

Using equation (17), one obtains

$$\Delta x \quad = \quad \frac{-4\,\Delta P_0}{3\,B}\,\sqrt{\left(\frac{D\,t}{\pi}\right)}\,, \tag{18}$$

and

12

$$\Delta V \quad = \quad \frac{-4\,H\,L\,\Delta P_O}{B}\,\sqrt{\left(\frac{D\,t}{\pi}\right)} . \qquad\qquad (19)$$

Taking $D=1\ m^2\,s^{-1}$, $t=1\ yr$, $H=60\ m$, $L=1000\ m$, $\Delta P_O=-10\ kPa$, and $B=27\ GPa$, one obtains $\Delta x=\sim 1.6\ mm$ and $\Delta V=\sim 280\ m^3$. For comparison, for an impermeable rock representing basement, with $D=0.002\ m^2\,s^{-1}$ (after Zhang et al., 2013) and $B=50\ GPa$, one obtains $\Delta x=\sim 0.04\ mm$ and $\Delta V=\sim 7\ m^3$, reflecting the much smaller values of x_M (Fig. 7(b)). The probability of the latter adjustment resulting in separation of asperities (cf. Fig. 5(b)) is much less.

Coulomb failure analysis

The tendency for coseismic slip on the seismogenic fault can be analysed using the standard Coulomb approach. The Coulomb failure parameter Φ:

$$\Phi \quad = \quad \tau - c\,(\sigma_N - P_f) , \qquad\qquad (20)$$

will thus be evaluated where σ_N, τ and c are the resolved normal stress, shear stress and coefficient of friction on the fault plane, and P_f is the fluid pressure in the fault. $\Phi=0$ marks this condition, with $\Phi<0$ indicating frictional stability under the current state of stress. In general, this condition for shear failure can also be visualized graphically using the standard Mohr circle construction, as a graph of τ against effective normal stress σ_N', defined as $\sigma_N - P_f$ (see below).

Treating the seismogenic fault as having uniform properties throughout its length, the reduction in P_f by ΔP_o will, on its own, act to make the fault more stable. This change in fluid pressure will have no direct effect on τ. The associated reduction in normal stress σ_N can be estimated as $B\times\varepsilon_{xx}$, so will have an effect on Φ that is smaller in magnitude than the direct effect of the decrease in P_f. Overall these considerations lead to the conclusion that a reduction in fluid pressure in a fault will 'clamp' the fault, increasing its stability. This is in accordance with the widespread observation that increases in P_f can 'unclamp' or destabilize faults, this being the accepted mechanism for the widespread occurrence in recent years of seismicity caused by fluid injection (e.g., Ellsworth, 2013; Keranen et al., 2014; Walsh and Zoback, 2015; Weingarten et al., 2015). On this basis, one might conclude that a decrease in the groundwater pressure within the seismogenic fault cannot be the cause of the Newdigate seismicity.

However, it is generally accepted that the mechanics of faults, notably whether they are stable or can slip seismically, are determined by the properties of strong patches – asperities – where the opposite surfaces of the fault are in frictional contact (e.g., Reiter, 1999). A fault surface consisting, on a microstructural scale, of a fractal size distribution of asperities with a small proportion of the fault surface in contact, in proportion to the normal stress applied to the fault, can mimic the effect, on a macroscopic scale, of a constant coefficient of friction (e.g., Archard, 1957; Mitchell et al., 2012). Brown and Scholz (1985) showed that natural rock surfaces follow fractal scaling for surface features of height up to $\sim 0.1\ m$. Laboratory simulations of faulting often include asperities on a microstructural scale, occupying only a small proportion of the overall area of a fault (e.g., Harbord et al., 2017; Selvadurai and Glaser, 2017). Most recently, the view has gained ground that the physics of co-seismic faulting is likewise governed by processes on a microstructural scale (e.g., Acosta et al., 2017; McDermott et al., 2017). For example, McDermott et al. (2017) deduced that asperities can be patches of fault with areas of no more than a few square metres, their properties being determined by mineral grains with dimensions of microns. Because these strong patches with fault surfaces in contact occupy only a small proportion of a fault surface, they act as stress concentrations. For example, in the laboratory experiments by Selvadurai and Glaser (2017), millimetre-sized asperities with micron-sized heights occupy a very small proportion of the fault area; in one experimental run, a decrease in the mean normal stress across the fault area by $\sim 0.3\ MPa$ caused decreases in the normal stress affecting individual asperities by $\sim 10\ MPa$.

Figure 5(b) illustrates how a small increase in separation of fault surfaces, Δx, can destabilize a fault through its effect on the extent of contact between asperities. Moving from configuration (i) to configuration (ii), two of the three asperities depicted will no longer contribute to fault stability. The third one will experience a significantly reduced normal stress, as a result of the increased separation of the fault surfaces. This will reduce the maximum shear stress that this asperity can sustain, in accordance with equation (20), whereas the shear stress that it is required to sustain to keep the fault stable will increase because the other asperities no longer contribute. Overall, it can thus be seen how a small increase in separation of fault surfaces might bring a fault significantly closer to the condition for slip, and might indeed result in coseismic slip.

Figure 8 here: Mohr circle diagrams

The geomechanical consequences of this model can now be illustrated using the standard Mohr circle construction (Fig. 8). In the absence of more definitive data (see the online supplement), a model stress field is adopted (based on analysis of the Preese Hall case study) at 2400 m depth from Westaway (2017) with σ_H=63.3 MPa, σ_V=54.3 MPa, and σ_h=39.2 MPa, with hydrostatic groundwater pressure P_f=23.5 MPa. A typical orientation is adopted for a patch of the seismogenic fault of strike 270°, dip 80° and rake 170° (cf. Table 3). Analyzing these values using the same software as was used for the Westaway (2017) analysis of Preese Hall (and for analysis of the Pohang case study by Westaway and Burnside, 2019), the optimum azimuth of the maximum principal stress is determined as 300° (or N60°W-S60°E), which predicts a rake of 150°. This differs from the observed rake of 170°, indicating that the assumed model stress field is not quite right for the present study area. This mismatch could be reconciled by adjustments to the magnitudes of the principal stresses or by incorporating inclined principal stresses, but in the interests of brevity such refinements are omitted here. Subject to this proviso, Fig. 8(a) indicates that the model stress field indicates Φ ~-2 MPa relative to a standard frictional failure threshold with c=0.6, the model normal and shear stresses across the fault being 21.4 and 10.6 MPa. The depicted state of stress on the seismogenic fault represents the average conditions across the fault; in reality, stability of this fault was maintained at asperities, probably occupying a small proportion of the fault area, at which the normal and shear stresses were much higher than the depicted average values.

In contrast, Figure 8(b) sets out to represent the conditions at the point of coseismic slip. It takes into account the inferred 10 kPa reduction in fluid pressure in the fault. It represents the effect of compaction of the Dinantian limestone reducing the number of asperities in contact and thus affecting the normal and shear stresses on the remaining asperities. Thus, the model σ_H has been increased by ~1.8 MPa and the model σ_h has been decreased by ~2.4 MPa, causing an increase in the model shear stress across the fault to 12.2 MPa and decreasing the model normal stress across it to ~20.3 MPa and bringing the model fault to the Coulomb condition for slip. Following the reasoning of Mitchell et al. (2013), this ~4% reduction in normal stress is interpreted as a consequence of a ~4% reduction in the proportion of the fault surface that is in frictional contact, as a result of the compaction of the adjoining rocks caused by their loss of fluid pressure.

Discussion

The proposed mechanism for the Newdigate seismicity depends on a pressure drop within the Dinantian limestone alongside the seismogenic strand of the Newdigate fault zone, as a result of depressurization of the groundwater within this fault. A simple approach to mitigation, albeit at considerable cost, would be to provide an injection well in or near this fault to replace the lost groundwater and thereby balance the groundwater pressure in and around the fault. It follows from the present analysis that if the approved plans for more wells at Horse Hill proceed, with much higher

production rates than for HH1, the pressure drawdown in the seismogenic fault will increase and – in the absence of the aforementioned mitigation - seismicity might recur.

In principle, testing of the proposed mechanism is possible, since the inferred volumetric strain implies vertical as well as horizontal compaction. Hicks et al. (2019) considered this aspect, concluding on the basis of other cases studies known to them that there was no precedent for strike-slip earthquakes to be caused by compaction. There is, however, no geomechanical reason why compaction cannot cause strike-slip earthquakes, if the compaction occurs in a region such as the Weald Basin where the stress field favours this mechanism. The predicted vertical compaction will result in subsidence of the Earth's surface, and so is in principle observable; its magnitude can be calculated as an integration similar to that for equation (14); for the parameter values already discussed, including the estimated ~60 m thickness of the Dinantian limestone, it will be a small fraction of 1 mm. Multiple techniques, including interferometric synthetic-aperture radar (InSAR) and repeated gravity and GPS measurements, can in principle measure vertical crustal motions such as this. A combined dataset of this type has been analysed for a region of southeast England, including the northern Weald Basin, by Aldiss et al. (2014). At the October 2018 workshop attention was also drawn to an InSAR-derived surface deformation map of Britain by GVL (2018), spanning October 2015 to October 2017. The Aldiss et al. (2014) analysis revealed vertical crustal motions at ~1 mm a^{-1}, caused by processes such as extraction of groundwater (or replenishment of groundwater reservoirs previously depleted by extraction). Such rates make it impossible to resolve the much smaller changes expected from compaction of the Dinantian limestone at Newdigate.

Much has been made by participants in the OGA (2018) workshop regarding the extent to which the Newdigate earthquake 'swarm' might fit the standard criteria identified by Davis and Frohlich (1993) for establishing whether instances of seismicity are anthropogenic (e.g., Baptie and Luckett, 2018). UKOG (2019a) have argued that this set of criteria is inapplicable as they relate to seismicity caused by fluid injection, which is not the causal mechanism in this case. However, familiarity with the literature in this field (e.g., Foulger et al., 2018) indicates that these criteria are widely used irrespective of the geomechanical cause of any particular anthropogenic earthquake. Verdon et al. (2019) proposed a different approach to assessing anthropogenic seismicity. This approach appears problematic, since it replaces the objective (yes / no) criteria recommended by Davis and Frohlich (1993) with subjective numerical scores. The development of a conceptual geomechanical model for the Newdigate earthquakes supersedes the other Davis and Frohlich (1993) criteria; nonetheless, an appraisal of this seismicity in terms of these criteria is included in the online supplement.

While preparation of this text was under way, it was announced in December 2019 that well HH2Z was experiencing significant water ingress, at rates approaching 1 l s^{-1}, from a fracture near the 'toe' of its horizontal section (UKOG, 2019c); during early 2020 this well toe was plugged to stop this ingress (UKOG, 2020a, 2020b). This instance indicates significant fracture permeability, as is required by the proposed conceptual model (Fig. 5).

Furthermore, also while text preparation was under way, OGA (2019) released details of the largest earthquake caused by 'fracking' of well Preston New Road-2 near Blackpool in northwest England. This event, of M$_L$ 2.9, occurred at 07:30 on 26 August 2019 at a depth reported by BGS as 2.5 km; the resulting peak ground velocity of 8 mm s^{-1} is broadly consistent with what is inferred for the largest Newdigate events in the present study (see the online supplement). This M$_L$ 2.9 event resulted, on 1 November 2019, in the imposition by the UK government of a moratorium on 'fracking' in England, superseding the previous regulation that earthquakes of M$_L$<0.5 were 'allowed'. This has created a strange regulatory situation where 'fracking' is forbidden on the basis of seismicity but there is no regulatory limit for seismicity caused by other technologies (such as conventional hydrocarbon production or, indeed, development of geothermal energy projects). It is suggested that a consistent

approach is needed, maybe based on the established procedure for regulating other forms of industrial nuisance vibration (cf., Westaway and Younger, 2014).

The remainder of this discussion will concentrate on geomechanical issues. Following each of the Newdigate earthquakes, the spatially averaged shear stress on the patch of fault that slipped will reduce by a value equal to the coseismic stress drop $\Delta\sigma$, moving the state of stress away from the Coulomb failure condition. However, if groundwater withdrawal from the Dinantian limestone continues, the possibility exists that the fault will ultimately adjust once again towards the failure condition by repetition of the same physical mechanism. Ultimately, maybe after multiple earthquake cycles, one can envisage so much previously stored elastic strain energy being released from the vicinity of the seismogenic fault that the activity eventually dies out. This mechanism might thus explain the decline in earthquake activity in the latter part of 2019 (Table 4), even though oil production has continued (and, indeed, its rate increased following the completion of well HH2Z). It is thus of interest to consider whether the existing dataset provides evidence for repeated slip on the same patches of fault; this aspect is now considered.

To investigate the area of the patch of fault that slipped in each earthquake, seismic moment M_O is first determined from magnitude M_W using the standard formula

$$\log_{10}(M_o / N\,m) = 9.05 + 1.5\,M_W \qquad (21)$$

(Hanks and Kanamori, 1979). For most of the Newdigate earthquakes, M_W values are unavailable from the Hicks et al. (2019) dataset; M_L is used as a proxy for M_W. Next, the radius a of the equivalent circular seismic source is determined from M_o, assuming a nominal value of the coseismic stress drop $\delta\sigma$:

$$M_o = \frac{16\,\delta\sigma\,(1-\nu)\,a^3}{3\,(2-\nu)} \qquad (22)$$

(e.g., Westaway and Younger, 2014), where ν is Poisson's ratio for the adjoining rock volume. The source area A is then determined as πa^2 and the mean slip u as $M_o / (\mu A)$. The value of μ comes from the standard formula $\mu \equiv 3\,B\,(1-2\nu) / (2(1-\nu))$. For Dinantian limestone ν ranges between 0.19 and 0.31 (Bell, 1981) so 0.25 is adopted, for which $\mu \equiv B$; as before B=50 GPa, from Bell (1981).

This task was carried out for the complete Hicks et al. (2019) earthquake dataset, plus the additional events listed in Table 4. The cumulative seismic moment thus obtained was ~1.5×10^{14} N m, equivalent to a single earthquake of M_W ~3.4. Assuming $\delta\sigma$=10 MPa, a plausible upper bound, the cumulative area of fault rupture is estimated as ~2.1×10^5 m^2 and the mean coseismic slip in the largest earthquake as ~2.2 cm. Taking 2 km as an upper bound to the length of the seismogenic zone, from Fig. 1, and 60 m as the thickness of the Dinantian limestone, the area of fault in this lithology is ~1.2×10^5 m^2. Calculated on this basis, the total area of coseismic ruptures exceeds the area of the fault, and would be even greater if a lower value of $\delta\sigma$ were to be assumed. Thus, either patches of fault slipped more than once, or that the seismicity propagated into the overlying and/or underlying lithologies, although the 'cloud' of hypocentres located by Hicks et al. (2019) indicates no clear propagation in any direction. The calculations also indicate that the eight largest earthquakes have source diameters larger than the estimated 60 m thickness of the limestone; evidently, these events either ruptured outside this layer or ruptured patches of fault that are elongated horizontally. Assuming the latter explanation, and that the overall population of earthquakes was distributed to produce a constant overall amount of coseismic slip across the fault, this amount is determined as ~2.5 cm, roughly as estimated for the largest individual earthquake. It is thus possible that the earthquake swarm was indeed 'self-limiting', and that once the full extent of the seismogenic fault had slipped by this distance, the fault was effectively 'de-stressed' and the activity died out, consistent with its observed cessation in late 2019 (Table 4). Further analysis of this aspect is evidently warranted, given the possibility that seismicity

might resume, as a result of pressure changes arising from the planned increase in production at the Horse Hill site.

As already noted, the proposed physical mechanism, whereby a decrease in the fluid pressure within a fault can destabilize the fault, is the opposite of what might be termed the 'usual' effect, the unclamping that will occur when the fluid pressure within a fault increases and causes the effective normal stress to reduce. The present analysis depends on the poroelastic compaction effect that will also occur within the rocks adjoining the fault, which is shown to be capable of causing separation of the fault surfaces by a distance of the order of 1 mm in the highly permeable Dinantian limestone, plus the inference that the characteristic height of asperities on fault surfaces in this lithology is less than this increase in separation, so the state of stress on these asperities is significantly affected. It is suggested that in these unusual circumstances, where a permeable fault occurs in permeable rocks, this poroelastic effect can outweigh the 'usual' effect whereby a decrease in fluid pressure would lead to increased fault stability.

Although fluid injection is nowadays recognized as a widespread cause of induced seismicity, it is worth noting that reductions in fluid pressure caused by fluid extraction has been linked to seismicity for far longer. The first instance recognized is by Pratt and Johnson (1926), for earthquakes accompanying oil production near Houston, Texas. Other case studies subsequently recognized include those by Calloi et al. (1956), Kovach (1974), Rothé and Lui (1983), Simpson and Leith (1985), Pennington et al. (1986), Wetmiller (1986), Grasso and Wittlinger (1990), Doser et al. (1991), Ottemöller et al. (2005), Dahm et al. (2015), and Hornbach et al. (2015), whereas works discussing physical mechanisms for such seismicity include those by Yerkes and Castle (1976), Simpson et al. (1988), Segall (1989), and Segall and Fitzgerald (1998). Hornbach et al. (2015) indeed considered a complex case study, at Azle near Fort Worth, Texas, where earthquake activity began in 2013 in a locality that had experienced both injection (of industrial wastewater) and production (of brine, oil and natural gas). The injection was initially suspected as the cause, on account of its very large volume, but the Hornbach et al. (2015) analysis indicates the pressure reduction caused by oil and gas production as the most important individual factor. Some of the above works (e.g., Pennington et al., 1986) have recognized the significance of processes required in the present conceptual model (e.g., compaction of limestone and failure of asperities), and others (e.g., Holland, 2013; Schultz et al., 2015; Igonin et al., 2019) have recognized that highly permeable connections can cause seismicity at significant distance from the source of the causative change in fluid pressure. However, no previous case study known to the present author has proposed a geometry between the source of depressurization and the seismogenic fault that resembles this conceptual model (Fig. 5).

The 'usual' effect of an increase in fluid pressure causing fault unclamping is to be expected if the fault is in impermeable rocks, where the fluid pressure only acts within the fault and not within the adjoining rock volume (e.g., Hackston and Rutter, 2016; Westaway, 2017). If the rock volume has zero permeability there will be no poroelastic effect. If it has very low permeability, increased pressure in an adjoining fault will increase the fluid pressure in it, which will dilate the volume and, on a microstructural scale, increase the contact area of asperities, partly cancelling the direct effect of the pressure increase. Conversely, if the rock volume has high permeability, increased pressure in an adjoining fault might cause sufficient poroelastic dilatation of the rock volume and so increase the contact area of asperities, such that, overall, the fault experiences net clamping. In general, for faults within permeable rocks, one can expect these two effects to counteract each other; whether the microscopic effect of asperities will predominate or not will depend on the conditions in each case. In this context, it is noteworthy that much of the seismicity associated with fluid injection in the USA occurs as a result of pressure increases in faults in impermeable basement rocks, rather than in the permeable rocks into which the injection takes place, an example being the case study documented by Hornbach et al (2015) (see also, e.g., Kim et al., 2013, and Zhang et al., 2013). In other instances,

for example that discussed by Justinic et al. (2013), authors have emphasised the proximity of hypocentres to injection points to highlight the possibility of a human cause, when many hypocentres are in fact rather deeper and indicate earthquakes within the underlying impermeable basement. Hincks et al. (2018) have noted that fluid injection into faults or fractures in basement or near the contact with basement at the base of permeable sediments is statistically much more likely to result in seismicity than injection well above basement. Consideration of poroelasticity provides an explanation for this empirical observation.

It has been argued (OGA, 2018) that the Brockham and Horse Hill wells are not hydraulically connected as pressure variations imposed in one are not seen in the other. However, due to the separation of these wells (~8 km; Fig. 1) and the finite hydraulic diffusivity of the intervening rocks, one would not expect instantaneous correlation. Given equation (11), with R=8 km, the approximate distance from well BRX2Y to the Newdigate seismicity cluster, $D=1$ m^2 s^{-1} would make t_D ~4 months; $D=20$ m^2 s^{-1} would make t_D ~6 days. With R=4 km, the approximate distance from HH1, $D=1$ m^2 s^{-1} would make t_D ~1 month; $D=20$ m^2 s^{-1} would make t_D ~1.5 days. Given these distances, the observed time lags between the starts of production and starts of seismicity of 9 days for well BRX2Y and 3 days for well HH1 indicate $D=14$ m^2 s^{-1} and $D=10$ m^2 s^{-1}, respectively. No study, known to the present author, has looked for any correlation of the seismicity with the sequence of activities (and associated pressure variations) at either well assuming these or any other duration of time lag. The pressure data that might demonstrate or refute any such correlation are not in the public domain.

In the absence of more detailed information, it is assumed (to calculate an upper bound to the pressure reduction) that the initial ~4 m^3 of oil obtained from well BRX2Y in March 2018 was produced from the wellbore, with no flow from the reservoir, possibly because of previous development of water coning around the production interval. Assuming well casing with an 8.625 inch external diameter and a 7.435 inch or 188.85 mm internal diameter, a standard size, ~4 m^3 of production would reduce the oil level within the well by ~140 m and thus reduce the pressure at the base of this oil column by ~1 MPa. The average pressure reduction ΔP_P during this production would thus be ~0.5 MPa. On the following day, the well was shut in, then on 25 March water injection (into well BRX3) was started, which led to some additional production (Hicks et al., 2019; Fig. 1). Taking Δt for the pressure transient as 8 hours (a working shift at the well site), and ΔP_P=0.5 MPa, with r=8 km and $D=14$ m^2 s^{-1}, equation (12) gives $\delta P_M \cong 3$ kPa. On reaching the patch of the seismogenic fault within the Dinantian limestone, such a pressure perturbation would act to unclamp the fault, in accordance with earlier discussion, potentially accounting for the start of the seismicity on 1 April 2018.

Clearly this is a very crude calculation: it does not incorporate the 2-D geometrical spreading that would be expected for a pressure transient within the calcite 'beef' fabric in the Portland sandstone, which would reduce the pressure perturbation at a given distance. On the other hand, it could be argued from the record of activity at Brockham (see online supplement) that the assumed duration of this transient should exceed ~8 hours, which would increase the predicted value of δP_M. It is suggested that subsequent production from the Portland sandstone at both BRX2Y and HH1 will cause additional pressure perturbations within the seismogenic fault, causing later seismicity, but their effect is not amenable to analytic calculations and will require numerical modelling. Once BRX2Y production ended, the good correlation between seismicity and production from the Portland reservoir at HH1 (Fig. 4(c)) supports the proposed explanation and is consistent with t_D being quite short, implying a high value of D and supporting the inference that this is based on the high permeability and hydraulic conductivity of calcite 'beef'. The net result of these pressure perturbations will be flow transients from the seismogenic fault towards the wells, superimposed on the pre-existing flow towards well BRX2Y, already discussed. It is suggested that these flow transients will be maintained by outflow of groundwater from, and compaction of, Dinantian limestone adjoining this fault.

A permeability of ~1 D in calcite 'beef' would correspond, given equation (4), for water with a viscosity of ~0.9 mPa s (appropriate for ~25 °C, as expected locally at ~600 m depth; e.g., Busby et al., 2011) to K ~1.1×10^{-5} m s^{-1}. From equation (3), with specific storage S$_S$ ~10^{-6} m^{-1}, a hydraulic diffusivity of ~11 m^2 s^{-1} can be determined, roughly as required for the proposed conceptual model to be feasible. Furthermore, the analysis has indicated estimated production of ~300 m^3 of water from the Dinantian limestone into the seismogenic fault during the course of a year, as a result of ~4700 m^3 of production from the Portland reservoir at HH1. Evidently, most of the groundwater flow to balance this production came from elsewhere. The associated time-averaged volume flow rate is thus ~10^{-5} m^3 s^{-1} or ~0.01 l s^{-1}. If sustained across a width of ~1 km (the along-strike length, estimated earlier, of the seismogenic fault) in a ~5 m thick layer of calcite 'beef', this would indicate a mean flow velocity of ~2×10^{-9} m s^{-1}. From equation (5) this would indicate a flow-parallel pressure gradient of ~2 Pa m^{-1}, which would require a pressure drop of ~8 kPa over ~4 km distance. To sustain this pressure drop plus the estimated 10 kPa pressure drop within the Dinantian limestone requires a time-averaged pressure decrease in the Portland reservoir at Horse Hill of at least ~18 kPa, a small proportion of the maximum pressure drop that has been reported. Modest pressure changes of this order, which might well be expected as a result of oil production, demonstrate the feasibility, in principle, of the proposed geomechanical model. Notwithstanding the repetition, it is noted again that availability of pressure data would facilitate testing of this model.

Conclusions

The seismicity at Newdigate, Surrey, during 2018-2019, has been reassessed, amending aspects where the Hicks et al. (2019) analysis has proved inaccurate. First-order correction for the seismic velocity model that they used for earthquake location, which was too slow for the local stratigraphy, adjusts the hypocentres ~400 m deeper than previously thought, to depths of ~2400 m, placing them within the Palaeozoic 'basement' beneath the Weald Basin rather than within its Jurassic sedimentary sequence. These earthquakes involved mainly right-lateral slip on a steeply north dipping fault, part of the Newdigate fault zone (Fig. 2).

Oil was produced during 2018-2019 in this vicinity from two wells in the Upper Portland Sandstone reservoir, Brockham-X2Y and Horse Hill-1. Previous workers, including Hicks et al. (2019), have dismissed the possibility that activity affecting these wells has caused the Newdigate seismicity. However, the correlation between phases of production from this reservoir and 'clusters' of earthquake activity (Fig. 4) is compelling, and warrants consideration of potential geomechanical mechanisms. A conceptual model that can account for this cause an effect connection is indicated schematically in Fig. 5. It is thus suggested that the seismicity occurred within a thin (estimated ~60 m thick) layer of permeable Dinantian limestone, which is hydraulically connected to the Portland reservoir via permeable strands of the Newdigate fault zone and by the highly permeable calcite 'beef' fabric within the Portland sandstone. It is hypothesized that past oil production at Brockham depressurized the Portland reservoir around this well and drew groundwater from the Dinantian limestone, causing it to compact and 'unclamp' the seismogenic fault but not sufficiently to reach the Coulomb failure criterion to initiate seismicity. The resumption of production at Brockham in March 2018 caused a negative pressure pulse to propagate through the hydraulic connection to the Dinantian limestone, which reached the failure threshold, initiating the first 'cluster' of Newdigate seismicity in April 2018. Likewise, a negative pressure pulse following resumption of production from the Portland reservoir at Horse Hill in February 2019 initiated a subsequent 'cluster' of seismicity. This mechanism requires hydraulic diffusivity ~10 m^2 s^{-1} in the calcite 'beef' and ~1 m^2 s^{-1} in the Dinantian limestone. At other times, the complexity of production patterns (from both BRX2Y and HH1 in summer 2018 and multiple suspensions of production from HH1 during 2019) and the absence of pressure data prevent any detailed conclusions being drawn, although the general correlation of seismicity with production from the Portland reservoir (Fig. 4) is compelling. The proposed 'unclamping' effect requires consideration of the fractal nature of asperities on the seismogenic fault and their response to

compaction of the adjoining limestone. Such behaviour, previously unrecognized in studies of seismicity caused by fluid extraction, is particularly significant in this instance because of the high permeability of the Dinantian limestone; in impermeable rocks a reduction in pore pressure would cause fault clamping rather than unclamping. In principle this model is testable, but required data, notably the history of pressure variations in the oil wells, is not currently in the public domain.

The recognition that this instance of seismicity is arguably caused by human activity, and the role of highly permeable hydraulic connections extending for many kilometres, has significant implications for regulation to mitigate the potential nuisance from future seismicity caused by oil production in the Weald Basin, and may well also help to inform the understanding of anthropogenic seismicity in other settings. The initial response to the Newdigate seismicity, which included claims that any connection with oil production was implausible before any geomechanical analysis had been done, was inappropriate.

Acknowledgements

References – for both manuscript and supplement (will be rationalized later)

Abramowitz, M., Stegun, I.A., 1972. Handbook of Mathematical Functions with Formulas, Graphs, and Mathematical Tables, 10th ed. Dover, New York, 1040 pp.

Acosta, M., Passelègue, F.X., Schubnel, A., Violay, M., 2018. Dynamic weakening during earthquakes controlled by fluid thermodynamics. Nature Communications, 9, 3074, 9 pp., doi: 10.1038/s41467-018-05603-9

Agosta, F., Prasad, M., Aydin, A., 2007. Physical properties of carbonate fault rocks, Fucino Basin (central Italy): implications for fault seal in platform carbonates. Geofluids, 7, 19–32.

Aldiss, D., Burke, H., Chacksfield, B., Bingley, R., Teferle, N., Williams, S., Blackman, D., Burren, R., Press, N., 2014. Geological interpretation of current subsidence and uplift in the London area, UK, as shown by high precision satellite-based surveying. Proceedings of the Geologists' Association, 125, 1–13.

Al Duhailan, M.A., Sonnenberg, S.A., 2014. The curious case of hydrocarbon-expulsion fractures: Genesis and impact on the Bakken Shales. Search and Discovery, 80398, 30 pp.

Al Duhailan, M.A., Sonnenberg, S.A., Longman, M., 2015. Analyzing beef fractures: Genesis and relationship with organic-rich shale facies. SPE Unconventional Resources Technology Conference, 20-22 July 2015, San Antonio, Texas, paper URTEC-2151959-MS, doi: 10.15530/URTEC-2015-2151959

Allen, D.J., Brewerton, L.J., Coleby, L.M., Gibbs, B.R., Lewis, M.A., MacDonald, A.M., Wagstaff, S.J., Williams, A.T., 1997. The physical properties of major aquifers in England and Wales. British Geological Survey Technical Report WD/97/34, 312 pp. Environment Agency R&D Publication 8. http://nora.nerc.ac.uk/id/eprint/13137/1/WD97034.pdf

Andrews, I.J., 2014. The Jurassic shales of the Weald Basin: geology and shale oil and shale gas resource estimation. British Geological Survey for Department of Energy and Climate Change, London, UK, 79 pp.

Angus Energy, 2018a. OGA – Surrey earthquakes. https://www.ogauthority.co.uk/media/5160/7c-angus-maps-for-oga-meeting.pdf

Angus, 2018. Brockham Portland & Kimmeridge Reservoirs. Addendum to the Field Development Plan. Angus Energy, Plc., London, 32 pp. https://www.whatdotheyknow.com/request/523935/response/1277768/attach/4/brockfdpadd%20Redacted.pdf?cookie_passthrough=1 (partly redacted version released under a Freedom of Information request)

Archard, J.F., 1957. Elastic deformation and the laws of friction. Proceedings of the Royal Society of London, Series A, Mathematical and Physical Sciences, 243, 190–205.

Baptie, B., 2006. UK Earthquake Monitoring 2005/2006. British Geological Survey, Nottingham. http://www.earthquakes.bgs.ac.uk/publications/annual_reports/2006_17th_annual_report.pdf

Baptie, B., Luckett, R., 2018. The Newdigate earthquake sequence, 2018. British Geological Survey Internal Report OR/18/059, 20 pp. https://earthquakes.bgs.ac.uk/research/NewdigateEarthquakesReport.pdf

Barton, C.A., Zoback, M.D., Moos, D., 1995. Fluid flow along potentially active faults in crystalline rock. Geology, 23, 683–686.

Bayerly, M., Brooks, M., 1980. A seismic study of deep structure in South Wales using quarry blasts. Geophys. J. R. astr. Soc. 60, 1-19.

BBC, 2018. Seventh tremor strikes in Surrey 'quake swarm'. British Broadcasting Corporation, London. https://www.bbc.co.uk/news/uk-england-44727326

BBC, 2019a. 'Surrey swarm' quakes 'not caused by oil extraction'. British Broadcasting Corporation, London. https://www.bbc.co.uk/news/uk-england-surrey-49480365

BBC, 2019b. Horse Hill: Oil drilling to expand in Surrey countryside. British Broadcasting Corporation, London. https://www.bbc.co.uk/news/uk-england-surrey-49665269

Bell, F.G., 1981. A survey of the physical properties of some carbonate rocks. Bulletin of the International Association of Engineering Geology, 24, 105–110.

Bense, V.F., Gleeson, T., Loveless, S.E., Bour, O., Scibek, J., 2013. Fault zone hydrogeology. Earth-Science Reviews, 127, 171–192.

Bisdom, K., Baud, E., Estrada, S., Sanz-Perl, Y., Gauthier, B., Bertotti, G., 2016. Coupled stress-fluid pressure modelling of stimulated rock volume in shale - impact of natural fractures and beef. 78th EAGE Conference and Exhibition, Vienna, Austria, 30 May - 2 June 2016. doi: 10.3997/2214-4609.201601164

Blake, D., Mlisa, A., Hartnady, C., 2010. Large scale quantification of aquifer storage and volumes from the Peninsula and Skurweberg Formations in the southwestern Cape. Water SA, 36 (2), 177-184.

Bommer, J.J., Dost, B., Edwards, B., Kruiver, P.P., Ntinalexis, M., Rodriguez-Marek, A., Stafford, P.J., van Elk, J., 2017a. Developing a model for the prediction of ground motions due to earthquakes in the Groningen gas field. Netherlands Journal of Geosciences, 96 (5), S203–S213.

Bommer, J.J., Stafford, P.J., Edwards, B., Dost, B., van Dedem, E., Rodriguez-Marek, A., Kruiver, P., van Elk, J., Doornhof, D., Ntinalexis, M., 2017b. Framework for a ground-motion model for induced seismic hazard and risk analysis in the Groningen gas field, the Netherlands. Earthquake Spectra 33, 2, doi: 10.1193/082916EQS138M.

Bommer, J.J., Stafford, P.J., Ntinalexis, M., 2017c. Empirical Ground-Motion Prediction Equations for Peak Ground Velocity from Small-Magnitude Earthquakes in the Groningen Field Using Multiple Definitions of the Horizontal Component of Motion. Updated Model for Application to Smaller Earthquakes. Nederlandse Aardolie Maatschappij BV, Assen, The Netherlands, 23 pp. https://nam-feitenencijfers.data-app.nl/download/rapport/62551a04-c1c3-4712-86e8-6c625ab5ee4c?open=true

Bond, C.E., Gibbs, A., Shipton, Z.K., Jones, S., 2007. What do you think this is? "Conceptual uncertainty" in geoscience interpretation. GSA Today, 17 (11), 4–10.

Brown, S.R., Scholz, C.H., 1985. Broad bandwidth study of the topography of natural rock surfaces. Journal of Geophysical Research, 90, 12,575-12,582.

Buckland, W., De la Beche, H.T., 1835. On the geology of the neighbourhood of Weymouth and the adjacent parts of the coast of Dorset. Transactions of the Geological Society, London, Series 2, 4, 1-46.

Busby, J., Kingdon, A., Williams, J., 2011. The measured shallow temperature field in Britain. Quarterly Journal of Engineering Geology and Hydrogeology, 44, 373–387.

Busby, J.P., Smith, N.J.P., 2001. The nature of the Variscan basement in southeast England: evidence from integrated potential field modelling. Geological Magazine, 138, 669–685.

Butler, M., Pullan, C.P., 1990. Tertiary structures and hydrocarbon entrapment in the Weald Basin of southern England. In: Hardman, R.F.P., Brooks, J. (eds), Tectonic Events Responsible for Britain's Oil and Gas Reserves. Geological Society, London, Special Publications, 55, 371-391.

Caine, J.S., Evans, J.P., Forster, C.B., 1996. Fault zone architecture and permeability structure. Geology, 24, 1025-1028.

Calloi, P., DePanfilis, M., DeFilippo, D., Marcelli, L., Spadea, M.C., 1956. Terrimoti della Val Padana del 15-16 Maggio 1951. Annali di Geofisica, 9, 63-105 (with summary in English).

Carey, J.W., Lei Zhou, Rougier, E., Mori, H., Viswanathan, H., 2015. Fracture-permeability behavior of shale. Journal of Unconventional Oil and Gas Resources, 11, 27-43.

Cavanagh, A., Gilfillan, S., Haszeldine, S., 2019. Further potential for earthquakes from oil exploration in the Weald. https://www.keithtaylormep.org.uk/sites/default/files/download/2019-02/Newdigate%20Short%20Summary%20Edinburgh%20Uni%20Feb%202019.pdf

Chadwick, R.A., 1986. Extension tectonics in the Wessex Basin, southern England. Journal of the Geological Society, London, 143, 465-488.

Chadwick, R.A., Kenolty, N., Whittaker, A., 1983. Crustal structure beneath southern England from deep seismic reflection profiles. Journal of the Geological Society, London, 140, 893-911.

Chadwick, R.A., Pharaoh, T.C., Williamson, J.P., Musson, R.M.W., 1996. Seismotectonics of the UK. British Geological Survey Technical Report, WA/96/3C. British Geological Survey, Keyworth, Nottingham, 172 pp. Available online: http://core.ac.uk/download/pdf/59774.pdf

Cobbold, P.R., Rodrigues, N., 2007. Seepage forces, important factors in the formation of horizontal hydraulic fractures and bedding-parallel fibrous veins ('beef' and 'cone-in-cone'). Geofluids, 7, 313–322.

Cobbold, P.R., Zanella, A., Rodrigues, N., Løseth, H., 2013. Bedding-parallel fibrous veins (beef and cone-in-cone): Worldwide occurrence and possible significance in terms of fluid overpressure, hydrocarbon generation and mineralization. Marine and Petroleum Geology, 43, 1-20.

Costain, J.K., 2017. Groundwater recharge as the trigger of naturally occurring intraplate earthquakes. In: Landgraf, A., Kübler, S., Hintersberger, E., Stein, S. (eds), Seismicity, Fault Rupture and Earthquake Hazards in Slowly Deforming Regions. Geological Society, London, Special Publications, 432, 91–118.

Cuadrilla, 2019. Preston New Road-1z: LJ/06-09(z) HFP Report. Cuadrilla Bowland Ltd., Preston, 25 pp. https://www.ogauthority.co.uk/media/5845/pnr-1z-hfp-report.pdf

Dahm, T., Cesca, S., Hainzl, S., Braun, T., Krüger, F., 2015. Discrimination between induced, triggered, and natural earthquakes close to hydrocarbon reservoirs: A probabilistic approach based on the modeling of depletion-induced stress changes and seismological source parameters. Journal of Geophysical Research, 120, 2491–2509.

Dake, L.P., 1998. Fundamentals of Reservoir Engineering. Developments in Petroleum Science series, volume 8, 17th edition. Elsevier, London, 498 pp.

Davies, R., Foulger, G., Bindley, A., Styles, P., 2013. Induced seismicity and hydraulic fracturing for the recovery of hydrocarbons. Marine and Petroleum Geology, 45, 171–185.

Davis, S.D., Frohlich, C., 1993. Did (or will) fluid injection cause earthquakes? - Criteria for a rational assessment. Seismological Research Letters, 64 (3-4), 207-224.

DECC, 2013. The Hydrocarbon Prospectivity of Britain's Onshore Basins. Department of Energy and Climate Change, London, 93 pp. https://www.ogauthority.co.uk/media/1695/uk_onshore_2013.pdf

Detournay, E., Cheng, A.H.-D., 1993. Fundamentals of poroelasticity. Chapter 5 in C. Fairhurst (ed.) Comprehensive Rock Engineering: Principles, Practice and Projects, Vol. II, Analysis and Design Method. Pergamon Press, Oxford, pp. 113-171.

De Wiest, R.J.M., 1966. On the storage coefficient and the equations of groundwater flow. Journal of Geophysical Research, 71, 1117-1122.

Dines, H.G., Edmunds, F.H., 1933. The geology of the country around Reigate and Dorking: memoir for 1:63,360 geological map sheet 286 (England and Wales). H.M.S.O., London, 204 pp.

Doser, D.I., Baker, M.R., Mason, D.B., 1991. Seismicity in the War-Wink gas field, Delaware Basin, West Texas, and its relationship to petroleum. Bulletin of the Seismological Society of America, 81, 971-986.

Ellsworth, W.L., 2013. Injection-induced earthquakes. Science, 341, 1225942, 7 pp. doi: 10.1126/science.1225942.

Europa, 2004. Application for Production Licence. Appendix B – Geotechnical Information. Europa Oil & Gas Ltd., London, 38 pp. https://ukogl.org.uk/map/php/pdf.php?subfolder=industry_reports&filename=41436.pdf

Evans, C.J., Brereton, N.R., 1990. *In situ* crustal stress in the United Kingdom from borehole breakouts. In: Hurst, A., Lovell, M.A., Morton, A.C. (eds), Geological Applications of Wireline Logs. Geological Society, London, Special Publications, 48, 327-338.

Evans, J.P., Forster, C.B., Goddard, J.V., 1997. Permeability of fault-related rocks, and implications for hydraulic structure of fault zones. Journal of Structural Geology, 19, 1393-1404

Fellgett, M.W., Kingdon, A., Williams, J.D.O., Gent, C.M.A., 2017. State of stress across UK regions. British Geological Survey GeoAnalytics and Modelling Directorate Open Report OR/17/048, 60 pp. http://nora.nerc.ac.uk/id/eprint/517414/1/OR17048.pdf

Ford, T.D., Torrens, H.S., 2001. A Farey story: the pioneer geologist John Farey (1766–1826). Geology Today, 17 (2), 59-68.

Foulger, G.R., Wilson, M.P., Gluyas, J.G., Julian, B.R., Davies, R.J., 2018. Global review of human-induced earthquakes. Earth-Science Reviews, 178, 438–514.

Gallois, R.W., Worssam, B.C., 1993. The geology of the country around Horsham: memoir for 1:50,000 geological map sheet 302 (England and Wales). H.M.S.O., London, 130 pp.

Gans, C.R., Furlong, K.P., Malservisi, R., 2003. Fault creep and microseismicity on the Hayward fault, California: Implications for asperity size. Geophysical Research Letters, 30, 2000, 4 pp., doi: 10.1029/2003GL017904

GeoSierra, 2017. Review of 2011 Preese Hall Well Stimulations and Proposed Alternate Stimulation Method for UK Bowland-Hodder Shale Gas. GeoSierra LLC, Norcross, Georgia. http://www.geosierra.com/files/122554754.pdf

GeoSierra, 2019. Newdigate Seismicity and Link to Horse Hill HH-1 Well Activities. GeoSierra LLC, Norcross, Georgia. http://www.geosierra.com/files/132555955.pdf

Gilfillan, S., Haszeldine, S., McGuire, B., Selley, R., 2018. Surrey quake fears. Letter to the Editor, The Times, 6 August 2018.

Goebel, T.H.W., Weingarten, M., Chen, X., Haffener, J., Brodsky, E.E., 2017. The 2016 M_w 5.1 Fairview, Oklahoma earthquakes: Evidence for long-range poroelastic triggering at >40 km from fluid disposal wells. Earth and Planetary Science Letters, 472, 50–61.

Gölke, M., Coblentz, D., 1996. Origins of the European regional stress field. Tectonophysics, 266, 11-24.

Grasso, J.R., Wittlinger, G., 1990. Ten years of seismic monitoring over a gas field area. Bulletin of the Seismological Society of America, 80, 450-474.

Grigoli, F., Cesca, S., Rinaldi, A.P., Manconi, A., López-Comino, J.A., Clinton, J.F., Westaway, R., Cauzzi, C., Dahm, T., Wiemer, S., 2018. The November 2017 M_w 5.5 Pohang earthquake: A possible case of induced seismicity in South Korea. Science, 360, 1003-1006.

Grünthal, G., 1998. European Macroseismic Scale 1998, EMS-98. Cahiers du Centre Européen de Géodynamique et de Séismologie, 15. Centre Européen de Géodynamique et de Séismologie, Luxembourg, 101 pp.

Guo BoYun, Sun Kai, Ghalambor, A., eds., 2008. Well Productivity Handbook. Elsevier, London, 334 pp.

GVL, 2018. United Kingdom Relative Deformation Map. Geomatic Ventures Limited, Nottingham. https://mangomap.com/geomatic-ventures-limited/maps/72883/united-kingdom-relative-deformation-map?preview=true

Haines, T., Michie, E.A.H, Neilson, J.E., Healy, D., 2016. Permeability evolution across carbonate hosted normal fault zones. Marine and Petroleum Geology, 72, 62-82.

Hainzl, S., 2004. Seismicity patterns of earthquake swarms due to fluid intrusion and stress triggering. Geophysical Journal International, 159, 1090–1096.

Harbord, C.W.A., Nielsen, S.B., De Paola, N., Holdsworth, R.E., 2017. Earthquake nucleation on rough faults. Geology, 45, 931–934.

Harding, P., Bridgland, D.R., Allen, P., Bradley, P., Grant, M.J, Peat, D., Schwenninger, J.-L., Scott, R., Westaway, R., White, T.S., 2012 Chronology of the Lower and Middle Palaeolithic in NW Europe: developer-funded investigations at Dunbridge, Hampshire, southern England. Proceedings of the Geologists' Association, 123, 584-607.

Haszeldine, S., Cavanagh, A., 2018. Weald Basin 2018 Earthquake Cluster Analysis: Does Horse Hill meet Davis & Frohlich (1993) criteria for induced earthquakes? https://www.ogauthority.co.uk/media/5173/10-weald-basin-earthquakes-induced-oga-workshop-haszeldine-cavanagh-oct-2018-low-res.pdf

Hawkes, P.W., Fraser, A.J., Einchcomb, C.C.G., 1998. The tectono-stratigraphic development and tectonic history of the Weald and Wessex Basins, Southern England. In: Underhill, J.R. (ed.), The Development, Evolution and Petroleum Geology of the Wessex Basin. Geological Society, London, Special Publications, 133, 33-69.

Hayhurst, R., 2018. Oil company says "We're not to blame for Surrey earthquake" – but local concerns remain. Drill or Drop? Magazine. https://drillordrop.com/2018/04/04/oil-company-says-were-not-to-blame-for-surrey-earthquake-but-local-concerns-remain/

Hayhurst, R., 2019. Latest earth tremor prompts call for release of data on oil operations. Drill or Drop? Magazine. https://drillordrop.com/2019/05/10/latest-earth-tremor-prompts-call-for-release-of-data-on-oil-operations/

Heidbach, O., Rajabi, M., Cui, X., Fuchs, K., Müller, B., Reinecker, J., Reiter, K., Tingay, M., Wenzel, F., Xie, F., Ziegler, M.O., Zoback, M.-L., Zoback, M.D., 2018. The World Stress Map database release 2016: Crustal stress pattern across scales. Tectonophysics, 744, 484-498.

Hesselbo, S.P., Jenkyns, H.C.A., 1995. A comparison of the Hettangian to Bajocian successions of Dorset and Yorkshire. In Taylor, P.D. (Ed.), Field geology of the British Jurassic. Geological Society, London, pp. 105-150.

Hettema, M., Papamichos, E., Schutjens, P., 2002. Subsidence delay: Field observations and analysis. Oil & Gas Science and Technology, 57, 443–458.

Hicks, S., Verdon, J., Baptie, B., Luckett, R., Mildon, Z., Gernon, T., 2019. A shallow earthquake swarm close to hydrocarbon activities: discriminating between natural and induced causes for the 2018–19 Surrey, UK earthquake sequence, Seismological Research Letters, https://pubs.geoscienceworld.org/ssa/srl/article-pdf/doi/10.1785/0220190125/4819219/srl-2019125.1.pdf

Hincks, T., Aspinall, W., Cooke, R, Gernon, T., 2018. Oklahoma's induced seismicity strongly linked to wastewater injection depth. Science, 359, 1251-1255.

Hitzman, M.W., Clarke, D.D., Detournay, E., Dieterich, J.H., Dillon, D.K., Green, S.J., Habiger, R.M., McGuire, R.K., Mitchell, J.K., Shemeta, J.E., Smith, J.L., 2013. Induced Seismicity Potential in Energy Technologies. The National Academies Press, Washington, DC, 263 pp. http://www.nap.edu/catalog/13355/induced-seismicity-potential-inenergy-technologies.

Holland, A.A., 2013. Earthquakes triggered by hydraulic fracturing in south-central Oklahoma. Bulletin of the Seismological Society of America, 103, 1784-1792.

Hornbach, M.J., DeShon, H.R., Ellsworth, W.L., Stump, B.W., Hayward, C., Frohlich, C., Oldham, H.R., Olson, J.E., Magnani, M.B., Brokaw, C., Luetgert, J.H., 2015. Causal factors for seismicity near Azle, Texas. Nature Communications, 6, 7728, 11 pp., doi: 10.1038/ncomms7728

Hornbach, M.J., Jones, M., Scales, M., DeShon, H.R., Magnani, M.B., Frohlich, C., Stump, B., Hayward, C., Layton, M., 2016. Ellenburger wastewater injection and seismicity in North Texas. Physics of the Earth and Planetary Interiors, 261, 54–68.

Horse Hill Developments Ltd., 2018a. FACTS ABOUT HORSE HILL. What we ARE doing & what we ARE NOT doing. Horse Hill Developments Ltd., London.

http://www.horsehilldevelopments.co.uk/ul/FACTS%20about%20HH%20Final%20Draft%20201810 18.pdf

Horse Hill Developments Ltd., 2018b. Horse Hill-1 rig-less intervention and well testing programme. Report HHDL-HH1-RIWTP-R0. Horse Hill Developments Ltd., London, 81 pp. https://brockhamoilwell.files.wordpress.com/2019/04/disclosure-201808357-2.pdf

Howett, F., 1964. Stratigraphy and structure of the Purbeck inliers of Sussex (England). Quarterly Journal of the Geological Society, London, 120, 77-113.

Igonin, N., Verdon, J.P., Kendall, J-M., Eaton, D.W., 2019. The importance of pre-existing fracture networks for fault reactivation during hydraulic fracturing. Earth and Space Science Open Archive, 10500976, 27 pp., doi: 10.1002/essoar.10500976.1. https://www.essoar.org/doi/pdf/10.1002/essoar.10500976.1

Jacob, C.E., 1940. The flow of water in an elastic artesian aquifer. Transactions of the American Geophysical Union, 2, 574-586.

Jones, H K, Morris, B L, Cheney, C S, Brewerton, L J, Merrin, P D, Lewis, M A, MacDonald, A M, Coleby, L M, Talbot, J C, McKenzie, A A, Bird, M J, Cunningham, J, and Robinson, V K. 2000. The physical properties of minor aquifers in England and Wales. British Geological Survey Technical Report, WD/00/4, 234 pp. Environment Agency R&D Publication 68.

Justinic, A.H., Stump, B., Hayward, C., Frohlich, C., 2013. Analysis of the Cleburne, Texas earthquake sequence from June 2009 to June 2010. Bull. Seismol. Soc. Am., 103, 3083–3093.

Karner, G.D., Lake, S.D., Dewey, J.F., 1987. The thermal and mechanical development of the Wessex Basin, southern England. In: Coward, M.P., Dewey, J.F., Hancock, P.L. (eds), Continental Extensional Tectonics. Geological Society, London, Special Publications, 28, 517-536.

Keranen, K.M., Weingarten, M., Abers, G.A., Bekins, B.A., Ge SheMin, 2014. Sharp increase in central Oklahoma seismicity since 2008 induced by massive wastewater injection. Science, 345, 448–451.

Kim Won-Young, 2013. Induced seismicity associated with fluid injection into a deep well in Youngstown, Ohio. Journal of Geophysical Research Solid Earth, 118, 3506–3518.

Kingdon, A., Fellgett, M.W., Williams, J.D.O., 2016. Use of borehole imaging to improve understanding of the in-situ stress orientation of Central and Northern England and its implications for unconventional hydrocarbon resources. Marine and Petroleum Geology, 73, 1-20.

Klein, R.J., Barr, M.V., 1986. Regional state of stress in Western Europe. In: Stephansson, O. (Ed.), Proceedings of the International Symposium on Rock Stress and Rock Stress Measurements, Stockholm, 1-3 September 1986. Centek, Lulea, pp. 33-44.

Kovach, R.L., 1974. Source mechanisms for Wilmington oil field, California, subsidence earthquakes. Bulletin of the Seismological Society of America, 64, 699-711.

Lake, S.D., Karner, G.D., 1987. The structure and evolution of the Wessex Basin, southern England: an example of inversion tectonics. Tectonophysics, 137, 347-356, 358-378.

Lang, W.D., 1914. The geology of Charmouth cliffs, beach and fore-shore. Proceedings of the Geologists' Association, 25, 293-360.

Lang, W.D., Spath, L.F., Richardson, W.A., 1923. Shales-with-'Beef', a sequence in the Lower Lias of the Dorset coast. Quarterly Journal of the Geological Society, London, 79, 47-99.

Lash, G.G., Engelder, T., 2005. An analysis of horizontal microcracking during catagenesis: Example from the Catskill delta complex. AAPG Bulletin, 89, 1433-1449.

Lewis, M.A., Cheney, C.S., Ó Dochartaigh, B.É., 2006. Guide to Permeability Indices. British Geological Survey, Information Products Programme, Open Report CR/06/160N. British Geological Survey, Keyworth, Nottingham, 29 pp.

Lunn, R.J., Shipton, Z.K., Bright, A.M., 2008. How can we improve estimates of bulk fault zone hydraulic properties? In: Wibberley, C.A.J., Kurtz, W., Imber, J., Holdsworth, R.E., Collettini, C. (eds), The Internal Structure of Fault Zones: Implications for Mechanical and Fluid-Flow Properties. Geological Society, London, Special Publications, 299, 231–237.

Maher Jr, H.D., Ogata, K., Braathen, A., 2017. Cone-in-cone and beef mineralization associated with Triassic growth basin faulting and shallow shale diagenesis, Edgeøya, Svalbard. Geological Magazine, 154, 201–216.

McDermott, R.G., Ault, A.K., Evans, J.P., Reiners, P.W., 2017. Thermochronometric and textural evidence for seismicity via asperity flash heating on exhumed hematite fault mirrors, Wasatch fault zone, UT, USA. Earth and Planetary Science Letters, 471, 85-93.

McKenzie, D.P., 1969. The relationship between fault plane solutions for earthquakes and the directions of the principal stresses. Bulletin of the Seismological Society of America, 59, 591–601.

McLennan, W., 2019. Surrey earthquakes: Is oil drilling causing tremors? British Broadcasting Corporation, London. https://www.bbc.co.uk/news/uk-england-47816810

McLimans, R.K., Videtich. P.E., 1989. Diagenesis and burial history of Great Oolite Limestone, southern England. American Association of Petroleum Geologists Bulletin, 73, 1195-1205.

Meng QingFeng, Hooker, J., Cartwright, J., 2017. Early overpressuring in organic-rich shales during burial: evidence from fibrous calcite veins in the Lower Jurassic Shales-with-Beef Member in the Wessex Basin, UK. Journal of the Geological Society, London, 174, 869-882.

Meng QingFeng, Hooker, J., Cartwright, J., 2018. Displacive widening of calcite veins in shale: Insights into the force of crystallization. Journal of Sedimentary Research, 88, 327-343.

Mitchell, E.K., Fialko, Y., Brown, K.M., 2012. Temperature dependence of frictional healing of Westerly granite: experimental observations and numerical simulations. Geochemistry, Geophysics, Geosystems, 14, 567–582.

Newson, M.D., 1973. The Carboniferous Limestone of the UK as an aquifer rock. The Geographical Journal, 139 (2), 294-305.

OGA, 2018. OGA Newdigate Seismicity Workshop –3 October 2018. Summary and conclusion. UK Oil & Gas Authority, Aberdeen. https://www.ogauthority.co.uk/media/5174/2018_11_23-newdigate-workshop-summary-finalv3.pdf

OGA, 2019. Interim report of the scientific analysis of data gathered from Cuadrilla's operations at Preston New Road. UK Oil & Gas Authority, Aberdeen, 20 pp. https://www.ogauthority.co.uk/onshore/onshore-reports-and-data/preston-new-road-pnr-1z-hydraulic-fracturing-operations-data/

Ottemöller, L., Nielsen, H., Atakan, K., Braunmiller, J., Havskov, J., 2005. The 7 May 2001 induced seismic event in the Ekofisk oil field, North Sea. Journal of Geophysical Research, 110, B10301, 15 pp., doi: 10.1029/2004jb003374.

Parnell, J., Honghan, C., Middleton, D., Haggan, T., Carey, P., 2000. Significance of fibrous mineral veins in hydrocarbon migration: fluid inclusion studies. Journal of Geochemical Exploration, 69, 623-627.

Pennington, W.D., Davis, S.D., Carlson, S.M., Dupree, J., Ewing, T.E., 1986. The evolution of seismic barriers and asperities caused by the depressuring of fault planes in oil and gas fields of South Texas. Bulletin of the Seismological Society of America, 76, 939-948.

Pine, R.J., Batchelor, A.S., 1984. Downward migration of shearing in jointed rock during hydraulic injections. International Journal of Rock Mechanics and Mining Sciences & Geomechanics Abstracts 21, 249-263.

Pratt, W.E., Johnson, D.W., 1926. Local subsidence of the Goose Creek oil field. Journal of Geology, 34, 577–590.

Pruiksma, J.P., Rózsás, Á., 2017. Vibration levels at foundations of houses in Groningen due to induced earthquakes. Report 2017 R10493-A. TNO, Utrecht, The Netherlands, 115 pp.

Pullan, C.P., Butler, M., 2018. Paleozoic gas potential in the Weald Basin of southern England. In: Paleozoic Plays of NW Europe, Monaghan, A.A., Underhill, J.R., Hewett, A.J., Marshall, J.E.A. (eds). Geological Society, London, Special Publications, 471, 333-363.

Reiter, M., 1999. Stress analyses of a simple fault asperity. In: Vail Rocks 1999, The 37th U.S. Symposium on Rock Mechanics, 7-9 June 1999, Vail, Colorado. American Rock Mechanics Association paper ARMA-99-0391, 8 pp.

Rothé, G.H., Lui, C.Y., 1983. Possibility of induced seismicity in the vicinity of the sleepy hollow oil field, southwestern Nebraska. Bulletin of the Seismological Society of America, 73, 1357-1367.

Schultz, R., Stern, V., Novakovic, M., Atkinson, G., Gu, Y.J., 2015. Hydraulic fracturing and the Crooked Lake sequences: Insights gleaned from regional seismic networks. Geophysical Research Letters, 42, 2750-2758.

Segall, P., 1989. Earthquakes triggered by fluid extraction. Geology, 17, 942–946.

Segall, P., Fitzgerald, S.D., 1998. A note on induced stress changes in hydrocarbon and geothermal reservoirs. Tectonophysics, 289, 117–128.

Selvadurai, P.A., Glaser, S.D., 2017. Asperity generation and its relationship to seismicity on a planar fault: a laboratory simulation. Geophysical Journal International, 208, 1009–1025.

Shepley, M.G., 2007. Analysis of flows from a large Carboniferous Limestone drainage adit, Derbyshire, England. Quarterly Journal of Engineering Geology and Hydrology, 40, 123-135.

Simpson, D.W., Leith, W., 1985. The 1976 and 1984 Gazli, USSR, earthquakes were induced? Bulletin of the Seismological Society of America, 75, 1465-1468.

Simpson, D.W., Leith, W.S., Scholz, C.H., 1988. Two types of reservoir-induced seismicity. Bulletin of the Seismological Society of America, 78, 2025-2040.

Spetzler, J., Dost, B., 2017. Hypocentre estimation of induced earthquakes in Groningen. Geophysical Journal International, 209, 453–465.

Stoneley, R., 1982. The structural development of the Wessex Basin. Journal of the Geological Society, London, 139, 543-552.

Tarney, J., Schreiber, B.C., 1977. Cone-in-cone and beef-in-shale textures from DSDP Site 330, Falkland Plateau, South Atlantic. Deep Sea Drilling Project Initial Reports, 36, 865-870.

Townend, J., Zoback, M.D. 2000. How faulting keeps the crust strong. Geology, 28, 399–402.

Trueman, S., 2003. The Humbly Grove, Herriard, Storrington, Singleton, Stockbridge, Goodworth, Horndean, Palmers Wood, Bletchingley and Albury Fields, Hampshire, Surrey and Sussex, UK Onshore. In: Gluyas, J., Hitchens, H.M. (eds.), United Kingdom Oil and Gas Fields Commemorative Millennium Volume. Geological Society, London, Memoir 20, pp. 929-941.

UKOG, 2019a. Why earth tremors in Surrey should not be blamed on oil exploration. Statement from UK Oil & Gas Plc, in response to "unscientific" claims made by Dr Cavanagh, Dr Gilfillan and Professor Haszeldine. UK Oil & Gas Plc, London. https://www.ukogplc.com/ul/Technical%20Response%20to%20Edinburgh%20University%20120419.pdf

UKOG, 2019b. Horse Hill Overview. UK Oil & Gas Plc, London. https://www.ukogplc.com/page.php?pID=60

UKOG, 2019c. HH-1 and HH-2z extended well test update. UK Oil & Gas Plc, London, 23 December 2019. https://www.lse.co.uk/rns/UKOG/hh-1-and-hh-2z-extended-well-test-update-xjk6frv4uqebsr1.html

UKOG, 2020a. Horse Hill-2z water shut off intervention commences. UK Oil & Gas Plc, London, 19 February 2020. https://irpages2.equitystory.com/websites/rns_news/English/1100/news-tool---rns---eqs-group.html?article=30267363&company=ukog

UKOG, 2020b. Dry oil flows to surface following successful Horse Hill-2z water shut-off programme. UK Oil & Gas Plc, London. 9 March 2020. https://irpages2.equitystory.com/websites/rns_news/English/1100/news-tool---rns---eqs-group.html?article=30354960&company=ukog

Verdon, J.P., Baptie, B.J., Bommer, J.J., 2019. An improved framework for discriminating seismicity induced by industrial activities from natural earthquakes. Seismological Research Letters, 90, 1592-1611.

Wald, D.J., Quitoriano, V., Heaton, T.H., Kanamori, H. 1999. Relationships between peak ground acceleration, peak ground velocity, and modified Mercalli intensity in California. Earthquake Spectra, 15, 557–564.

Walsh, F.R., Zoback, M.D., 2015. Oklahoma's recent earthquakes and saltwater disposal. Science Advances, 1, e1500195, 9 pp., doi: 10.1126/sciadv.1500195.

Walsh, J.J., Watterson, J., 1988. Dips of normal faults in British Coal Measures and other sedimentary sequences. Journal of the Geological Society, London, 145, 859-873.

Wang QiQi, 2016. Characterization of bedding-parallel fractures in shale - Morphology, size distribution and spatial organization. Master of Science thesis, The University of Texas at Austin, 324 pp.

Webster, T., 1826. Observations on the Purbeck and Portland Beds. Transactions of the Geological Society, London, Series 2, 2, 37-44.

Wees, V.J., Buijze, L., van Thienen-Visser, K., Nepveu, M., Wassing, B., Orlic, B., Fokker, P., 2014. Geomechanics response and induced seismicity during gas field depletion in the Netherlands, Geothermics, 52, 206–219.

Weingarten, M., Ge SheMin, Godt, J.W., Bekins, B.A., Rubinstein, J.L., 2015. High-rate injection is associated with the increase in U.S. mid-continent seismicity. Science, 348, 1336–1340.

Weisstein, E.W., 2019. Erfc. From MathWorld - A Wolfram Web Resource. http://mathworld.wolfram.com/Erfc.html

Westaway, R., 2006. Investigation of coupling between surface processes and induced flow in the lower continental crust as a cause of intraplate seismicity. Earth Surface Processes and Landforms 31, 1480-1509.

Westaway, R., 2016. The importance of characterizing uncertainty in controversial geoscience applications: induced seismicity associated with hydraulic fracturing for shale gas in northwest England. Proceedings of the Geologists' Association, 127, 1–17.

Westaway, R., 2017. Integrating induced seismicity with rock mechanics: a conceptual model for the 2011 Preese Hall fracture development and induced seismicity. In: Rutter, E.H., Mecklenburgh, J., Taylor, K.G. (eds). Geomechanical and Petrophysical Properties of Mudrocks. Geological Society, London, Special Publications, 454, 327–359.

Westaway, R., Bridgland, D.R., White, M.J., 2006. The Quaternary uplift history of central southern England: evidence from the terraces of the Solent River system and nearby raised beaches, Quaternary Science Reviews, 25, 2212-2250.

Westaway, R., Burnside, N.M., 2019. Fault 'corrosion' by fluid injection: potential cause of the November 2017 MW 5.5 Korean earthquake. Geofluids, 1280721, 23 pp., doi: 10.1155/2019/1280721

Westaway, R., Younger, P.L., 2014. Quantification of potential macroseismic effects of the induced seismicity that might result from hydraulic fracturing for shale gas exploitation in the UK. Quarterly Journal of Engineering Geology and Hydrogeology, 47, 333–350.

Westaway, R., Younger, P.L., 2016. Unravelling the relative contributions of climate change and ground disturbance to subsurface temperature perturbations: case studies from Tyneside, UK. Geothermics, 64, 490–515.

Westwood, R.F., Toon, S.M., Styles, P., Cassidy, N.J., 2017. Horizontal respect distance for hydraulic fracturing in the vicinity of existing faults in deep geological reservoirs: a review and modelling study. Geomechanics and Geophysics for Geo-Energy and Geo-Resources, 3, 379–391.

Wetmiller, R.J., 1986. Earthquakes near Rocky Mountain House, Alberta, and their relationship to gas production facilities. Canadian J. Earth Science, 23, 172-181.

Wigley, P., 2015. Exploration in the UK Weald Basin: Déjà vu. Search and Discovery, 70182, 8 pp. http://www.searchanddiscovery.com/pdfz/documents/2015/70182wigley/ndx_wigley.pdf.html

Willacy, C., van Dedem, E., Minisini, S., Li JunLun, Blokland, J.-W., Das, I., Droujinine, A., 2019. Full-waveform event location and moment tensor inversion for induced seismicity. Geophysics, 84 (2), KS39–KS57. doi: 10.1190/GEO2018-0212.1

Wilson, M.P., Worrall, F., Davies, R.J., Almond, S., 2018. Fracking: How far from faults? Geomechanics and Geophysics for Geo-Energy and Geo-Resources, 4, 193–199.

Worden, C.B., Gerstenberger, M.C., Rhoades, D.A., Wald, D.J., 2012. Probabilistic relationships between ground-motion parameters and modified Mercalli intensity in California. Bulletin of the Seismological Society of America, 102, 204-221.

Xodus, 2018. 2018 Competent Person's Report to UK Oil & Gas Investments PLC. Xodus Group, London, 112 pp. https://www.ukogplc.com/ul/UKOG%202018%20CPR%20060618.pdf

Yerkes, R.F., Castle, R.D., 1976. Seismicity and faulting attributed to fluid extraction. Engineering Geology, 10, 151-167.

Younger, P.L., 1993. Simple generalized methods for estimating aquifer storage parameters. Quarterly Journal of Engineering Geology, 26, 127-135.

Zanella, A., Cobbold, P.R., Boassen, T., 2015. Natural hydraulic fractures in the Wessex Basin, SW England: widespread distribution, composition and history. Marine and Petroleum Geology, 68, 438-448.

Zhang Bo, Yin CongYuan, Gu ZhiDong, Zhang JinJiang, Yan ShuYu, Wang Yang, 2015. New indicators from bedding-parallel beef veins for the fault valve mechanism. Science China: Earth Sciences, 58, 1320–1336.

Zhang, YiPeng, Person, M., Rupp, J., Ellett, K., Celia, M.A., Gable, C.W., Bowen, B., Evans, J., Bandilla, K., Mozley, P., Dewers, T., Elliot, T., 2013. Hydrogeologic controls on induced seismicity in crystalline basement rocks due to fluid injection into basal reservoirs. Groundwater, 51, 525–538.

Zimmerman, R.W., Bodvarsson, G.S., 1996. Hydraulic conductivity of rock fractures. Transport in Porous Media, 23, 1–30.

Zoback, M.L., Zoback, M.D., 2007. Lithosphere stress and deformation. Treatise on Geophysics, 6, 253-273.

Table 1: Stratigraphy of the Horse Hill 1 borehole

Table 2: Layered Velocity Model used by Hicks et al. (2019)

Table 3: Source parameters for Newdigate earthquakes with focal mechanisms

Table 4: Newdigate seismicity since the start of June 2019

Figure captions

Figure 1. Map of the study area, modified from Fig. 2(a) of Hicks et al. (2019). The original geographical (latitude-longitude) co-ordinate system has been retained, but 'greyed out', with a new co-ordinate system added, indexed to the British National Grid (BNG). As is discussed in the main text, the original scale bar by Hicks et al. (2019) is much too small and has also been 'greyed out'. Faults are identified thus: BHF, Box Hill Fault; BRF, Brockham Fault; BUF, Buckland Fault; CF, Crawley Fault; COF, Collendean Fault; FGF, 'Faygate Fault'; HF, Holmbush Fault; HHF, Horse Hill Fault; HWF, Holmwood Fault; KFF, Kingsfold Fault; LHF, Leigh Fault; NGF, Newdigate Fault; OKF, Ockley Fault; WB1F, Whiteberry-1 Fault; and WCF, Westcott Fault. Most of these structures are depicted as shown by Hicks et al. (2019), although some are misplaced, as discussed in the text. The Crawley and Holmwood faults, not recognized by Hicks et al. (2019), are shown schematically where they cross seismic line TWLD-90-15, the southward continuation of which (beyond the excerpt shown in Fig. 2) is also shown schematically. The 'Faygate Fault' is a mistaken concept by Hicks et al. (2019), so is shown 'greyed out' (see text and online supplement). Focal mechanisms are illustrated as standard equal area projections of the lower focal hemisphere, with compressional quadrants of the P-wave radiation pattern shaded. Horse Hill 1 well track is from https://ukogl.org.uk/map/php/well_deviation_survey.php?wellId=3041. The source of information for positions of seismic lines, including line TWLD-90-15, was not reported by Hicks et al. (2019); they are from the schematic location map provided by the UK Onshore Geophysical Library (https://ukogl.org.uk/), which is indexed to the BNG, and was transformed to geographical co-ordinates by Hicks et al. (2019). Seismograph station GATW ceased operation on 17 May 2019 due to

equipment theft. It was replaced by station GAT2, ~230 m northwest, which became operational from 6 June.

Figure 2. 2-D seismic section along seismic line TWLD-90-15, modified from Fig. 6 of Hicks et al. (2019). The original was indexed by Hicks et al (2019) to the British National Grid (BNG), rather than the geographical co-ordinates used for Fig. 1; as discussed in the online supplement, after careful consideration these co-ordinates were accepted as accurate. The labelled horizons were not explained by Hicks et al. (2019), but appear to be the top Portland Group, top Kimmeridge Clay Formation, and top Coralline Oolite Formation (cf. Table 4). Faults designated by Hicks et al. (2019) are identified thus: COF, Collendean Fault; LHF, Leigh Fault; and NGF, Newdigate Fault. CF denotes the Crawley Fault. Hicks et al. (2019) did not explain how they depth-converted this seismic section. As is discussed in the main text and online supplement, it is suspected that they used their velocity model for earthquake location (Table 2) for this depth conversion. Their depth scale is 'greyed out', whereas the new version, using the seismic interval velocities from the HH1 well (Table 1) is emphasized. Additional interpretation has also been added, including the interpreted top Penarth Group / base Lias Group reflector and its offset by the main strand of the Newdigate Fault, and some of the additional lesser fault strands forming the multi-stranded Newdigate fault zones, other strands being evident in Fig. 3 and in the uninterpreted version of this seismic section provided by Hicks et al. (2019) in their online supplement.

Figure 3. Excerpt from the record section for seismic line TWLD-90-15, as provided by UKOGL, illustrating the Newdigate Fault. As geo-located in the online supplement, this excerpt extends between BNG references TQ 21585 39125 and TQ 20326 46935, a distance of ~8 km.

Figure 4. Time series of Newdigate earthquakes and other activities affecting the Horse Hill 1 and Brockham X2 wells, based on Fig. 3 of Hicks et al. (2019). Note that their original Fig. 6(d) has been omitted as it depicts an incorrect timeline for production at Brockham up to 2016: the correct timeline is shown in Fig. 11 of Angus (2018). **(a)** Installation dates of stations forming the local temporary seismic monitoring network. From Fig. 3(a) of Hicks et al. (2019). **(b)** Detected earthquakes, cumulative number of events, and inferred variations in the completeness threshold magnitude M_C. From Fig. 3(b) of Hicks et al. (2019). Note that some of the magnitudes M_L depicted here differ slightly from those listed in Supplementary Fig. S2 of Hicks et al. (2019), which feature in discussion in the text. **(c)** Summary timeline for activities at the Horse Hill 1 well, indicating (based on the information sources discussed in the text and details in part (d)) the phases of production from each reservoir. Notes refer to details discussed in the text, thus, regarding the HH1 well: 1, first known intervention affecting the well, 5 April 2018; 2, removal of bridge plug that had isolated the Portland reservoir from the surface, 4 July 2018; 3, production from KL3; 4, production from KL4; and 5, 'co-mingled' production from both KL3 and KL4. Regarding the BRX2Y well, based on the timeline reported by Hicks et al. (2019): 6 denotes the restart of production on 22 March 2018; 7 denotes a later resumption, with injection of water starting on 25 June and (net) production restarting on 28 June (but with both injection and production occurring on 27 June); and 8 denotes the end of production on 15 October 2018. **(d)** More detailed operations timeline for activities at the Horse Hill 1 well, with flow-period averaged production and cumulative production over time. From Fig. 3(c) of Hicks et al. (2019), with further details, including dates, provided in their supplementary Table S4. The information provided by Hicks et al. (2019) is much more detailed than that which has been otherwise released into the public domain, and must have been obtained from the developer. However, their reporting of the information does not identify the hydrocarbon reservoirs to which the activities relate (see part (c)), which is essential to reveal the pattern of correlation between seismicity and activities affecting the Portland reservoir (see also the online supplement).

Figure 5. Cartoons summarizing the proposed conceptual model linking the Newdigate seismicity to reductions in fluid pressure in oil wells. **(a)** Large-scale processes. Production of oil (1) will reduce the pressure within the Portland reservoir near the production well. This will cause flow of oil towards the well from more distal parts of the reservoir (2). This will be accompanied by flow of groundwater into the volume vacated by the oil, which is inferred to be hydraulically connected to the 'hyper-permeable' fabric in the underlying Lower Portland Sandstone (3), which will cause flow within this fabric (4). This flow will draw groundwater from greater depths (5), up one or more strands of the Newdigate fault zone, which is assumed permeable, reducing the pressure in the section where this fault transects the Dinantian limestone. This pressure reduction will act to draw groundwater from the permeable Dinantian limestone into the fault (6). The associated compaction of the Dinantian limestone will cause separation of its two surfaces across the seismogenic fault (7). Surface interventions affecting the wells, such as bleeding pressure following shut-in, will reduce the pressure inside the well and have a similar overall effect. **(b)** Processes on a micro-structural scale on the seismogenic fault, where separation of the fault surfaces by a small distance Δx, from configuration (i) to configuration (ii), affects three model asperities (1, 2 and 3). After this change, at asperity 1 the fault surfaces are no longer in contact, at asperity 2 what was an interference fit between the fault surfaces has become a clearance fit, and at asperity 3 the rocks forming asperity 3 have decompressed elastically, so they remain in contact but with a reduced normal stress and thus a reduced limiting shear stress that can maintain fault stability.

Figure 6. Map of the structure of British National Grid 100 km × 100 km quadrangle TQ, showing the depth of base Jurassic (in feet below O.D., with contours at 200 ft intervals) and locations where the base Jurassic is offset by faults. H and N appear to denote the Holmwood, and Newdigate faults (cf. Figs 1 and 2), although the latter is misplaced. Modified from part of Fig. 4(a) of Butler and Pullan (1990).

Figure 7. Graphs of the predicted variation in pressure δP with distance x from the model seismogenic fault, calculated using equation (1) at times t of 1 week, 1 month and 1 year after a pressure change ΔP_O=-10 kPa is imposed in the fault. **(a)** For hydraulic diffusivity D=1 m^2 s^{-1}, representing Carboniferous Limestone. **(b)** For D=0.002 m^2 s^{-1}, representing crystalline basement rocks (after Zhang et al., 2013).

Figure 8. Mohr circle diagrams representing the state of stress at 2400 m depth associated with the Newdigate seismicity. **(a)** For a model stress field with σ_H=63.300 MPa, σ_V=54.300 MPa, and σ_h=39.200 MPa. Hydrostatic groundwater pressure P_f=23.544 MPa causes $\sigma_H^{'}$=39.756 MPa, $\sigma_V^{'}$=30.756 MPa, and $\sigma_h^{'}$=15.656 MPa, resulting in $\sigma_L^{'}$=28.723 MPa and $\sigma_M^{'}$=27.706 MPa. The resolved shear stress and normal stress on the fault, 10.401 and 21.622 MPa, plot below the Coulomb failure line for c=0.6, indicating that the fault is stable. **(b)** For revised conditions consistent with the set of processes in Fig. 5, representing the average model stress field on the fault, given the reduced proportion of asperities that remain in frictional contact. Groundwater pressure adjusts by 0.010 MPa below its hydrostatic value, to P_f=23.534 MPa, and the principal stresses adjust to σ_H=65.130 MPa and σ_h=36.870 MPa keeping σ_V=54.300 MPa. As a result, $\sigma_H^{'}$=41.956 MPa, $\sigma_V^{'}$=30.766 MPa, and $\sigma_h^{'}$=13.336 MPa, resulting in $\sigma_L^{'}$=28.566 MPa and $\sigma_M^{'}$=27.466 MPa. The resolved shear stress and normal stress on the fault, 12.199 and 20.332 MPa, now plot on the Coulomb failure line for c=0.6, indicating that the fault is frictionally unstable.

Table 1: Stratigraphy of the Horse Hill 1 borehole

Subdivision	MD (m)	TVDSS (m)	TWT (s)	V_I (m s^{-1})	Notes
Younger subdivisions (Early Cretaceous; Berriasian to Barremian)					
Weald Clay	7.6	-66.9	NR	ND	
Hastings Beds	158.5	84.0	NR	ND	
Grinstead Clay	211.8	137.3	NR	ND	
Lower Tunbridge Wells Sands	234.7	160.2	NR	ND	
Wadhurst Clay	245.4	170.8	NR	ND	
Ashdown Beds	298.1	223.6	NR	ND	
Purbeck Group (latest Jurassic and earliest Cretaceous; Tithonian and Berriasian)					
Purbeck Durlston Beds	396.8	322.3	NR	ND	1
Purbeck Carbonates	464.8	390.3	NR	ND	
Purbeck Main Anhydrite	604.7	530.2	0.370	2500	
Portland Group (Late Jurassic; Tithonian)					
Upper Portland Sandstone	622.4	547.7	0.384	2531	
Lower Portland Sandstone	708.4	632.5	0.451	5011	
Ancholme Group (latest Middle Jurassic and Late Jurassic; Callovian to Tithonian)					
Kimmeridge Clay	755.9	677.6	0.469	2787	
Kimmeridgian Micrite 1	851.3	765.4	0.532	2861	
Kimmeridgian Micrite 2	939.7	835.5	0.581	2961	
Top Corallian	1359.1	1139.0	0.786	3289	
Corallian Limestone	1523.7	1272.2	0.867	3743	
Oxford Clay	1539.2	1285.3	0.874	3540	
Kellaways Beds	1666.0	1403.9	0.941	3725	
Great Oolite Group (Middle Jurassic; Bathonian and Callovian)					
Cornbrash	1681.6	1418.8	0.949	2600	2
Main Great Oolite	1682.8	1420.1	0.950	5095	
Fuller's Earth	1732.8	1468.5	0.969	4886	
Inferior Oolite Group (Middle Jurassic; Aalenian and Bajocian)					
Inferior Oolite	1767.5	1502.7	0.983	5584	
Lias Group (Early Jurassic; Hettangian to Toarcian)					
Upper Lias	1941.6	1675.8	1.045	4244	
Middle Lias	2048.0	1781.9	1.095	4796	
Lower Lias	2158.3	1892.2	1.141	4301	
Older subdivisions (Triassic and older)					
Rhaetic	2470.1	2204.0	1.286	5318	
Mercia Mudstone	2528.6	2262.5	1.308	4434	3
Dolomitic Conglomerate	2581.7	2315.6	NR	ND	
Carboniferous Limestone	2593.2	2326.8	1.337	ND	
Upper Devonian	2659.4	2393.3	NR	ND	4
TD	2686.8	2420.7	NR	ND	5

Data for tops of stratigraphic subdivisions (as used by UKOGL; not all expressed using modern formal stratigraphic nomenclature, which is available from https://www.bgs.ac.uk/lexicon) are from the online well log (https://ukogl.org.uk/map/php/pdf.php?subfolder=wells\tops&filename=3041.pdf), supplemented by values from Pullan and Butler (2018), NR indicating 'not reported'. Measured Depth (MD) is measured below a datum at 66.9 m O.D., below the local ground level of 74.5 m O.D. at the wellhead, at TQ 25254 43600. TVDSS is True Vertical Depth below O.D.; TWT is echo time. Values of interval velocity, V_I, are determined in this study, ND indicating 'not determined'. Notes:

1., The Durlston Beds (or Durlston Formation) are nowadays regarded as earliest Cretaceous; the rest of the Purbeck Group is Late Jurassic.

2., The Cornbrash Formation is too thin here for its interval velocity to be reliably determined.

3., Interval velocity for the Mercia Mudstone and the Dolomitic Conglomerate combined

4., TVDSS for the top Devonian estimated given the vertical orientation of the deepest part of the well.

5., The well bottoms (at TD) in Upper Devonian mudstone.

Table 2. Velocity Model from Hicks et al. (2019)

H (km)	V_P (km s^{-1})	V_S (km s^{-1})
0.0	2.2	1.2
0.2	2.4	1.4
0.4	2.6	1.5
0.7	2.7	1.5
1.2	3.1	1.8
1.5	3.6	2.0
1.8	4.7	2.7
2.1	5.0	2.8
2.4	5.5	3.1
7.6	6.4	3.7
18.9	7.0	4.1
34.2	8.0	4.6

This velocity model was used by Hicks et al. (2019) for earthquake relocation and moment tensor inversion. H denotes the depth to the top of each layer; V_P and V_S denote the P-wave and S-wave velocities. Note that this velocity model is significantly slower that that in Table $1; it results in a two-way time to depth 2326.8 m, corresponding to the top of the Carboniferous Limestone at Horse Hill, of 1.466 s rather than the actual 1.337 s.

2326.8 m 1.337 1.4656

Table 3: Source parameters for Newdigate earthquakes with focal mechanisms

No.	Date	Time (UTC)	Epicentre (BNG reference)	Depth (m)	ΔN (m)	ΔE (m)	Δz (m)	$\Delta\alpha$ (°)	N_P	N_S	Δt_o (s)	z_{DD} (m)	M_L	M_W 1	M_W 2	z_C (m)	Strike (°)	Dip (°)	Rake (°)	f_C (Hz)	r_o (m)	$\Delta\sigma$ (MPa)
1	18 Jul 2018	03:59:56	TQ 22005 41393	1990	1397	803	1011	151	15	13	0.04	ND	2.01	2.20	2.03	2.00	282	74	178	6.4	48	0.25
2	18 Jul 2018	13:33:18	TQ 21920 41474	1860	1463	737	1014	145	15	15	0.02	ND	2.54	2.56	2.45	2.20	276	75	169	4.3	25	0.27
3	14 Feb 2019	07:43:33	TQ 22959 41543	2220	297	330	379	98	9	7	0.09	2050	2.47	2.52	2.27	2.80	255	86	173	7.7	142	1.05
4	19 Feb 2019	17:03:57	TQ 22872 41538	2050	220	429	393	106	5	4	0.04	2040	1.98	1.95	1.77	2.20	256	61	-163	11.2	86	0.56
5	27 Feb 2019	03:42:21	TQ 22622 41517	2110	286	352	316	98	14	11	0.13	2300	3.18	3.25	2.87	3.60	260	78	178	5.8	169	2.62
6	04 May 2019	00:19:19	TQ 22796 41516	2190	143	165	294	94	13	10	0.11	2440	2.35	2.31	2.17	2.40	255	85	167	16.9	64	8.06

Data from supplementary table S2 of Hicks et al. (2019). The events are numbered to match Fig. 1. For events 1 and 2 only conventional hypocentral locations were determined, which yielded the epicentral co-ordinates and focal depths. Double difference focal depths (z_{DD}) were not determined (ND). For the other events, the epicentral co-ordinates and z_{DD} are determined from the double difference location procedure and the 'Depth' by conventional location. ΔN, ΔE and Δz are the uncertainties in northing, easting, and depth, based for events 3-6 on the double difference solutions. $\Delta\alpha$ is the maximum gap between ray path azimuths to seismograph stations that recorded each event, N_P and N_S being the numbers of P- and S-wave records. Δt_o is the rms residual in origin time. M_L and M_W are local magnitude and moment magnitude. M_W 1 and the centroid depth z_C are determined from the moment tensor; M_W 2 is from P-wave spectra. Strike, Dip and Rake are for the nodal plane of the focal mechanism that is regarded as the fault plane, being subparallel to the Cudworth Fault (Fig. 2). Mean corner frequency f_C, source radius r_o, and stress drop $\Delta\sigma$ are determined from seismogram spectra.

Table 4: Newdigate seismicity since the start of June 2019

Date	Time (UTC)	Latitude (°N)	Longitude (°W)	BNG	Depth (km)	M_L	Note
9 June 2019	02:43:18.2	51.159	0.237	TQ 23382 41449	2.7	-0.5	
9 June 2019	23:00:15.0	51.133	0.295	TQ 19393 38462	3.3	-0.1	
6 July 2019	01:03:20.4	51.161	0.242	TQ 23027 41663	2.5	-0.7	
6 July 2019	01:03:23.7	51.161	0.242	TQ 23027 41663	2.5	-0.7	
6 July 2019	01:03:30.1	51.159	0.241	TQ 23102 41442	2.1	-0.8	
6 July 2019	01:03:40.2	51.159	0.241	TQ 23102 41442	2.2	-0.7	
6 July 2019	03:57:15.3	51.160	0.239	TQ 23239 41557	2.5	0.1	
20 July 2019	22:02:26.0	51.158	0.251	TQ 22405 41315	2.1	-0.6	
29 July 2019	03:35:25.5	51.160	0.242	TQ 23029 41552	2.2	-0.1	
6 Aug 2019	02:32:00.9	51.157	0.239	TQ 23247 41223	2.2	-0.5	
12 Aug 2019	00:46:46.6	51.160	0.241	TQ 23099 41554	2.1	-0.7	
12 Aug 2019	00:46:49.2	51.160	0.241	TQ 23099 41554	2.1	-1.4	
2 Sep 2019	05:13:04.9	51.160	0.237	TQ 23379 41560	2.0	1.1	1
3 Sep 2019	20:19:13.2	51.161	0.237	TQ 23376 41672	2.0	0.2	
6 Sep 2019	07:09:45.5	51.161	0.237	TQ 23376 41672	2.0	1.0	
21 Sep 2019	14:43:45.2	51.160	0.237	TQ 23379 41560	2.2	0.6	
31 Oct 2019	19:25:16.4	51.160	0.238	TQ 23309 41558	2.0	0.8	

Cataloguing here is complete to 27 April 2020. Data are from https://earthquakes.bgs.ac.uk; these earthquakes have been located using standard BGS procedures, as reported by the International Seismological Centre (http://www.isc.ac.uk). Co-ordinate transformations to the British National Grid, as part of this study, use https://www.bgs.ac.uk/data/webservices/convertForm.cfm
Note:
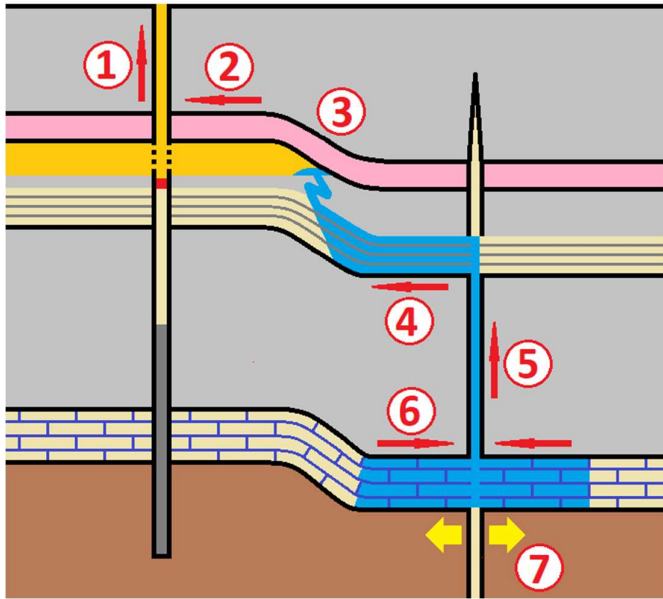1…Felt in Newdigate; maximum EMS intensity 2.
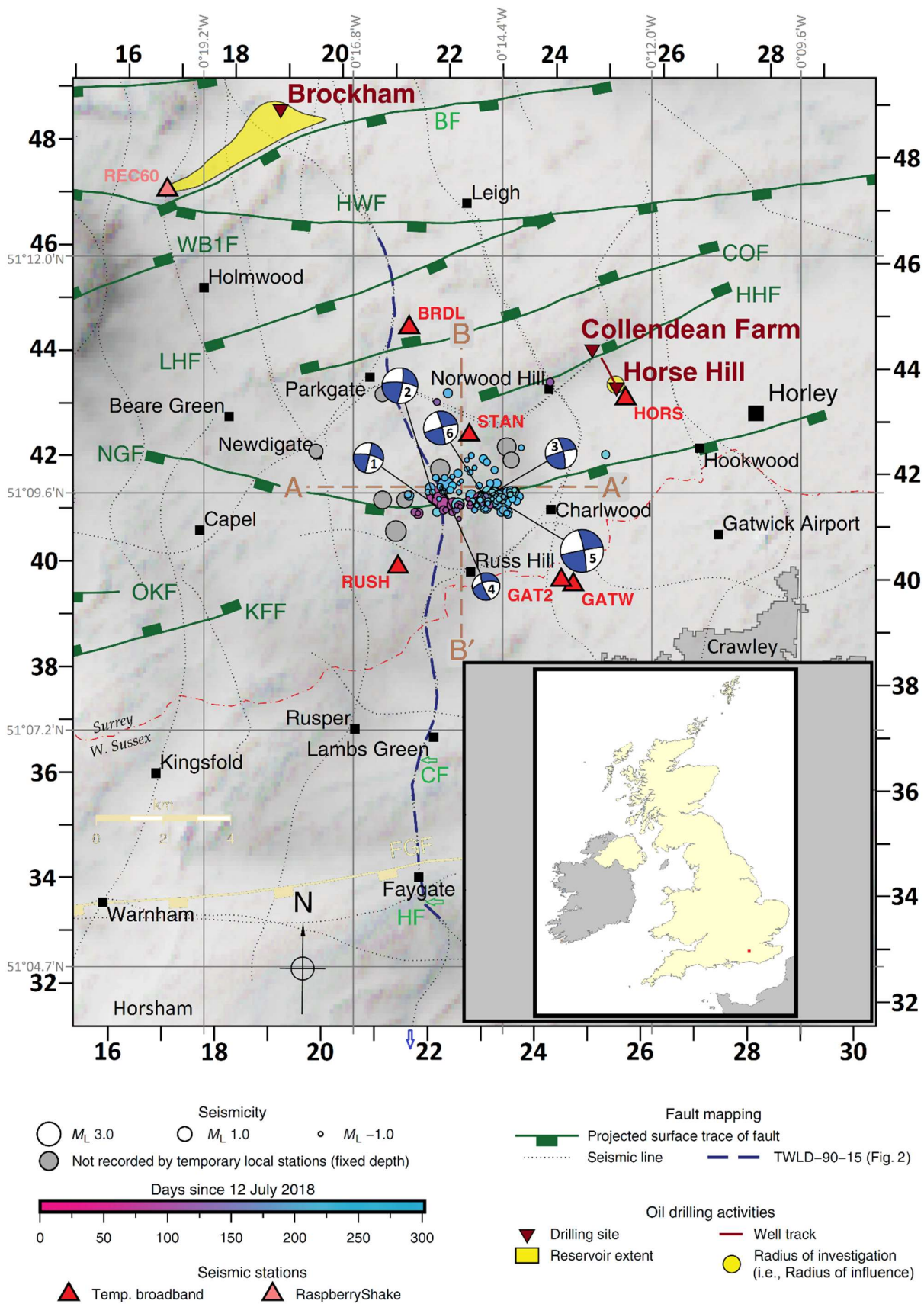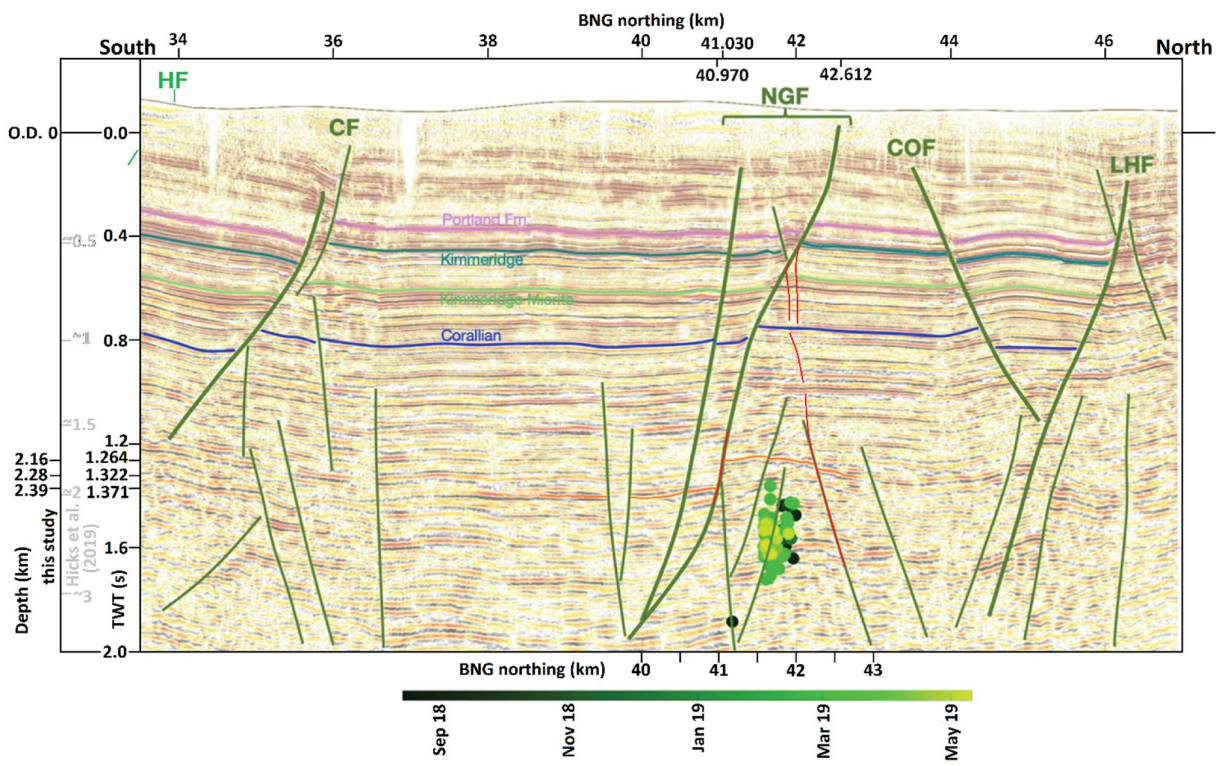
Figure 1

Figure 2

Figure 3

Figure 4

(a)

(b)
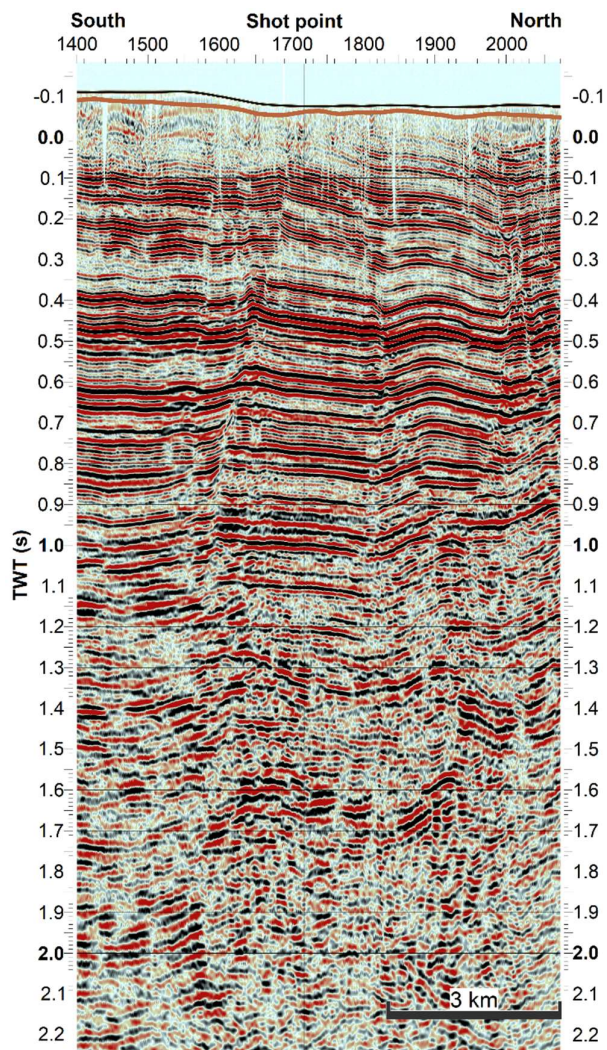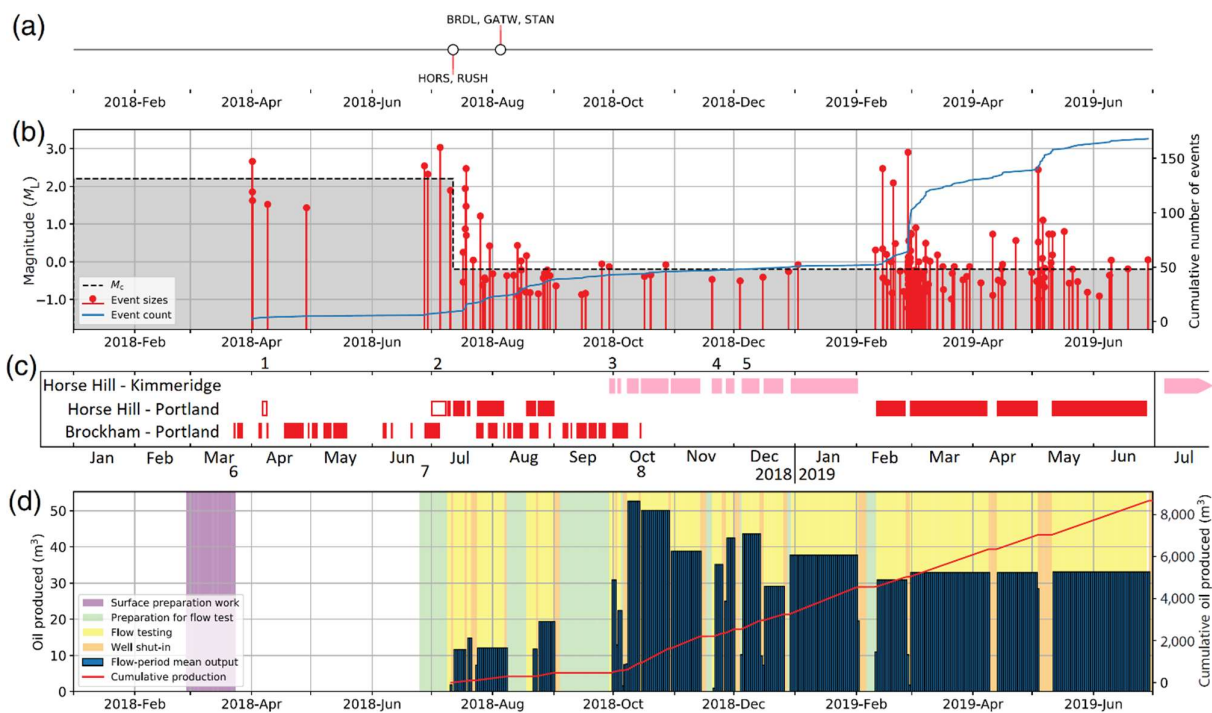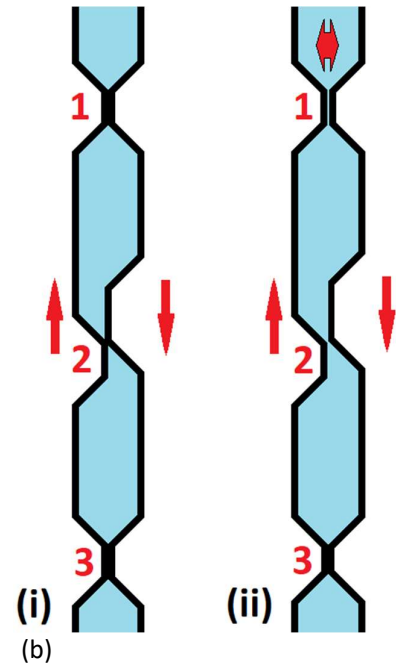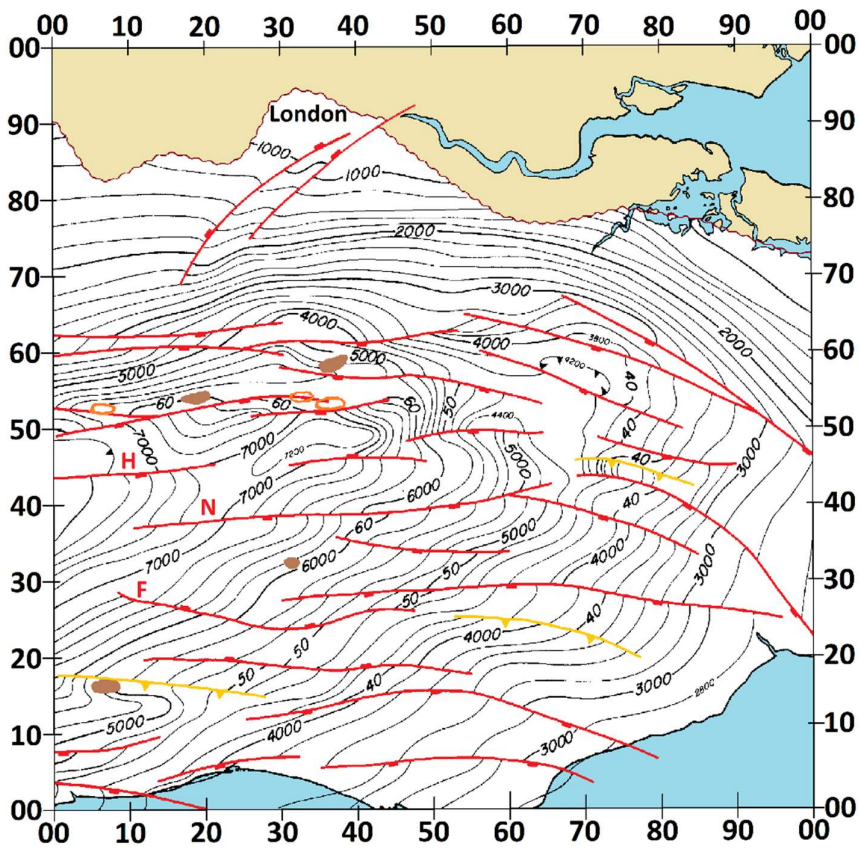
Figure 5

Key:

———— Contours of depth (below O.D.) of base Jurassic

⬤ Area with no Jurassic subcrop   ● Oil accumulation

———— Mesozoic normal fault   ⬭ Natural gas accumulation

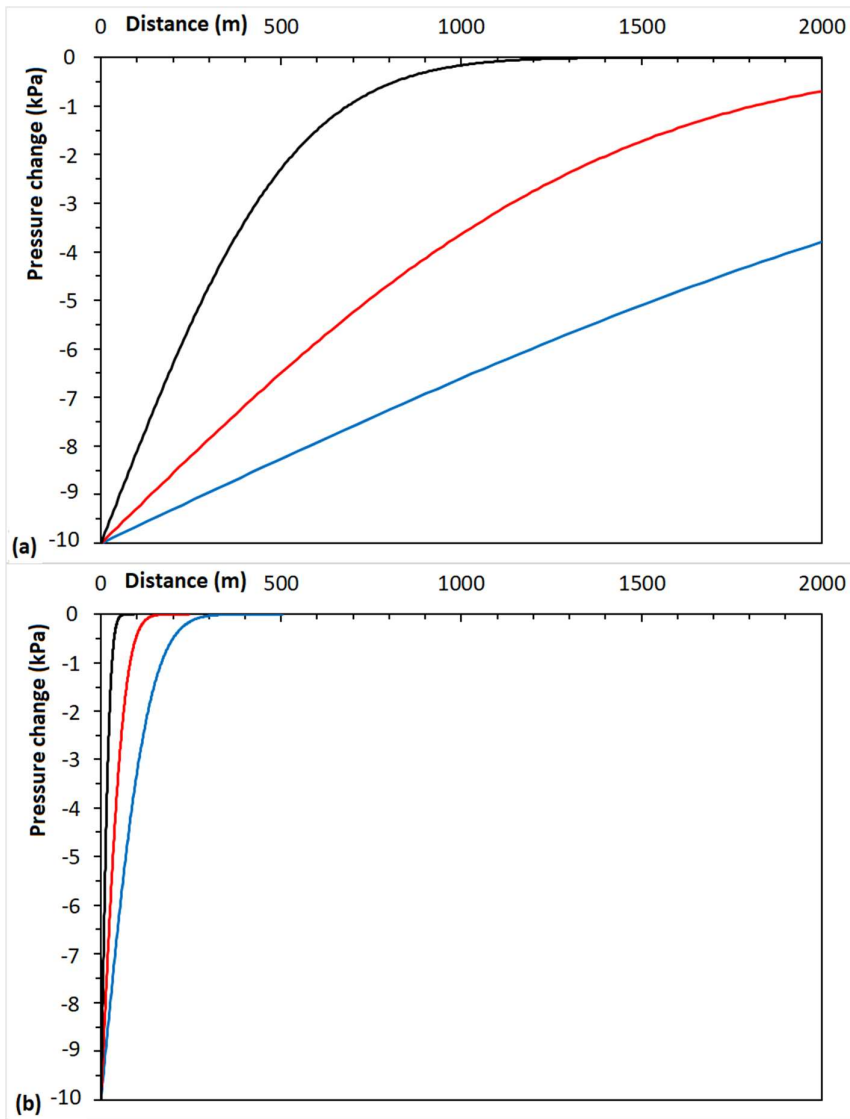———— Mesozoic normal fault with significant Cenozoic reverse slip
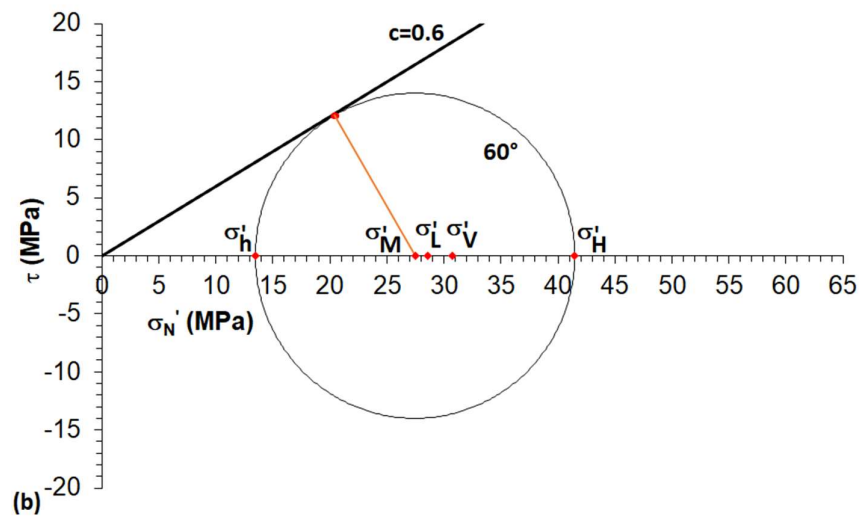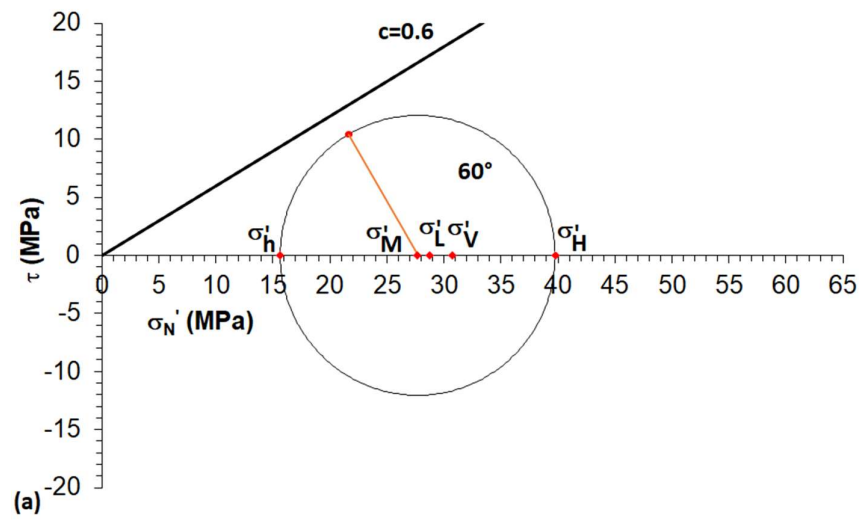
Figure 6

Figure 7

Figure 8

Seismicity at Newdigate, Surrey, during 2018-2019:
A candidate mechanism indicating causation by nearby oil production

Rob Westaway,
James Watt School of Engineering, University of Glasgow, Glasgow G12 8QQ, UK
robert.westaway@gla.ac.uk

Supplementary material

Contents:

1. Reporting of activities in the Brockham and Horse Hill wells

As is evident from the extensive media coverage (e.g., BBC, 2018; Hayhurst, 2018; McLennan, 2019), from the outset, on 1 April 2018, a potential connection between the 'swarm' of earthquakes in the Newdigate area of Surrey and local oilfield activities (in the nearby Brockham and Horse Hill wells) was immediately suspected, but was dismissed by one developer (Hayhurst, 2018a). Concerns about the possibility that activities in these wells were indeed causing these earthquakes were raised through correspondence in The Times newspaper in August 2018 (Gilfillan et al., 2018). A workshop, convened by the Oil & Gas Authority (OGA), followed on 3 October 2018, a summary of its proceedings being reported by OGA (2018), including the statement that '*the workshop participants concluded that, based on the evidence presented, there was no causal link between the seismic events and oil and gas activity although one participant was less certain and felt that this could only be concluded on "the balance of probabilities" and would have liked to see more detailed data on recent oil and gas surface and subsurface activity.*' The workshop presentations included a candidate conceptual model linking the seismicity to site activity, by Haszeldine and Cavanagh (2018), which – its authors admitted – could not be tested at that stage because essential data needed were unavailable. Nonetheless, later in October 2018 the Horse Hill developer issued a communication to local residents, which stated that '*in light of a few misleading and mischievous rumours being circulated, we thought you would appreciate the facts, from the Horse Hill mouth, so to speak. … Following the number of unexplained tremors in Surrey earlier in the year, earthquake-monitoring devices were installed at various nearby locations. A subsequent meeting organised by the OGA with various stakeholders and the British Geological Survey has concluded that there is no link between exploring for hydrocarbons and the tremors. This came as no surprise to us since there was no activity at Horse Hill during the majority of the tremors*' (Horse Hill Developments Ltd., 2018). This was in the context of the developer initiating a planning application to the local authorities for permission to drill five more wells at the site.

By February 2019, additional data regarding the nature and timing of operations at the Horse Hill-1 well had been placed in the public domain. On 5 February Cavanagh et al. (2019) wrote to SCC pointing out the clear correlation between these operations and the Newdigate seismicity and noting other evidence that might reasonably be taken as indicative of a cause and effect connection and was worthy of further investigation. On 12 February, UKOG (2019) wrote a response, which stated that '*in our view Cavanagh et al's document reads more like a protester statement than a serious scientific document*'. UKOG (2019) made many specific criticisms, some of which seem unreasonable. For example, they criticised the application of the Davis and Frohlich (1993) criteria for assessment of whether seismicity is natural or anthropogenic, on the basis that these criteria only apply to seismicity caused by fluid injection, which has not occurred at this site. However, as is well known to subject specialists, these criteria are applicable to anthropogenic seismicity irrespective of its particular mechanism. In any case, Cavanagh et al. (2019) did not refer to Davis and Frohlich (1993), although their previous submission (by Haszeldine and Cavanagh, 2018) did. Haszeldine and Cavanagh (2018) showed that this instance of seismicity satisfies all the criteria for anthropogenic seismicity advocated by

Davis and Frohlich (1993) except one, that a geomechanical mechanism linking the two could not be demonstrated, this being due to a lack of data. Subsequently, Verdon et al. (2019) proposed a new procedure (superseding that by Davis and Frohlich, 1993) for assessing whether seismicity is anthropogenic. Applying these criteria, they reached a strong conclusion that the Newdigate seismicity was a natural occurrence. Several assessments contributed to this conclusion. First, Verdon et al. (2019) claimed that the earthquakes are not correlated in time with well activities, even though Cavanagh et al. (2019) had already shown otherwise. Second, Verdon et al. (2019) claimed that there was no plausible geomechanical mechanism linking the seismicity to well activities. Rather than presenting any geomechanical calculations, they argued this on the basis of the smallness of the fluid volumes involved in the activities at Horse Hill, which they claimed would not affect fluid pressure (and thus, the state of stress) at distances greater than a few hundred metres from the well. They also noted that the seismicity propagated towards the Horse Hill well, whereas if well activities were the cause it would propagate away.

HH-1 April 2018 Re-Completion Operations Sequence

Preparatory Work:

1.

2.

3.
4.

Re-completion operations:

1.
2.
3.

4.
5.
6.
7.
8.
9.
10.
11.
12.
13.
14.

Figure S1. Redacted excerpt from a submission by the Horse Hill developer to OGA detailing the well testing activities to be carried out in 2018, as part of the permitting process (https://www.whatdotheyknow.com/request/513050/response/1369572/attach/3/hhrecomp%20marked%20for%20redaction%20Redacted.pdf?cookie_passthrough=1). This redacted document was released on 21 May 2019 as part of a Freedom of Information request, following a protracted email exchange between the requester and the OGA (see https://www.whatdotheyknow.com/request/horse_hill_request_for_informati6ncoming-1239081 for details). In this case, the redaction was pointless, as an unredacted version (https://brockhamoilwell.files.wordpress.com/2019/04/disclosure-201808357-2.pdf) had been placed in the public domain by 10 May 2019 (see https://drillordrop.com/2019/05/10/latest-earth-tremor-prompts-call-for-release-of-data-on-oil-operations/).

In August 2019 Hicks et al. (2019) published a more detailed analysis of the Newdigate seismicity (Figs 01 and 2). They noted that the propagation deduced previously was an artefact of mislocation, thus undermining part of the evidence that influenced Verdon et al. (2019). Despite, once again, not presenting any geomechanical calculations, Hicks et al. (2019) concluded that '*On balance, and based on the available evidence, we find it currently unlikely that nearby industrial activities induced the seismic swarm*'. This work has been widely reported (e.g., BBC, 2019a), albeit noting that the scientific community is divided over these

conclusions. In early September 2019, the Horse Hill planning application was approved, the media reporting (e.g., BBC, 2019b) noting the issue of seismicity and that this decision might well be subject to legal challenge.

Technical data from the Brockham and Horse Hill sites that are relevant to the present study will now be summarized. Hicks et al. (2019) had access to proprietary information, but the present study has been reliant on public domain sources. These include public announcements by the developers (required to comply with UK law on transparent disclosure of information that can affect valuation of company shares), online postings by objectors to these projects, and documents provided by regulatory authorities. Some of the latter category of document have only entered the public domain as a result of Freedom of Information (FOI) requests, which are possible under UK law as the OGA is a public body; in the process, many such documents have undergone redaction to eliminate information that might supposedly be commercially sensitive (as in Fig. S1).

Brockham
The first well at Brockham, Brockham 1 (BGS ID TQ14NE95, at TQ 18832 48653), was drilled in 1987. The oil reservoir is in the uppermost ~3 m of the Portland Upper Sandstone, its top at 570 m TVDSS (Angus, 2018), or ~622 m below local ground level. At the October 2018 workshop it was reported (https://www.ogauthority.co.uk/media/5160/7c-angus-maps-for-oga-meeting.pdf) that production up to 2016 in this field had amounted to ~490,000 barrels of fluid. Approximately 62,000 barrels of formation water had been re-injected, making net production ~428,000 barrels or ~68,000 m^3 (Angus, 2018, stated 36,900 m^3, this figure presumably excluding produced water). During this production, the reservoir pressure decreased from ~900 to ~500 psi, a decrease by ~400 psi or ~3 MPa. At this time, and following the subsequent resumption, production was from well Brockham X2Y (BRX2Y; BGS ID TQ14NE141; at TQ 18850 48660), a sidetrack off the original Brockham X2 or BRX2 well (BGS ID TQ14NE136, drilled in 1998), which was left shut in when production ceased in 2016. Water injection to maintain this production has been into well Brockham X3 (BRX3; BGS ID TQ14NE139; drilled in 2007 as a sidetrack from well Brockham-1). Well Brockham X2Y is deviated SW from the wellhead, achieving a ~600 m separation between production and injection (Angus, 2018). Well Brockham X4 (BRX4; BGS ID TQ14NE137; at TQ 18841 48650) was also drilled in 2007. Subsequent events at this site are recorded through press releases by its operator (http://www.angusenergy.co.uk/media/news/; see also https://www.ogauthority.co.uk/media/5159/7b-angus-earthquake-summary-report.pdf), a document outlining the plans for the site, released under a FOI request (Angus, 2018), and online postings by objectors (e.g., https://drillordrop.com/brockham-surrey/). Thus, in November 2016 the developer obtained an environmental permit to drill a sidetrack (called BRX4Z) from well BRX4, to test and potentially produce from the deeper Kimmeridgian and Corallian formations; drilling took place in January 2017. However, no planning permission was obtained; the operator stated at the time that it was covered by existing planning consents, even though this existing permission (https://planning.surreycc.gov.uk/planappdisp.aspx?AppNo=2007/0443) makes no mention of any sidetrack from this well. Pending resolution of this planning dispute, work on testing sidetrack BRX4Z was suspended.

On 23 March 2018, production from well BRX2Y resumed from the Portland reservoir, as indicated in Fig. 4. From Hicks et al. (2016), ~4.0 m^3 (~25 barrels) of oil were produced on 23 March followed by ~1.1, ~0.9 and ~1.0 m^3 (~7, ~6 and ~6 barrels) on 25-27 June, the latter accompanied by water injection. Production during subsequent months was intermittent (Fig. 4), including ~2.7 m^3 (~17 barrels) on each of 7 and 8 June, ~2.1 m^3 (~13 barrels) on 11 June, and ~1.6 m^3 (~10 barrels) on 21 June. As detailed in Fig. 4, fluid injection occurred on 26 June, the day before the first earthquake of the second 'cluster', followed by renewed production, but the detailed schedule for these actions has not been placed in the public domain. On 8 August 2018 the developer's retrospective application for planning permission to legitimate sidetrack BRX4Z was approved (https://planning.surreycc.gov.uk/planappdisp.aspx?AppNo=SCC+Ref+2017%2f0215); production from BRX2Y ceased in October 2018 (Fig. 4) as work at the site switched to testing this sidetrack.

Horse Hill
The Horse Hill 1 well (HH1; BGS ID TQ24SE93; at TQ 25255 43600) was drilled in 2014. It was logged to its original total depth (Table 1), before being plugged below the Kimmeridgian. Flow testing in 2016 attracted media attention as the 'Gatwick Gusher'. A press release

(http://otp.investis.com/clients/uk/solo_oil/rns/regulatory-story.aspx?cid=983&newsid=1054418; see also https://www.lse.co.uk/rns/UKOG/horse-hill-1-flow-test-yjc35j83vlmcg7a.html) reported that for this testing this well had been perforated over a 35 m interval in the Portland reservoir, ~615 m below ground level, from which oil production at 323 bopd was maintained over an 8.5 hour period. Xodus (2018) noted that to achieve this production rate required acid stimulation of the reservoir, which created a permeability of ~2 mD (mean) to ~20 mD (maximum). Testing in the Kimmeridgian involved two 30 m perforated intervals, centred at depths of 840 and 900 m, in the Kimmeridge Limestone 4 (KL4) and Kimmeridge Limestone 3 (KL3) units. Production rates during testing in 2016 were of 901 bopd from KL4 and 464 bopd from KL3, during short (4-7.5 hour) flow periods. According to UKOG (2019), following this testing, the well was left in a 'suspended' state, with three pressure-tight bridge plugs set, one above each of the intervals that had been tested (see also Horse Hill Developments Ltd., 2018b).

When the seismicity began on 1 April 2018, a potential connection with the HH1 well was immediately suspected. As has been reported (https://drillordrop.com/2018/04/04/oil-company-says-were-not-to-blame-for-surrey-earthquake-but-local-concerns-remain/), the developer issued this statement '*We strongly refute the far-fetched, unscientific and malicious connection made between Horse Hill and the earthquake in Surrey on April 1st. … There is no drilling, testing or underground works taking place at Horse Hill or at any of our sites at present. All such work at Horse Hill ceased over two years ago.*' OGA (2018) later summarized the activity involving this well thus: '*Subsurface operational activity at the Horse Hill 1 site included a flow test in 2016 of 1940 bbls of oil from the Portland and Kimmeridge zones combined, but then activity ceased until 3 July 2018 when the extended well test of the Portland began, long after the first seismic event on 1 April 2018.*' … '*There is no annular pressure evidence of impaired wellbore integrity in the Horse Hill 1 well because of the seismic events, nor evidence of migration of gas outside the wellbore between different zones. The strata are normally pressured and at formation pressures all gas is solution gas and there is no free gas.*' … '*Flow testing at Horse Hill 1 well created pressure drawdown but the radius of influence is small (~200-1000m).*' A summary of the operations at the well, provided by its operator for the October 2018 workshop (https://www.ogauthority.co.uk/media/5168/6-horse-hill-development-limited-operational-summary-of-activity-at-horse-hill-1-wellsite.pdf), indicated that no activity took place between March 2016, when the well was perforated and the aforementioned flow testing was carried out, and June 2018. However, some of the entries in this record are truncated, so the full information cannot be read. This document anyway proved incomplete, requiring OGA (2018) to add as a footnote that prior '*to the recent commencement of the Horse Hill 1 testing in 2018, there had been no sub-surface work at the Horse Hill site since 18 March 2016. Surface activity included the excavation of a nearby new cellar starting on 21 March 2018 using a JCB for a future well and the site was visited by tankers to remove rainwater collected above the impermeable layer. Well integrity tests were conducted by checking annular pressures on 5-6 April 2018. No pressure was detected in either annuli and pressure tests were satisfactory. A workover crane arrived on site on 25 June 2018 in preparation for flow testing and the well was re-entered on 3 July 2018 and the retrievable bridge plug was removed from the well to test the Portland Sandstone. No injection was done, but liquids were drawn out of the well using a downhole pump. On 17 August 2018, a 113 ft interval in the well was perforated using a Geodynamics tool with 6 shots per foot and charges of 39 gm. The modelled stressed rock penetration is 18 inches from this activity.*'

UKOG (2019) added: '*A cursory glance … at publicly available information from the Health and Safety Executive would have revealed that the hydrocarbon bearing horizons in the well were completely isolated from the surface by three pressure tight plugs, as would be the case for any well suspended for future operations. The shallowest plug above the Portland was subsequently removed during operations in July 2018, the deeper plugs above Kimmeridge Limestone 3 and 4 were removed some months later. Therefore, there was no communication to the surface within the well until testing operations commenced.*'

Documents reporting on activities affecting the HH1 well in 2018 include the developer's application to recomplete the well (https://www.whatdotheyknow.com/request/513050/response/1427741/attach/3/Re%20Completion%20Application%20WONS%2010944%200%20RC%201%20Version%201%20LR%2024%204%20Redacted.pdf)

and   associated   supporting   material
(https://www.whatdotheyknow.com/request/513050/response/1369572/attach/2/ewtapp%20marked%20for%20redaction%20Redacted.pdf?cookie_passthrough=1;
https://www.whatdotheyknow.com/request/513050/response/1369572/attach/3/hhrecomp%20marked%20for%20redaction%20Redacted.pdf?cookie_passthrough=1). However, although these documents report some details, such as the design of the test string to be used in the Portland reservoir, overall they have been heavily redacted, as in Fig. S1.

Cavanagh et al. (2019) reported that prior '*to flow testing in April and July, Horse Hill appears to have encountered a natural source of overpressure in the … Kimmeridge, as observed in the 'gas lift' reported for the well. We infer that management of this pressure (probably by bleeding the well annulus prior to testing) likely altered the … stress balance, which then impacted on the Newdigate fault, causing the earthquakes.*' … '*Freedom of Information requests and social media posting from the fenceline of Horse Hill clearly indicate that well preparations for flow testing immediately precede the Newdigate earthquakes. We infer that the Horse Hill well and site engineering logs (not released at this time for scrutiny) may provide additional information on well intervention pressure changes as the trigger for the 2018 Newdigate cluster.*'
In response to this claim, UKOG (2019a) wrote that '*the annulus pressure bleed-off cited by Cavanagh et al. relates to the annulus above the pressure tight plug set above the Portland, i.e. in the shallow part of the well inside unperforated steel casing that is isolated from the oil-bearing sections below. This is standard safety practice for all wells to ensure there is no build up of any biogenic gas from bacterial action in the near surface section. The annular bleed off, amounting to a few tens of psi, therefore, has no physical connection with anything in the deeper isolated oil bearing section below.*'

The above-mentioned report by UKOG (2019a) that there was some pressure change in the well is at odds with the report by OGA (2018) that '*no pressure was detected*'. There has been no subsequent disclosure of pressure data, despite an FOI request. There has also been no disclosure regarding the integrity of the bridge plug that isolated the Portland reservoir from the surface, ahead of its removal on 4 July 2018 (as reported by https://www.ogauthority.co.uk/media/5168/6-horse-hill-development-limited-operational-summary-of-activity-at-horse-hill-1-wellsite.pdf). Regarding the Cavanagh et al (2019) account, as part of the present study no FOI request or social media posting has been identified that establishes any intervention in the well before 1 April 2018. As noted above, the first reported intervention in the well was the measurement of pressure starting on 5 April 2018 (OGA, 2018). According to the published log of site activities (https://www.ogauthority.co.uk/media/5168/6-horse-hill-development-limited-operational-summary-of-activity-at-horse-hill-1-wellsite.pdf), the first intervention in the well ahead of the July 2018 flow testing in the Portland reservoir occurred on 1 July 2018, when it is reported that flow was circulated around the well (presumably its upper part, above the Portland bridge plug).

It has been suggested (Hayhurst, 2019) that the Horse Hill-1 well became pressurized while suspended between 2016 and 2018 and this pressure was released when activity at the well site resumed in the spring of 2018, potentially having an effect on the seismicity at this time. The state of this well during this suspension has been reported by Horse Hill Developments Ltd. (2018b); as they have indicated, the interval of the well open to the Portland reservoir was at this time isolated from the shallow part of the well by a removable bridge plug. This would mean that for any pressure change in the shallow part of the well (potentially caused by activity at the well pad) to affect the Portland reservoir would require this bridge plug to have failed. As already noted, this bridge plug was removed on 4 July 2018; the Portland reservoir at this site was thereafter hydraulically connected with the surface in this well.

During the phase of production in well HH1 from the Portland reservoir, the developer reported rates of 140-160 bopd, plus gas production rates of an additional ~50 bpd before the gas separator, equivalent to ~15000 cubic feet per day or ~425 m^3 per day at standard pressure (https://www.lse.co.uk/rns/UKOG/uk-oil-and-gas-plc-ewt-updates-portland-and-kimmeridge-oil-discovery-gzgkrfuq4fzq6lq.html). During this testing, the developer reported sustained pumping with stable bottom hole pressures of ~200 psi (~1.4 MPa) below the initial reservoir pressure of ~915 psi (~6.3 MPa), and that bottom hole pressures recovered rapidly back to

initial reservoir pressure during periods of shut-in, indicating good connectivity within the oil pool in the Portland reservoir.

On 10 September 2018 the operator announced (https://www.lse.co.uk/rns/UKOG/uk-oil-and-gas-plc-ewt-updates-portland-and-kimmeridge-oil-discovery-gzgkrfuq4fzq6lq.html) that the flow testing of the Portland reservoir had ended and work was under way to re-complete the well to test the Kimmeridgian reservoirs. It is inferred from this announcement that this phase of flow testing ended around the end of August 2018, the precise date having not been reported. An additional ~4 m of perforated section had been created in the well, resulting in a sustainable production rate estimated as 362 bopd. On 5 October 2018, the operator announced (https://www.lse.co.uk/rns/UKOG/uk-oil-and-gas-plc-extended-well-test-and-regulatory-update-xgqw1sw82jyk4k1.html) that analysis of the testing established that this well is in hydraulic connection with a Portland reservoir of 7-11 million barrels of oil. This was considered a commercial discovery, although rather less than the range of estimates of 20-44 million barrels deduced from modelling of the original flow testing in 2016 (Xodus, 2018). This was followed by an announcement on 10 October (https://www.lse.co.uk/rns/UKOG/uk-oil-and-gas-plc-ewt-update-horse-hill-1--xa4zpctdu1tpii9.html) that an initial 50 hour flow test from the KL3 reservoir had been completed. Flow rates of up to 771 bopd were attained, significantly higher than in 2016. A subsequent announcement (https://www.lse.co.uk/rns/UKOG/uk-oil-and-gas-plc-kimmeridge-oil-production-continues-at-hh-1--5g16kgournvimc5.html) reported that production from the KL4 reservoir began in late November, the sustainable production rate being 300 barrels of oil per day, and that simultaneous pressure measurements established that the KL3 and KL4 reservoirs are hydraulically connected. As a result, it was decided to produce from both sources together, which began on 4 December.

Early on 18 February 2019, the developer announced (https://www.lse.co.uk/rns/UKOG/uk-oil-and-gas-plc-portland-oil-production-resumes-at-horse-hill-1zdan7c12i5yeog.html) that production had ceased from the Kimmeridgian reservoir and had resumed from the Portland reservoir. The developer appeared to have not announced the exact date, but it is reported as 11 February 2019 in Fig. 4(d), from Hicks et al. (2019). The announcement of resumed Portland production included the statement '*For prudent reservoir management purposes, the average test production rate from the 114 ft vertical perforated Portland section has been maintained below the previously reported 362 bopd calculated optimised sustainable rate.*' An online comment on this (https://drillordrop.com/2019/02/18/oil-production-updates-for-horse-hill-and-lidsey/), included '*Hmmm…..Prudent reservoir management purposes? No worries about changing the pressure enough to cause further earthquakes then?*' The reservoir pressure draw-down at this time was described as 'modest' (https://www.lse.co.uk/rns/UKOG/uk-oil-and-gas-plc-horse-hill-1-production-test-update-eyt2n45v64zsvqx.html), although with no quantitative information. Production from the Portland reservoir ceased for 60 hours in mid April (https://www.lse.co.uk/rns/UKOG/uk-oil-and-gas-plc-oil-production-test-update--diew7rpxvbd4576.html), before resuming at a steady 220 bopd through into May, when it was announced (https://www.lse.co.uk/rns/UKOG/uk-oil-and-gas-plc-horse-hill-1-production-test-update-eyt2n45v64zsvqx.html) that it would cease in June and resume in the Kimmeridgian reservoir, in order to permit safe drilling of new Horse Hill-2 (HH2) well through the Portlandian succession (https://www.lse.co.uk/rns/UKOG/uk-oil-and-gas-plc-horse-hill-1-production-test-update-8mg2yi5vjywnu71.html). Production from the Portland ceased in late June, when the volume produced reached 29568 barrels (equivalent to ~4700 m^3), and resumed in the Kimmeridgian on 6 July (https://www.lse.co.uk/rns/UKOG/uk-oil-and-gas-plc-horse-hill-1-50000-barrels-of-oil-production--xd4jh1jjpiw92j9.html; https://www.lse.co.uk/rns/UKOG/uk-oil-and-gas-plc-horse-hill-1-production-test-update-8mg2yi5vjywnu71.html).

On 30 September the start of drilling of well HH2 was announced (https://www.lse.co.uk/rns/UKOG/hh-2-2z-drilling-commences-spud-at-horse-hill-aw1qz6dh9uts74p.html) This vertical pilot well was drilled to ~900 m depth and logged, concentrating on the Portlandian section, to optimize the design of a side track in the Portland reservoir to be known as Horse Hill 2Z (HH2Z), before being plugged back to the kick-off point for this lateral. Well HH2Z has been designed with a total length of ~5,800 ft (~1800 m) from the surface, with a ~1000 m horizontal section in the most productive zone of the Portland reservoir. The aim of this long

production interval is to achieve much higher production rates than are feasible from the Portland reservoir using HH1. By 8 October, drilling of well HH2 had reached a depth of 615 m, near the top Portlandian, with preparations under way to recover core (https://www.lse.co.uk/rns/UKOG/drilling-update-horse-hill-lx7s8ddu8e14cc8.html). The lateral, well HH2Z, was duly completed in November 2019 (https://www.lse.co.uk/rns/UKOG/hh-2z-completed-horse-hill-7qxv12c1g58vjb2.html). Flow testing took place in December 2019, ending by 18 December, when a maximum rate of fluid production of 1087 bpd was achieved (https://www.lse.co.uk/rns/UKOG/hh-1-and-hh-2z-extended-well-test-update-xjk6frv4uqebsr1.html), indeed much higher than the maximum rate from well HH1. Production at this site then switched back to the Kimmeridgian reservoir in well HH1.

The production figures reported by Hicks et al (2019) in Fig. 4 are not consistent with the above-mentioned values reported by the developer. For example, during the initial Portland testing phase for well HH1 in July-August 2018, Hicks et al (2019) reported the maximum production rate as 19.4 m^3 per day or 122 bopd (Fig. 4(d)), whereas the developer reported rates of 140-160 bopd, plus the aforementioned gas production (https://www.lse.co.uk/rns/UKOG/uk-oil-and-gas-plc-ewt-updates-portland-and-kimmeridge-oil-discovery-gzgkrfuq4fzq6lq.html). During the February-June 2019 phase, Hicks et al (2019) reported the maximum production rate as 33.0 m^3 per day or 207 bopd (Fig. 4(d)), whereas the developer reported a steady rate above 220 bopd (https://www.lse.co.uk/rns/UKOG/uk-oil-and-gas-plc-horse-hill-1-50000-barrels-of-oil-production--xd4jh1jjpiw92j9.html). No attempt is made here to resolve discrepancies such as these.

2. Geolocation issues

The study area has been illustrated using the map (Fig. 01), and seismic cross-section (Fig. 2) from Hicks et al. (2019). However, the original versions of both these figures have required significant amendment regarding accuracy issues. These aspects will now be discussed. The issues covered include the scaling and the depictions of faults and seismic lines for Fig. 01, and the vertical and horizontal geolocation of Fig. 2.

First, the original version of the map, presented by Hicks et al. (2019), had a scale bar that was too small and thus gave a misleading impression of the distance between the Horse Hill-1 and Brockham wells and the seismicity. The original scale bar is shown 'greyed out' in Fig. 01. This map also shows seismic lines. The source of information for positions of seismic lines, including line TWLD-90-15 that is illustrated in Fig. 2, was not reported by Hicks et al. (2019); it is evident that they are from the UK Onshore Geophysical Library (OGL; https://ukogl.org.uk/) location map, which is itself indexed to the BNG, so the information provided therein must have been transformed to geographical co-ordinates by Hicks et al. (2019). Moreover, the OGL index map is highly schematic and so cannot be used for accurate location, although careful comparison of it with definitive maps can indicate the routes followed by seismic lines along roads and rural tracks and, thus, indirectly provide accurate location.

Faults
Hicks et al. (2019) explained (in Note S6 of their online supplement) that (rather than using the existing literature) they located faults in the study area through their own analysis of 2-D seismic reflection profiles, including making their own interpretations of how to interpolate faults between these profiles. Where points of comparison are available, Fig. 01 can be seen to lack accuracy. For example, definitive geological maps (available online via BGS Digimap) and the structural map available as Fig. 22 of Gallois and Worssam (1993) indicate that there is no significant fault at the position indicated in Fig. 01 for the 'Faygate Fault'. The Holmbush Fault crosses seismic line TWLD-90-15 at BNG reference TQ 21766 33846, south of the village of Faygate and also south of the intersection with the east-west seismic line depicted in Fig. 01 south of this village, which follows the main road (the A264) between Crawley and Horsham. The depiction of this fault by BGS Digimap is consistent with that by Gallois and Worssam (1993): at outcrop it has modest upthrow to the south (as a result of reverse slip during the Cenozoic basin inversion) and separates the Early Cretaceous (Valangian) Tunbridge Wells Sand Formation (https://www.bgs.ac.uk/lexicon/lexicon.cfm?pub=TWS) to the south from the younger (Hauterivian-Barremian) Weald Clay Formation (https://www.bgs.ac.uk/lexicon/lexicon.cfm?pub=WC) to the north. This geological boundary corresponds to the transition in the landscape from the 'Low Weald' in the Weald Clay, which is mostly agricultural land,

to the 'High Weald' in the Tunbridge Wells Sand, which is forest and heathland, and is unequivocal. Initial attempts to correctly geo-locate the information presented by Hicks et al. (2019) assumed that their 'Faygate Fault' is in fact the Holmbush Fault but was depicted by them in Fig. 01 several hundred metres too far north.

A further difficulty concerning Fig. 01 is that according to both Digimap and Gallois and Worssam (1993) seismic line TWLD-90-15 crosses another significant fault, the Crawley Fault, at BNG reference TQ 21657 36444, just south of the village of Lamb's Green. However, no fault is depicted in this vicinity in Fig. 01.

Another significant issue affecting Fig. 01 concerns the faulting in the vicinity of the Brockham well; here, too, Hicks et al. (2019) have proposed a reinterpretation of the structure rather than familiarizing themselves with the established interpretation, from documentation provided for the petroleum licensing process (e.g., Europa, 2004). Thus, in Fig. 01, the Brockham oil reservoir is depicted as separated from the source area of the Newdigate earthquakes by two faults, the Brockham and Holmwood faults, both with downthrow to the south (Fig. 01). In contrast, the definitive interpretation (Europa, 2004), envisages the structure rather differently. In their view, as the Holmwood Fault approaches the Brockham Fault from the east, it bends to WNW strike, joining the Brockham Fault circa TQ 17520 47483. Furthermore, although the Holmwood Fault has substantial downthrow to the south in older deposits, at the stratigraphic level of the top Portland Sandstone the downthrow is reversed, due to the effect of Cenozoic reverse-slip reactivation, but its throw is small, circa 10 ms in terms of TWT. A subsidiary normal fault splays WSW from the Holmwood Fault circa TQ 18991 46988, but has a similar small offset at the level of the top Portland Sandstone and dies out circa TQ 16163 46416. The Brockham Fault bends around the southern end of the Brockham oil reservoir, located within the Upper Portland Sandstone, before resuming westward strike, with a subsidiary normal fault splaying WSW from it circa TQ 15961 47458. Thus, between TQ 17520 47483 and TQ 15961 47458, a distance of ~1.5 km, the top Portland Sandstone is offset by ~40 ms in terms of TWT.

Seismic section – horizontal scale
Regarding the horizontal scale of Fig. 2, the clearest indication of an apparent lack of accurate geolocation by Hicks et al. (2019) is again provided by the position of their 'Faygate Fault'. With the horizontal scale used by Hicks et al. (2019), this fault projects to the surface at a point ~11 km from the northern end of the profile, whereas when Fig. 01 is correctly scaled and the fault positioned in the correct place it is ~13 km from this northern end. The southern end of the profile is also much closer to this fault as depicted in Fig. 01 than in Fig. 2.

Having noted these difficulties, an initial attempt was made to rectify them by correctly geo-locating Fig. 2. Figure 2 shows seismic line TWLD-90-15; from OGA records, this was shot in 1990 using Vibroseis, with 12.5 m shot spacings, its overall length of 24.55 km spanning shot points 112 to 2078. However, the seismic section depicted is clearly shorter than the total length of the seismic line and thus does not necessarily reach either of its ends. Nonetheless, checking against the OGA index map and its schematic locations to actual locations on real roads indicates that the northern end of Fig. 2 does in fact coincide with the northern end of the seismic line, at shot point 2078, located using the OGA index map at BNG reference TQ 20322 46930 (at Gad Brook Bridge, Bunce Common). However, to position and scale Fig. 2 correctly, using this constraint, another point of reference is needed. After trying multiple options, a provisional geo-location of Fig. 2 was achieved as follows. A clear feature of Fig. 2 is the section of it that has been muted, in a location ~600 m north of the surface trace of the Faygate Fault. This part of the seismic line was shot along a minor road that heads northward through the village of Faygate, crossing over the Crawley-Horsham railway on a bridge (at BNG reference TQ 21777 34426). When shooting seismic lines in the UK, it is standard to skip Vibroseis shot points that would otherwise endanger sensitive infrastructure, such as railway bridges and their approach embankments; it is inferred that this was done in this particular instance. Using the OGL index map (which shows shot points with numbers that are multiples of 100) and definitive local maps, from Digimap, the shot point that was muted was tentatively identified as number 1034, making this point 13050 m from the northern end of the seismic line. Provisional horizontal scales could thus be added to Fig. 2, a first one assuming that the seismic line runs due north-south. A second scale is also added, showing the shot point

numbers, which can be used to locate other points on the profile, by interpolating between the known co-ordinates of adjacent shot points with numbers that are multiples of 100. This provisional attempt at geo-location is illustrated in Fig. S2.
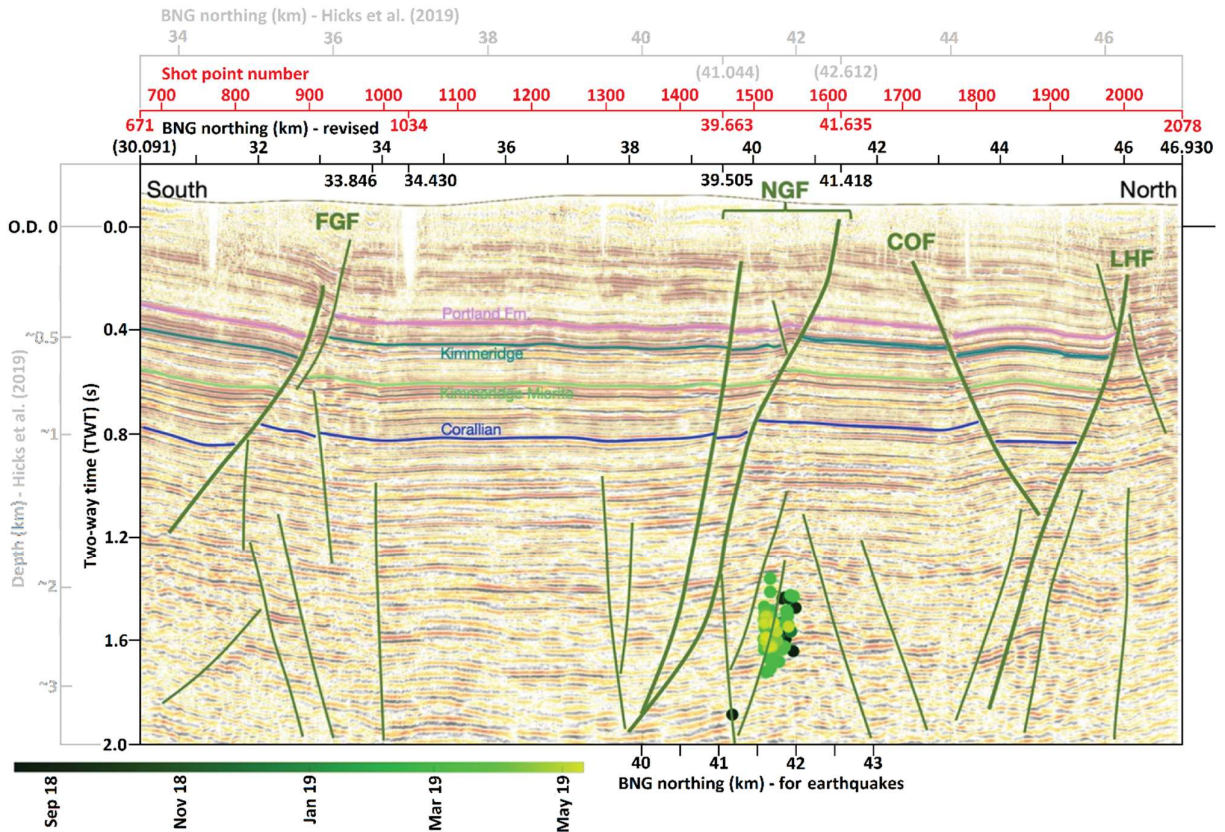

Figure S2. Seismic section along seismic line TWLD-90-15, modified from Fig. 6 of Hicks et al. (2019), annotated to facilitate the attempt, discussed in the supplementary text, to try to reconcile the position of the 'Faygate Fault', depicted here, with the depiction of the same fault in Fig. 01. The original was indexed to the British National Grid (BNG), rather than the geographical co-ordinates used for Fig. 01; the co-ordinates reported by Hicks et al. (2019) have been 'greyed out'. New co-ordinates have been added, based on geo-location of features in the seismic section and by counting the shot points, as described in the text. Further consideration, including inspection of the original seismic section and metadata from UKOGL, established that the 'Faygate Fault' (FGF), depicted here, is the Crawley Fault of previous authors (e.g., Gallois and Worssam, 1993), and this fault was depicted by Hicks et al. (2019) in the wrong place in Fig. 01.

To test this geo-location, the resulting co-ordinates of the Newdigate Fault (the structure associated with the 2018-2019 seismicity, according to Hicks et al., 2019, as already noted) were calculated at the Earth's surface and at a point on its footwall cutoff at a two-way time (TWT) of 1.264 s. Using the shot point co-ordinates gave TQ 22031 41635 and TQ 21884 39663 as the BNG references of these two points, whereas approximating the seismic line as straight, due north-south, gave TQ 22085 41418 and TQ 21917 39505. Conversely, the original interpretation of the seismic section by Hicks et al. (2019) placed these two points circa TQ 21426 42612 and TQ 22162 41044. The two provisional revised geo-locations are consistent to within a margin of ~200 m in this locality and, if correct, would indicate that Hicks et al. (2019) placed this fault ~1 km too far north. Extrapolation on the basis of counting shot points places the southern end of the excerpt of seismic line TWLD-90-15 in Fig. 2 at shot point 671, with co-ordinates TQ 21694 30698. The alternative extrapolation, assuming that the excerpt is oriented north-south, places its southern end at TQ 21194 31091. Because this southerly part of the seismic line includes a number of significant changes in direction, as it follows forest tracks through the High Weald, the extrapolation by counting shot points is likely to be the more accurate of the two.

Given the need to check this apparent mislocation, imagery and metadata for seismic line TWLD-90-15 were obtained from the UKOGL/Beneath Britain archive. The metadata included a list of shot point co-ordinates and excerpts from large-scale maps showing the surveyed location of the seismic line. However, as will become clear, these two forms of metadata are not consistent, with discrepancies of up to ~100 m; the map has been assumed to be definitive. It was thus established that the northern end of the excerpt depicted by Hicks et al. (2019) is indeed of the northern end of the seismic line, ending at shot point 2078. The co-ordinates of shot point 2076 are reported as TQ 20358 46937. However, if this were so, the seismic line would have run ~30 m east of the road in Bunce Green, through a row of houses, rather than along the road. The true northern end of the line appears to be at Gad's Bridge, circa TQ 20326 46935.

The muted section of the seismic line, thought in the tentative geo-location process to be at Faygate, turned out to be at shot point 1224. Shot point 1221 was reported at BNG reference TQ 21785 36777 but this point is ~100 m NW of the road followed by the seismic line through Lamb's Green. The UKOGL location map also shows the seismic line too far to the west, but from it the correct location of shot point 1200 can be estimated as circa TQ 21734 36513. It follows that shot point 1224, where the section is muted, is ~300 m farther NNE, so circa TQ 21915 36771.

The southern end of the Hicks et al. (2019) excerpt of the seismic section turns out to be circa shot point 921. Shot point 930 was reported at BNG reference TQ 22332 33383, from which the position of shot point 935 can be estimated as TQ 22404 33297. This is near, roughly 200 m south of, the position estimated by Hicks et al. (2019), which is circa BNG northing 33500. To this margin of uncertainty, it can be seen that this end of the seismic section is depicted in the correct place in Fig. 01.

The structure named by Hicks et al. (2019) as the 'Faygate Fault' projects to the Earth's surface in the vicinity of shot point 1171. Taking shot point 1200 at TQ 21734 36513, as before, the position of shot point 1171 can be estimated as circa TQ 21546 36256. On this basis it can be seen that the BNG northing co-ordinates provided by Hicks et al. (2019) for the surface projection of their 'Faygate Fault' is circa 36300. Overall, it is therefore concluded that the seismic section in Fig. S2 was in fact accurately geo-located by Hicks et al. (2019). Any mislocation is small, no more than ~200 m, and would be difficult to improve upon given the uncertainty in the reported shot point co-ordinates for this seismic line. However, the realisation that their 'Faygate Fault' projects to the Earth's surface in the same place as the previously recognized Crawley Fault (surface trace on seismic line at TQ 21657 36444; see above) means that these faults are one and the same; the name Crawley Fault should be given precedence. Moreover, the surface trace of the 'Faygate Fault' in Fig. 01 is depicted >2 km south of its position by Hicks et al. (2019) in Fig. S2.

The Holmbush Fault can be recognized on the OKOGL version of the record section for seismic line TWLD-90-15 at shot point 971, although the small throw on this fault in the shallow subsurface makes it near the limit of seismic resolution. The co-ordinates of shot point 971 are listed as TQ 21966 33725; this point is on the route taken by the seismic line, but ~200 m ESE of the outcrop of the fault as recognized by Digimap and by Gallois and Worssam (1993). The position of this fault is labelled on Fig. S2 and Fig. 2, the image presented by Hicks et al. (2019) being less clear than that from UKOGL.

The excerpt of seismic line TWLD-90-15, provided in Fig. R to illustrate the structure of the Newdigate Fault, spans between shot point 1400 and the northern end of the seismic line at shot point 2078. Its southern end point now requires geo-location. According to the metadata for the seismic line, shot point 1405 was located at TQ 21796 39007, but these co-ordinates are >200 m east of the route followed. Taking this and the depiction of the seismic line on the UKOGL map into account, the co-ordinates of shot point 1400 can be estimated as TQ 21585 39125.

Seismic section – vertical scale
The existing tie between the Horse Hill-1 well and a seismic section (reported by Pullan and Butler, 2018) can form the basis of validating the vertical scale deduced by Hicks et al. (2019) in Fig. 2(a). This well is deviated NNW by 604 m, as shown in Fig. 01. From OGA documentation, it deviates to a maximum inclination of 45°,

gradually returning to a vertical orientation near the well bottom. The detailed structure in the vicinity of this well is illustrated in a seismic section provided as Fig. 22 of Pullan and Butler (2018). Table 1 indicates that the base of the Jurassic succession is encountered in this well at a depth (TVDSS) of 2204 m that corresponds to a two-way time of 1.286 s; given the near-vertical orientation of the bottom part of the well, this point is ~604 m NNW of the wellhead. Pullan and Butler (2018) reported that at the western end of their seismic section, ~2 km west of the wellhead, the two-way time to the base Jurassic is ~1.2 s, which they converted to a depth of ~6900 ft or ~2100 m. Their seismic line intersects that in Fig. 2 at TQ 21062 43513, near shot point 1785; around this point Pullan and Butler (2018) indicated that the base Jurassic is again at ~2100 m depth.

Experience of other seismic sections in the Weald Basin, such as those depicted by Andrews (2014) and Pullan and Butler (2018), indicates that the Lias Group sediments, in the lower part of the Jurassic succession, typically do not produce strong seismic reflections. The underlying strong reflectors thus represent the Penarth Group of Late Triassic age (https://www.bgs.ac.uk/Lexicon/lexicon.cfm?pub=PNG; formerly known as the Rhaetic beds; Table 1). On this basis, the base of the Jurassic succession can be tentatively interpreted as indicated in Fig. 2(b). The seismic reflector thus interpreted appears (Figs 2, 3) offset across the Newdigate Fault by 0.107 s two-way time, between 1.264 s at its footwall cutoff (circa TQ 22163 41030, shot point 1567) and 1.371 s at its hanging-wall cutoff (circa TQ 22135 40970, shot point 1562). Using the interval velocity for the Lower Lias (Table 1; nowadays formally designated as the Scunthorpe Mudstone Formation; https://www.bgs.ac.uk/lexicon/lexicon.cfm?pub=SMD) the height of this footwall escarpment is estimated as ~230 m; its ~60 m estimated width thus indicates a dip of ~75°, a reasonable value for a low-displacement normal fault (cf. Walsh and Watterson, 1988).

Comparison with the Horse Hill 1 well log (Table 1) suggests that the footwall cutoff of the Newdigate Fault is at a depth of ~2160 m, placing the hanging-wall cutoff at ~2390 m. The position of the Newdigate Fault where it offsets the base of the Jurassic succession, thus interpreted, is in roughly the same place as that estimated by Butler and Pullan (1990), although these authors estimated only a small displacement (Fig. 6). It is also in roughly the same place as where Pullan and Butler (2018) reported a ~300 m north-south increase in the depth of the base Jurassic, from ~7000 ft (~2130 m) to ~8000 ft (~2440 m), although these authors depicted this as occurring over a distance of ~2 km, rather than as a fault offset. The depth-conversion used by Hicks et al. (2019) (illustrated in Fig. 2) places these interpreted footwall and hanging-wall cutoffs at depths of ~1800 and ~2000 m, rather shallower than the depths deduced from the present analysis. It is thus evident that Hicks et al. (2019) used the velocity model in Table 2 for depth conversion of their seismic section, and this procedure has made the structure too shallow relative to what would be obtained for the velocity model in Table 1.

Earthquake locations
Hicks et al. (2019) reported epicentral positions using geographical co-ordinates; in Table 3 these have been converted to BNG references. In their original version of Fig. 2, Hicks et al. (2019) plotted hypocentral co-ordinates as BNG northings, not as latitudes. Again using the online co-ordinate converter, it has been confirmed for a representative subset of these events that their hypocentres were correctly positioned as BNG northings relative to the seismic section, as geo-located by Hicks et al. (2019), in Fig. 2.

The vertical mislocation of the earthquake 'cloud' in Fig. 2 is now considered. The base Jurassic (Lias Group / Penarth Group) unconformity beneath a representative point (at TQ 21983 41750) is at 1.322 s TWT; depth conversion relative to the footwall cutoff of the Newdigate Fault (assuming that the additional TWT is in Lower Lias rocks; cf. Table 1) places this point 2.28 km below O.D. (Fig. 2(b)). Interpolating the Hicks et al. (2019) depth conversion from Fig. 2(b)) for the same point gives a depth of ~1.85 km, ~400 m less. At greater depths, the Hicks et al. (2019) velocity model (Table 2) incorporates P-wave velocities of 4.7, 5.0 and 5.5 km s^{-1} that are reasonable for the rocks encountered, such as the Penarth Group and Carboniferous Limestone, so no significant additional systematic error in depth conversion will result. In the absence of repeating the location process for all the Newdigate earthquakes, using a more accurate velocity model, the present best estimate is to apply a uniform adjustment, throughout the earthquake 'cloud', by ~400 m. The focal depths

of the majority of the earthquakes listed in Table 3 thus adjust from ~1.9-2.2 km to ~2.3-2.6 km. An equivalent adjustment should be made to the vertical scale of the seismic section in Fig.2 which, as already noted, was depth-converted by Hicks et al. (2019) using their velocity model for earthquake location that now appears too slow. As a result, if the seismic section is depth-converted using the faster set of velocities in Table 1, and the set of hypocentral depths are amended as noted above, then their relative vertical positions remain unchanged. Nonetheless, as a result of this depth adjustment, the earthquake 'cloud' can be reliably placed beneath the Jurassic succession, not within this succession as Hicks et al. (2019) thought.

A further issue is that the Hicks et al. (2019) velocity model does not take into account the evident fault offsets and tilts of layer boundaries, which will affect the paths of seismic waves between the earthquake sources and the seismograph stations. Each of these factors was shown to be significant for obtaining reliable locations for the induced earthquakes at Preese Hall in 2011 (Westaway, 2016, 2017). Extensive numerical tests have been carried out on this aspect, from which it has been concluded that the low-angle dips (~1-2°) of the beds in the present study area and the ~200 m throw on the Newdigate Fault (Fig. 2) affect hypocentral co-ordinates by no more than ~100 m. In this particular case, these aspects are therefore of lesser importance than the adjustment to correct for the incorrect velocity model for earthquake location, so will not be considered further.

3. State of stress

Kingdon et al. (2016) and Fellgett et al. (2017) provided syntheses of data pertaining to the stress field across much of Britain. However, these authors wrote little about the Weald Basin; Fellgett et al. (2017) noted that many hydrocarbon wells in this area have yielded stress data but it had not yet been analysed by BGS, other than to note that the vertical stress gradient in the top 1.4 km is ~22-25 kPa m^{-1} (i.e., lithostatic). The World Stress Map (Heidbach et al., 2016) provides no data from the Weald Basin but interpolates a stress field for it using data from surrounding regions. The submission regarding the stress field to the OGA (2018) workshop (https://www.ogauthority.co.uk/media/5152/2-bgs-andy-chadwick-uk_stress.pdf) noted the input from Fellgett et al. (2017) and emphasized the significant uncertainty regarding the magnitude and orientation of the stress field in the Weald Basin.

The view is well established that, to first order, the stress field in Britain is dominated by effects of adjoining plate boundaries, 'ridge push' from the Mid-Atlantic Ridge and the effect of the convergent plate boundary in the Mediterranean region, and this results in a roughly NW-SE maximum principal stress, σ_H (e.g., Klein and Barr, 1986; Gölke and Coblentz, 1996). The minimum principal stress σ_h is thus roughly NE-SW, the intermediate principal stress being vertical, σ_V. However, it is also well understood that local effects cause significant variations in the stress field; the predicted orientation determined by plate tectonics cannot be assumed for the purposes of site-specific geomechanical calculations (e.g., Pine and Batchelor, 1984). The analyses by Kingdon et al. (2016) and Fellgett et al. (2017) indeed indicate significant local variations in the stress field. These are to be expected from the growing knowledge of active crustal deformation of Britain, which includes lateral variations in uplift rates and strong evidence of Quaternary slip on faults, such as the Portsdown Fault to the south and southwest of the Weald Basin (e.g., Westaway et al., 2006; Harding et al., 2012). Such effects will cause complex local changes to the state of stress, making it significantly 'rougher' rather than the smooth variations expected from simple considerations of plate tectonics (Westaway, 2006). As was discussed by Westaway (2016, 2017), an important realization to have emerged relatively recently in Britain is that the differential stress in the crust is high, consistent with the observed seismicity and crustal deformation, which makes it possible for small changes in the local state of stress to bring 'critically stressed' faults to the condition for slip and to thus cause earthquakes. The Westaway (2017) analysis of the induced seismicity at Preese Hall in 2011 developed a model stress field for this locality; this consisted of σ_H oriented at azimuth N7°E-S7°W and σ_h oriented at S83°E-N83°W, the model principal stresses at 2400 m depth being σ_h=39.2 MPa, σ_V=54.3 MPa, and σ_H=63.3 MPa. This north-south maximum principal stress in the Blackpool area of northwest England, derived initially at the Preese Hall well, was confirmed by Cuadrilla (2019) using data from the Preston New Road 1 well.

Table S1: Stress field data for the Weald Basin

Name	BGS ID	BNG reference	Code	σ_H	G	Surf. (m O.D.)	Depth (TVD SS) (m)				
							KC	CC	OC	ULC	MLC
Palmer's Wood 1	TQ35SE94	TQ 36450 52620	PAL1	NE-SW	V	140	517	789	860	1073	1180
Godley Bridge 1	SU93NE21	SU 95232 36640	GB1	N65°E-S65°W	V	71	1028	1527	1578	2017	2149
Iden Green 1	TQ83SW1	TQ 81325 31568	IDE	N40°W-S40°E	D	48	328	563	634	828	884
Wallcrouch 1	TQ62NE3	TQ 66050 29800	WLC	NW-SE	V	116	310	713	783	1079	1164
Stanmer 1	TQ31SW13	TQ 32631 11423	STA	N30°W-S30°E	V	198	488	695	748	989	998

Data listed are for the five wells in the Weald Basin (in the 110 km × 60 km rectangle with corners at SU 900 000 and TR 000 600) that have yielded caliper data indicating the orientation of the maximum horizontal stress, σ_H, according to Chadwick et al., 1996). Orientations of σ_H have been measured from Fig. 5.3 of Chadwick et al. (1996). The wells have been identified by matching their locations to Fig. 11 of Andrews (2014) to obtain the abbreviations of their names listed in the Code column, then using the table in Appendix E of Andrews (2014) to get the well names and depth information, then finally using the online BGS borehole viewer (http://mapapps.bgs.ac.uk/geologyofbritain/home.html) to obtain the BGS IDs and BNG references of the wells. Column G, for 'geometry', indicates whether each well is vertical or deviated. Surface levels (Surf.) and depths of stratigraphic boundaries are converted into metres, from Appendix E of Andrews (2014). The boundaries listed are: KC, top Kimmeridge Clay; CC, top Corallian Clay; OC, top Oxford Clay; ULC, top Upper Lias Clay; and MLC, top Mid Lias Clay.

At the OGA (2018) workshop a map was presented (https://www.ogauthority.co.uk/media/5152/2-bgs-andy-chadwick-uk_stress.pdf) to indicate the orientation of the stress field in the Weald Basin, with no source given. This map is from Evans and Brereton (1990); despite its age it continues to provide the most recent published information available. To facilitate the present analysis, this dataset has been curated (Table S1), identifying the boreholes that yielded the σ_H orientations, also providing summary stratigraphic details at these sites. As can be seen, three of the five measurements show the roughly NW-SE orientation that is expected, the other two show a roughly perpendicular orientation. Kingdon et al. (2016) have noted issues with the Evans and Brereton (1990) study, including input data of relatively poor quality by modern standards and an unclear analysis workflow. In their view, instances like this of highly discrepant data in the Evans and Brereton (1990) dataset resulted from the combination of erroneous data and poor analysis. This deduction is supported by the present analysis, implying that the data indicating a roughly NW-SE orientation of σ_H in the Weald Basin are valid.

4. The *Davis and Frohlich* criteria for anthropogenic seismicity

The Davis and Frohlich (1993) criteria will now be applied to the Newdigate earthquake sequence.

The first criterion is '*Are these events the first known earthquakes of this character in the region?*' The Newdigate earthquakes occurred in what is usually one of the most aseismic parts of Britain (e.g., Hicks et al., 2019), and are unprecedented for their epicentral area, inviting the answer '*yes*' to this question. However, Baptie and Luckett (2018) noted the preceding Billingshurst earthquake swarm (Baptie, 2006; Table S2) as a potential basis for concluding that the Newdigate earthquake swarm was not in fact unprecedented. Nonetheless, other wells were producing in the Weald Basin in 2005, notably those at Storrington (TQ 068 149), which were drilled from the 1980s onwards and continue to produce from the Middle Jurassic Oolitic Limestone (e.g., McLimans and Videtich, 1989). The closest of the earthquake epicentres listed in Table S2 is >10 km from the Storrington well pad, more than the 5 km separation recognized by Davis and Frohlich (1993) as significant for identification of induced seismicity (see below). However, the sparseness of the BGS seismograph network in 2005 makes mislocation of these earthquakes by many kilometres a strong possibility.

Table S2: The 2005 Billingshurst earthquake swarm

Date	Time	Latitude (°N)	Longitude (°W)	BNG reference	Depth (km)	M_L
18 June 2005	07:50:55.7	51.069	0.511	TQ 04425 31017	5.0	1.4
19 June 2005	11:49:34.3	51.064	0.512	TQ 04366 30460	5.0	1.6
16 July 2005	18:29:09.2	51.008	0.392	TQ 12910 24410	5.0	2.2

Data from the International Seismological Centre online catalogue (http://www.isc.ac.uk/iscbulletin/search/catalogue/), with BNG co-ordinates calculated as part of the present study. Focal depth was held fixed at 5 km during the location process for all these events.

The second Davis and Frohlich (1993) criterion is '*Is there a dear correlation between injection and seismicity*'. In the present context, this should be reworded as '*Is there a dear correlation between injection or production and seismicity*'. As already noted, Fig. 4(c) indicates a compelling correlation between production from the Portland reservoir and the Newdigate seismicity, so the answer to this question is clearly '*yes*'.

The third criterion is '*Are epicenters near wells (within 5 km)?*'. As Fig. 01 shows, the Newdigate earthquake epicentres cluster ~4 km from the Horse Hill-1 well, so this question can be likewise answered 'yes'. However, it should be clear that this 5 km threshold should be seen as a general indication rather than a hard-and-fast rule, earthquakes that are accepted as anthropogenic having occurred much farther from any causative well (up to ~40 km according to Goebel et al., 2017, based on the Hornbach et al., 2016, case study). The centre

of the Newdigate earthquake epicentre cluster is ~8 km from the Brockham site; the 5 km distance threshold proposed by Davis and Frohlich (1993) is moot.

The fourth criterion is '*Do some earthquakes occur at or near injection depths? If not, are there known geologic structures that may channel flow to sites of earthquakes?*' In the present context, the first of these questions should be reworded as '*Do some earthquakes occur at or near depths of injection or production?*' As already noted, the earthquakes cluster around 2400 m depth whereas the production is from a reservoir at ~600 m. The earthquakes are thus much deeper than the reservoir. However, the conceptual model (Fig. 5) and supporting explanatory text indicate structures that might well direct flow between the seismogenic fault and the well bottom. This question can be therefore answered 'yes'. Like the previous question, this question is made moot by the conceptual model.

The fifth criterion is '*Are changes in fluid pressure at well bottoms sufficient to encourage seismicity? Are changes in fluid pressure at hypocentral locations sufficient to encourage seismicity?*' The absence in the public domain of quantitative data on pressure changes in the Portland reservoir means that the first of these questions cannot be answered at this stage. The expectation, from the conceptual model, is that a small reduction in groundwater pressure within the strands of the Newdigate fault zone (smaller than a plausible estimate for the reduction in reservoir pressure) will cause significant changes to the state of stress that will bring the fault to the Coulomb condition for slip. However, no proof is possible as this would require detailed data on the size and shape of asperities on this fault and accurate data on the local state of stress, both of which are currently unavailable. Nonetheless, the conceptual model predicts changes to the state of stress that facilitate slip (Fig. 8).

The conclusion drawn from this summary is that the conceptual model in Fig. 5 provides a plausible explanation for the Newdigate earthquake swarm. Nonetheless, uncertainty remains, but much of it could be eliminated by release of appropriate data. As noted above, the principal data required to validate or refute this hypothesis are site engineering logs including pressure logs.

5. Regulatory issues

Following the Preese Hall seismicity in 2011, the UK Government imposed extremely tight regulation on seismicity caused by fracking, requiring any developer to suspend operations following the any earthquake of magnitude M_L ≥0.5. This form of regulation has been criticised by many people, notably by Westaway and Younger (2014), for two main reasons. First, earthquakes of magnitude 0.5 at depths of, say, 2-3 km are too small to be felt. Moreover, given the sparseness of the network of permanent seismograph stations in Britain, which does not guarantee event detection below magnitude ~2 (e.g., Baptie and Luckett, 2008), such small events are unlikely to even be detected but for the regulatory requirement for the operator to install a temporary local seismograph network. Second, it does not make sense to regulate anthropogenic seismicity by magnitude but, instead, by felt effects, expressed either as seismic intensity (as already noted) or as peak ground velocity (PGV). As Westaway and Younger (2014) indeed noted, other forms of industrial nuisance vibration, such as quarry blasting, have been uncontroversially regulated in the UK for many years on the basis of PGV, the specification being to keep PGV measured at any residential property below 6 mm s^{-1} during the working day, with lower thresholds at other times. Wald et al. (1999) and Worden et al. (2012) noted that PGV 6 mm s^{-1} corresponds to seismic intensity 3 on the Modified Mercalli (MM) intensity scale used in the USA, which is defined similarly to the European Macroseismic Scheme (EMS-98; Grünthal, 1998) used in Europe. However, the UK regulation (effective between 2012 and 2019) governing seismicity caused by fracking did not apply to earthquakes caused by other activities such as geothermal energy projects or 'conventional' extraction of hydrocarbons.

According to BGS (https://earthquakes.bgs.ac.uk/research/SurreyEarthquakes.html), seven of the Newdigate earthquakes in 2018 and four in 2019 have been strong enough to be felt. For the largest, on 27 February 2019, >1600 people reported felt effects to BGS; these were interpreted as indicating a peak EMS intensity of 5. The resulting distribution of seismic intensity from this event (illustrated by https://earthquakes.bgs.ac.uk/research/SurreyEarthquakes.html) is quite unusual, with intensity 5 persisting

to distances of ~10 km from the epicentre, but no higher intensity observed nearer the epicentre. The distinction between intensities 5 and 6 is significant; intensity 5 means that an earthquake is strongly felt and buildings shake, but there is no damage so the earthquake represents a nuisance. On the other hand, intensity 6 denotes (slight) damage to buildings, for example, plaster cracking and pieces of it falling off walls, so it indicates a hazard rather than a nuisance. A possible explanation for the observed distribution in seismic intensity, after Westaway and Younger (2014), recognizes that the vertically upward direction from a strike-slip earthquake source, such as those beneath Newdigate (Fig. 01), is along a node of the radiation pattern for both P- and S-waves, so – but for effects of geological structure, such as scattering of the seismic waves – the amplitude of the ground shaking in this direction would be zero. Stronger seismic radiation occurs obliquely to the vertical, but the greater amplitudes radiated are offset by the greater geometrical spreading and anelastic attenuation caused by the longer ray paths to the Earth's surface. But for this quirk of seismology, the residents of Newdigate might well have experienced damage to their property. The seismicity at Newdigate is thus of significance, far more so than M_L ~0.5 events caused by fracking. Following the granting in September 2019 of permission to develop more oil wells from the Horse Hill well pad, much higher production rates can be expected, which will cause greater pressure reductions in the reservoir. The proposed geomechanical model (Fig. 5) thus raises the possibility of more seismicity in future, although it does not specify whether this will involve more frequent events or larger events, with M_L significantly greater than 3.

To explore this issue further, the dataset for the sequence of earthquakes in the Groningen area of The Netherlands is utilized. These earthquakes have occurred as a result of reduction in the pressure in a gas reservoir in Triassic sandstone at a depth of ~3 km (e.g., Spetzler and Dost, 2017; Willacy et al., 2019). Much work has gone into the prediction of PGV from these earthquakes as a function of magnitude and epicentral distance to determine potential impacts (e.g., Bommer et al., 2017a,b,c; Pruiksma and Rózsás, 2017). The largest event, the Huizinge earthquake (M_L 3.6) of 16 August 2012, produced the largest single-component record of PGV, 34.6 mm s^{-1}, at a seismograph station at an epicentral distance of 2 km (Bommer et al., 2017c). Many records of earthquakes with M_L ~3 indicate PGV ~10 mm s^{-1} near the epicentre (Pruiksma and Rózsás, 2017). Bommer et al. (2017c) developed an empirical equation that, at the epicentre, predicts PGV 2-4 mm s^{-1} for M_L 2, 10-17 mm s^{-1} for M_L 3, and 52-82 mm s^{-1} for M_L 4, the range of vales for each magnitude depending on definition of PGV (e.g., single-component or vector sum of all three components). Omitting any correction for several complicating factors, including the different geological structure at Groningen and its effect on attenuation of seismic waves, the different focal mechanisms of the Groningen earthquakes, and the different definition of M_L in the Netherlands, one may use the ratio of focal depths (~2.4 km for Newdigate and ~3.0 km for Groningen) to crudely estimate PGV for the Newdigate earthquakes. The Bommer et al. (2017c) predictions for M_L 3 can be adjusted by a ratio of 3.0/2.4 or 5/4 and indicate epicentral PGV in the range 13-21 mm s^{-1} at Newdigate. Values in this range greatly exceed the UK regulatory limit for non-earthquake-related ground vibrations of 6 mm a^{-1}. By similar calculation, the predicted values for M_L 4 will adjust to 65-103 mm s^{-1} for Newdigate, exceeding the Wald et al. (1999) threshold of 81 mm s^{-1} for intensity 6 (and the revised 67 mm s^{-1} threshold, from Worden et al., 2012), for which minor damage might be expected. These considerations might help to inform debate about the potential environmental impact of activities at the Horse Hill site.